ISSN 1732-9353 (suspended)
eISSN 2543-7496

Scientific Review

Engineering and Environmental Sciences

Przegląd Naukowy
Inżynieria i Kształtowanie Środowiska

Vol. 35 (1) 2026 Issue 111
Quarterly

SCIENTIFIC REVIEW
ENGINEERING AND ENVIRONMENTAL SCIENCES
Quarterly

EDITORIAL OFFICE ADDRESS
Wydział Budownictwa i Inżynierii Środowiska SGGW, ul. Nowoursynowska 159, 02-776 Warsaw, Poland
tel. (+48 22) 59 35 363, 59 35 210, 59 35 302
e-mail: srees@sggw.edu.pl
https://srees.sggw.edu.pl

Electronic version of the Scientific Review Engineering and Environmental Sciences is primary version

All papers are indexed in the data bases as follows: AGRO(Poznań), BazTech, Biblioteka Nauki, **CrossRef**, **DOAJ**, **Google Scholar**, **Index Copernicus**, INFONA, POL-Index, **SCOPUS**, SIGŻ(CBR)

Scientific Review

Engineering and Environmental Sciences

Przegląd Naukowy

Inżynieria i Kształtowanie Środowiska

Vol. 35 (1) 2026 Issue 111

Contents

Wydawnictwo SGGW, Warsaw 2026

 Wydawnictwo SGGW  wydawnictwosggw

Editorial work – Anna Dołomisiewicz, Tomasz Ruchniewicz

ISSN 1732-9353 (suspended) eISSN 2543-7496

Scientific Review Engineering and Environmental Sciences (2026), 35 (1), 3–19

Sci. Rev. Eng. Env. Sci. (2026), 35 (1) https://srees.sggw.edu.pl

ISSN 1732-9353 (suspended) eISSN 2543-7496 DOI 10.22630/srees.10861

Received: 08.10.2025
Accepted: 19.12.2025

Sleyther Arturo De La CRUZ VEGA✉
Cristian Milton MENDOZA FLORES
Kevin Arturo ASCOY FLORES
Ccori Siello VEGA NEYRA
Universidad Cesar Vallejo, Faculty of Engineering and Architecture, Peru

Soil improvement with the addition of natural materials, such as cactus mucilage

Keywords: addition, standard Proctor, soil, cactus mucilage

Introduction

Improving soil simply means making the ground intended for construction stronger and firmer, ensuring that buildings do not collapse or experience other problems (De la Cruz Vega & Cornelio, 2022). In some places, the soil is very soft or cannot support much weight, therefore some materials need to be used to strengthen it. Usually, products like lime or cement are used, but those can be quite expensive and harmful to the environment (Alarcón et al., 2020).

Growing concern about pollution has encouraged the search for more natural and sustainable alternatives in many industries, including the construction sector. Accordingly, interest in natural materials has increased, as they help protect the environment and encourage a reconsideration of the ways in which buildings and infrastructure are designed and constructed (Silva et al., 2020). In recent decades, they have reemerged in sustainable architecture and engineering, driven by their

✉sdelacruzv@ucv.edu.pe

renewability, lower environmental footprint, and the rediscovery of techniques that improve their mechanical performance and durability (Przybek, 2025).

One of the natural materials used is cactus mucilage – a sticky, gel-like substance derived from the cactus *Opuntia ficus-indica* (More & Gogate, 2019). This gel improves soil by increasing soil particles cohesion and by promoting healthy conditions in the soil (More & Gogate, 2019). This makes the soil less water-permeable, as well as stronger and firmer, which is highly beneficial for construction purposes and also for protecting the environment (Luna-Zapién et al., 2023).

To evaluate the effectiveness of this gel, a test was conducted to measures soil compaction, which is important for the safety of constructions (Medina-Torres et al., 2000). Before the test, basic soil properties, such as particle size and sieve retention, were checked (Medina-Torres et al., 2000). After adding the gel, the soil exhibited improved compactability (Bacchetta et al., 2024). This effect was observed because the gel, when mixed with water, enhances the soil's workability (Soto Juscamayta, 2023). In very wet soil, the gel makes the cohesion of fine particles, such as clay, more effective and allows them to deform without fracturing (Luna-Zapién et al., 2023). However, if the soil becomes too soft or sticky, its workability can decrease,, which can lead to construction problems, such as excessive settlement or structural damage (Kulshreshtha et al., 2022).

A study by Campos (2022) investigated the effects of cactus mucilage affects on soils used in road subgrades. Three different concentrations were tested 25%, 35%, and 40% using the Proctor method together with an assessment of natural soil conditions. The results showed a clear improvement in soil properties, starting with a reduction in the plasticity index to 3% after incorporating 40% cactus mucilage. In turn, the optimal moisture content was reduced by 8.3%, while the maximum dry density increased to 2.168 $g \cdot cm^{-3}$, indicating that mucilage may represent a good option for improving road subgrades, especially for clayey soils. Huamán Roca and Reaño Quiespe (2022) conducted a similar study on the Huilcarpay highway, with similar objectives, adding San Pedro cactus mucilage, using concentrations of 0%, 30%, 60%, and 90%. The study showed the maximum dry density achieved with the addition of 90% mucilage was 1.45 $g \cdot cm^{-3}$, and the plasticity index was 30.87%, suggesting that San Pedro cactus mucilage improves the physical and mechanical properties of the soil. Aranda-Jiménez and Suárez-Dominguez (2014) chose to use the following concentrations: 0%, 0.5%, 1%, 1.5%, 2%, and 2.5%, and the dry density increased from 1.85 $g \cdot cm^{-3}$ in the undisturbed soil to 1.91 $g \cdot cm^{-3}$ with the highest dose of 2.5%, indicating that small doses of mucilage can improve soil densification, facilitating soil handling.

Finally, Tanta (2022) analyzed cactus mucilage in the subgrade of the Rosario–Sivia highway using mucilage concentrations of 0%, 3%, 6%, and 9%. The maximum dry density of the natural soil without mucilage was 1.655 $g \cdot cm^{-3}$; with 3% mucilage, the density was slightly lower (1.600 $g \cdot cm^{-3}$). The optimal moisture content was 25.3%, indicating that cactus mucilage is effective in reducing soil plasticity. This background demonstrates that cactus mucilage has the potential to significantly enhance the soil properties, enabling its use in conditions that would otherwise be unsuitable for road subgrades.

Material and methods

Type of research

This research is applied in nature, as it uses scientific knowledge to address a specific problem within the field of geotechnical engineering. According to Torales and Barrios (2023), this type of research transforms theoretical principles into practical solutions oriented towards real-world contexts. Similarly, Cordero (2009) explains that its purpose is to generate concrete impacts in technical, social, and operational areas, extending beyond theoretical contributions. In this study, cactus mucilage is used as a natural additive to improve soil properties, representing a sustainable, economical alternative aligned with current environmental protection demands. As noted by Olivera Granada (2022), the incorporation of natural materials in civil engineering enhances both the technical performance and the sustainability of projects, strengthening the transition toward more responsible construction practices.

Research design

The study adopts a quasi-experimental design, characterized by the manipulation of a variable – in this case, the dosage of cactus mucilage – without requiring the random assignment of treatments. According to Zurita-Cruz et al. (2018), this design enables the analysis of cause-and-effect relationships in situations where full control of the study conditions is not feasible. Ramos-Galarza (2021) states that this approach is suitable for measuring effects while maintaining some degree of internal control, even in the absence of strict randomization. Likewise, Manterola and Otzen (2015) indicate that this design is particularly useful in applied research where external factors cannot be completely controlled, but results with practical

validity are still desired. In the present investigation, samples were distributed without random assignment and were subjected to different proportions of mucilage under carefully controlled laboratory conditions to ensure the consistency of the results.

Research approach

A quantitative approach was used, which involved working with numerical measurements to analyze the relationship between the variables under study (Sánchez Flores, 2019). This approach relies on standardized instruments and precise procedures that allow for objective and replicable results (Hernández Sampieri et al., 2014). As emphasized by Huamán Rojas et al. (2022), it is essential in quantitative research to formulate clear hypotheses and test them through verifiable procedures in order to generate valid and generalizable conclusions. In this case, laboratory tests, such as the Standard Proctor test, were conducted to rigorously evaluate the effect of cactus mucilage on the soil's mechanical behavior.

Research methods

The methodological process consisted of several stages, each designed to ensure the validity, reliability, and reproducibility of the results. These stages were conducted in accordance with technical criteria and internationally recognized standards, ensuring the overall quality of the research.

Soil collection

The soil used in the study was collected from Luzuriaga street in the Barranca District, selected for its representativeness of the study area. The sample was extracted through a shallow excavation, with care taken to avoid disturbing or altering its natural properties (Agostini et al., 2014). The amount of material to be collected was determined in accordance with established technical guidelines to ensure representativeness. The entire process was carried out in accordance with national and international standards, primarily ASTM specifications (ASTM International, 2012).

Initial soil analysis

The collected soil underwent characterization tests, including granulometry, Atterberg limits, and specific gravity, in accordance with applicable ASTM and AASHTO standards. These analyses established a baseline of the physical

and mechanical properties of the natural soil, enabling subsequent comparison with the samples treated with mucilage.

Preparation and analysis of cactus mucilage

The mucilage was extracted from fresh cladodes, followed by a controlled process that preserved its physicochemical properties. Parameters such as viscosity, density, and pH were evaluated, as these directly influence how the mucilage interacts with soil particles. Additionally, X-ray analysis was used to determine its chemical composition, providing insight into its potential as an additive capable of modifying soil structure.

Preparation of soil–mucilage mixtures

Mixtures were prepared with varying the proportions of mucilage added to the soil. Environmental variables such as humidity, temperature, and resting time were controlled to ensure comparability between samples. This control made it possible to attribute any observed differences in the results could be attributed specifically to the mucilage rather than to external factors.

Compaction and mechanical behavior tests

The mixtures were subjected to the standard Proctor test to determine optimum moisture content and maximum dry density (Flores et al., 2020; Guevara Lopez & Canaza-Rojas, 2023). With these data, compaction curves were generated – an essential tool in geotechnical engineering for understanding how soil density varies with moisture content and with the inclusion of additives. This analysis is fundamental for the design and construction of civil works, as it helps engineers to predict soil behavior under applied loads (American Association of State Highway and Transportation Officials [AASHTO], 2001).

Comparison and analysis of results

Finally, the results obtained from the natural soil samples were compared with those from the mixtures treated with cactus mucilage. This comparison made it possible to evaluate the influence of the natural additive on the compaction properties, optimum moisture content, and mechanical behavior of the soil, thereby determining its potential as a sustainable alternative for soil improvement.

Results and discussion

Cactus mucilage

Table 1 shows the names of cactus mucilage by scientific name, country, and species. This information makes it possible to identify how its nomenclature varies in different regions (Villa Uvidia et al., 2020), which is useful for understanding references from other locations, facilitating knowledge sharing, and supporting its application in diverse contexts.

TABLE 1. Names of cactus mucilage used in other countries

Scientific name	Country	Plant common name	Mucilage common name
Opuntia ficus-indica	Mexico	Nopal	Nopal mucilage
	Peru	Cactus	Cactus mucilage
	Argentina	Tuna	Prickly pear mucilage
	Chile	Tuna	
	Ecuador	Tuna	
	Bolivia	Tuna	
Opuntia spp.	United States	Nopal	Nopal mucilage
	Colombia	Nopal	
	Venezuela	Nopal	

Source: own work.

Table 1 presents to the elemental composition of cactus mucilage determined using the Ed XRF technique, a practical and well-known technique for accurately identifying the mineral components present in the mucilage. This method provides a clear characterization of mucilage's structure and composition, which is essential for properly understanding its chemical and physical properties and for supporting its use in various industrial or research applications (Vargas Mamani et al., 2019).

Figure 1 shows a world map highlighting the regions or countries where the use of cactus mucilage in soil compaction has been applied or explored. The areas marked in green include parts of Latin America, North and East Africa, West Asia, and India, suggesting that this method is relevant mainly in arid or semi-arid regions where cactus species are common and accessible.

FIGURE 1. Regions where cactus mucilage is used for soil compaction
Source: own work.

The results of cactus mucilage chemical analysis (Table 2) reveal a high water content (96.43%), suggesting its primarily aqueous nature. Significant levels of potassium, calcium, and magnesium were found among the inorganic components, present both in elemental and oxide forms, suggesting their involvement in the structure of the mucilage and its water-retaining capacity. Other elements were also detected, including phosphorus, iron, zinc, manganese, and copper, but in smaller proportions, which could indicate their role in the chemical stability and bioactive properties of the mucilage. This water-rich composition, with a diverse mineral fraction, makes the mucilage a suitable material for consideration in various applications related to industry or research.

TABLE 2. Composition of cactus mucilage obtained by X-ray fluorescence spectrometry at a sample' moisture content of 96.43%

Content of the chemical elements	Value [%]	Content of the oxides	Value [%]
Potassium (K)	1.7810	Potassium oxide (K_2O)	2.6042
Calcium (Ca)	0.8190	Magnesium oxide (MgO)	0.6014
Magnesium (Mg)	0.5913	Calcium oxide (CaO)	0.3110
Chlorine (Cl)	0.2883	Phosphorus pentoxide (P_2O_5)	0.0372
Phosphorus (P)	0.0402		
Sulfur (S)	0.0333	Chlorine (Cl)	0.0040
Iron (Fe)	0.0050	Iron oxide (Fe_2O_3)	0.0033
Zinc (Zn)	0.0034	Sulfur trioxide (SO_3)	0.0024
Manganese (Mn)	0.0031	Manganese oxide (MnO)	0.0017
Copper (Cu)	0.0019	Zinc oxide (ZnO)	0.0008

Source: own work.

Although Table 1 presents the elemental composition of Opuntia mucilage, it is important to note that this composition is not universal for all cactus species. While variations are generally small, differences may occur depending on the genus and species, environmental conditions, soil mineral content, plant maturity, and even the season. Therefore, the chemical profile reported here should be interpreted as specific to this particular sample, and it may differ slightly from the mucilage obtained from other specimens growing in different regions.

Table 3 shows that cactus mucilage has a high viscosity, indicating a thick, gelatinous appearance, typical of substances with water-retaining capacity. The density of these substances is quite similar to that of water, suggesting they do not significantly alter soil structure.

TABLE 3. Properties of cactus mucilage

Property	Value
Viscosity	1,087.9 cSt
Density	0.9948 $g \cdot cm^{-3}$
Potential of hydrogen (pH)	4.61

Source: own work.

However, they also improve material cohesion and water retention. The slightly acidic pH of the mucilage indicates a chemical environment that could favor certain biochemical reactions and even enhance formulation stability. Ultimately, these aspects give cactus mucilage significant potential for use in soil improvement, especially in infrastructure projects where improved material cohesion and water retention are sought (De la Cruz Vega, 2023).

Undisturbed soil

The results of the particle-size analysis of the tested soil sample are presented in Table 4, enabling the determination of the particle-size distribution and the classification of the soil according to the established criteria – an essential step for evaluating soil behavior (Gutiérrez Rodríguez, 2023).

The results obtained from Table 4 show a granulometric analysis of the analyzed soil sample, indicating a composition of 14.08% gravel, 85.51% sand, and 0.42%

fine material, which allows it to be classified as a primarily sandy and clean soil due to its low fine-particle content. According to the USCS classification system, the soil is classified as well-graded sand (SW), given that it presents a continuous and wide distribution of particle sizes within the sandy range. With respect to AASHTO, since less than 35% of the sample passes the Sieve No 200 and it is mainly sand with some gravel, the soil corresponds to Group A-1-b.

TABLE 4. Granulometry of the soil sample

Sieve	Mesh [mm]	Weight [g]	Soil retained [%]	Cumulative of soil retained [%]	Soil passing [%]
3″	76.200	0	0	0	100
2″	50.800	0	0	0	100
1 1/2″	38.100	0	0	0	100
1″	25.400	52.308	1.74	1.74	98.26
3/4″	19.050	34.808	1.16	2.90	97.10
1/2″	12.700	90.288	3.01	5.91	94.09
3/8″	9.525	42.478	1.42	7.33	92.67
1/4″	6.350	109.378	3.65	10.98	89.02
No 4	4.760	93.048	3.10	14.08	85.92
No 8	2.380	494.968	16.50	30.58	69.42
No 16	1.190	567.208	18.91	49.48	50.52
No 30	0.595	537.688	17.92	67.41	32.59
No 50	0.297	489.528	16.32	83.72	16.28
No 100	0.150	376.848	12.56	96.29	3.71
No 200	0.075	98.928	3.30	99.58	0.42
Bottom	–	12.518	0.42	100	–
	Total	2,999.994			

Source: own work.

During the analysis of the samples from Tanks 1, 2, and 3, the liquid limit was determined (Fig. 2). For this purpose, samples with different moisture contents were prepared, and the number of blows required to close the cut groove was recorded. After performing the corresponding calculations, a liquid limit value of 19.16 was obtained for the sample.

De La Cruz Vega, S. A., Mendoza Flores, C. M., Ascoy Flores, K. A., Vega Neyra, C. S. (2026). Soil improvement with the addition of natural materials, such as cactus mucilage. *Sci. Rev. Eng. Env. Sci.*, *35* (1), 3–19. DOI 10.22630/srees.10861

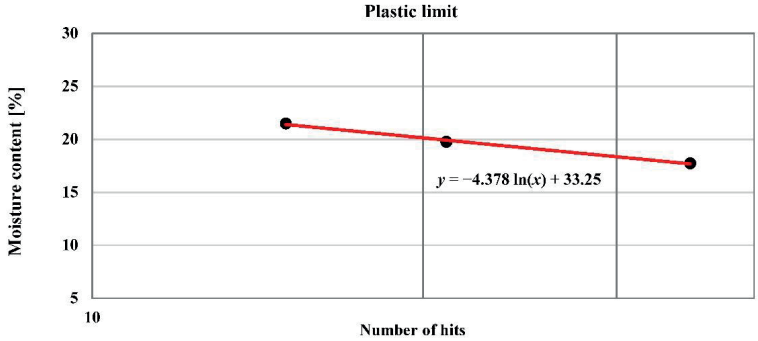

FIGURE 2. Liquid limit of the soil sample
Source: own work.

Standard Proctor test of soil with cactus mucilage dosages

The results of the tests are analyzed to identify patterns, trends, and significant variations in soil properties. Data are updated against certain standards, and useful recommendations are made based on the results obtained, which will determine applicable improvements in land use in the study area (Castro-Solis et al., 2024). The standard Proctor test was performed on undisturbed soil samples with different dosages of cactus mucilage, with the aim of determining the maximum dry density and optimal soil moisture content (Reyes, 2010). To this end, different doses of cactus mucilage were supplied to the soil (4%, 6%, 8% CM).

Dry density data obtained from the standard Proctor tests are presented in Figure 3. Among the samples tested, the soil with 6% cactus mucilage stands out for exhibiting the highest value. This dosage results in improved compactability and greater stability compared with the other dosages. These findings suggest that incorporating 6% mucilage enhances soil cohesion, thereby increasing its strength and resistance to applied loads.

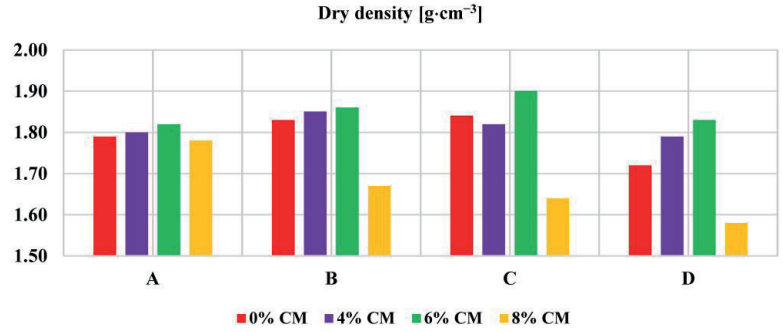

FIGURE 3. Comparative graph of dry density values of soil with cactus mucilage (CM)
Source: own work.

Figure 4 presents the test results showing that using 4% and 6% mucilage provided higher dry densities (1.85 and 1.90 g·cm^{-3}, respectively) compared to the original soil without mucilage (1.84 g·cm^{-3}). In this case, the 6% dosage provided the highest density, resulting in greater soil compaction and stability. Moisture content also increased, from 12.27% (undisturbed) to 19.11% (with 6% cactus mucilage). When the mucilage content was 8%, the dry density decreased, as extreme humidity impairs compaction processes due to the hygroscopic properties of the mucilage, leading to poor soil compaction.

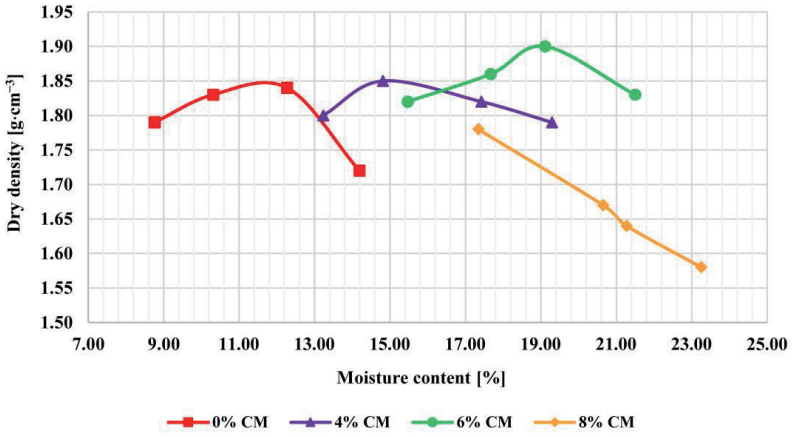

FIGURE 4. Comparative graph of dry density values of soil with cactus mucilage (CM)
Source: own work.

The 6% cactus mucilage dosage used in this research was the most effective, achieving a maximum dry density of 1.90 g·cm^{-3} and an optimum moisture content of 19.11%. This represents a significant improvement in soil compaction compared to the undisturbed sample. These results partially coincide with Campos (2022), who, after employing higher concentrations of nopal mucilage (40%), reported a higher dry density of 2.168 g·cm^{-3}, but with a lower optimum moisture content of 8.3%. This is likely due to differences in soil type and the nature of the mucilage used. Huamán Roca and Reaño Quiespe (2022) did use high concentrations of San Pedro cactus mucilage, up to 90% concentration, but their results yielded a lower dry density of 1.45 g·cm^{-3}. This suggests that the type of cactus used, as well as the excess addition, may hinder the soil's densification capacity.

Building on the findings of this research, Aranda-Jiménez and Suárez--Dominguez (2014) demonstrate how small doses of mucilage, for example, 2.5%, can progressively increase soil dry density, reaching 1.91 g·cm^{-3}, thus confirming the effectiveness of more controlled dosages. Finally, Tanta (2022) concluded that low mucilage concentrations (up to 9%) do not significantly affect the dry density of 1,600 g·cm^{-3} achieved in the study, although they did contribute to reducing plasticity. All these studies support the notion that a controlled dosage, such as the 6% used in this study, can improve soil mechanical properties without reaching the values that impair compaction due to high moisture content or saturation of the material.

The mucilage acts as a natural binder, joining the soil particles without producing any internal structural modification of the material. Its main function is to improve cohesion and compaction, which increases the stability of the soil without altering its fundamental physical composition. Additionally, once compacted, this improved soil can be covered with an asphalt layer, which serves as protection against moisture, erosion, and environmental changes, helping preserve the properties achieved during the stabilization process.

The results in Table 5 show that dry density varies noticeably with the amount of cactus mucilage added. The natural soil (0%) exhibits a mean dry density of 1.84 g·cm^{-3} with very low variability, reflecting consistent measurements. A slight increase is observed at 4% mucilage, where the mean rises to 1.85 g·cm^{-3}, although variability increases moderately. The 6% dosage yields the highest dry density (1.90 g·cm^{-3}), supported by its confidence interval, which lies entirely above those intervals of the previous treatments, indicating a significant improvement in compaction. In contrast, the 8% dosage results in the lowest density (1.78 g·cm^{-3}), with a confidence interval clearly separated from the others, confirming that this higher dosage reduces the soil's compactability. Overall, the data indicate that 6% mucilage provides the most favorable compaction performance among the tested dosages.

TABLE 5. Statistical indicators (*SD*, *SEM*, *CI*)

Cactus mucilage dosage [%]	Mean [g·cm^{-3}]	*SD*	*SEM*	95% *CI*
0	1.84	0.010	0.006	1.828–1.852
4	1.85	0.015	0.009	1.833–1.867
6	1.90	0.020	0.012	1.876–1.924
8	1.78	0.018	0.010	1.760–1.800

Source: own work.

The results of the Shapiro–Wilk test indicate that all mucilage dosages (0%, 4%, 6%, and 8%) exhibit *p*-values greater than 0.05, meaning none of the distributions deviate significantly from normality. Since normality is not rejected for any group, the dataset meets one of the key assumptions required for parametric analysis. Therefore, it is statistically appropriate to apply a one--way ANOVA to evaluate differences in dry density among the various mucilage treatments (Table 6).

TABLE 6. Shapiro–Wilk normality test results

Content of cactus mucilage [%]	W statistic	*p*	Normal distribution?
0	0.8925	0.3948	yes
4	0.8604	0.2616	yes
6	0.9281	0.5835	yes
8	0.9736	0.8636	yes

Source: own work.

The one-way ANOVA analysis shows a statistically significant effect of mucilage percentage on the soil's dry density ($F = 8.37$; $p = 0.0028$). Since the *p*-value is less than 0.05, the null hypothesis, asserting that all group means are equal, is rejected. Therefore, it is concluded that the different mucilage dosages produce real variations in dry density (Table 7).

TABLE 7. Analysis of variance (ANOVA)

Source of variation	Sum of squares (*SS*)	Degrees of freedom (*df*)	Mean square (MS)	*F*	*p*
Between groups	0.1183	3	0.03940	8.37	0.0028
Within groups	0.0565	12	0.00471	–	–
Total	0.1748	15	–	–	–

Source: own work.

This result confirms that mucilage is not merely a physical additive but significantly modifies the soil's compaction behavior. In practical terms, the 6% dosage is the most efficient, yielding the highest dry density, whereas the 8% dosage reduces compaction efficiency due to the excessive moisture contributed by the mucilage.

Conclusions

Adding cactus mucilage to soil significantly improves it, especially in terms of compaction and the moisture required to achieve good compaction. The best results were obtained with about 6% mucilage; at that amount, the soil compacted well and had just the right moisture to remain strong. However, it is important to note that adding too much mucilage introduces excessive moisture, which reduces soil compaction.

For example, when 8% was used, there was too much moisture, and instead of improving the soil, it actually made it looser and less dense. Therefore, it is important to find the right balance – not too little, not too much. Another advantage of mucilage is that it helps distribute moisture evenly throughout the soil, resulting in more uniform compaction and fewer air pockets. This is key to ensuring the ground remains stable and can bear weight.

Reviewing other studies, it is clear that cactus mucilage can improve soil, but the results vary depending on soil type and the amount of mucilage used. Overall, 6% appear to provide optimal balance between strengthening the soil and controlling moisture. Since it is natural, it is a promising alternative to chemical stabilizers – not only for environmental benefits but also for cost savings.

Acknowledgments

The authors sincerely thank Universidad César Vallejo for the valuable support provided throughout the research.

References

Agostini, M., Monterubbianesi, M. G., Studdert, G. A., & Maurette, S. (2014). A simple and practical method for determining bulk density. *Ciencia del Suelo*, *32*(2), 171–176. http://www.scielo.org.ar/scielo.php?script=sci_arttext&pid=S1850-20672014000200003

Alarcón, J., Jiménez, M., & Benítez, R. (2020). Stabilization of soils through the use of oily sludge. *Journal of Construction Engineering*, *35*, 5–20. https://pdfs.semanticscholar.org/e533/a1b0d5339bc5bb182d9ccc6abc1f2ddffcc8.pdf

American Association of State Highway and Transportation Officials [*AASHTO*]. (2001). *Standard method of test for moisture-density relations of soils using a 4.54-kg (10-lb) rammer and a 457-mm (18-in.) drop* (*AASHTO T 180-03*).

Aranda-Jiménez, Y. G., & Suárez-Domínguez, E. J. (2014). Cactus stalk waterproof effect in compressed earth blocks. *Nova Scientia*, *6*(11), 311–323. https://www.scielo.org.mx/scielo.php?pid=S2007-07052014000100017&script=sci_abstract&tlng=en

ASTM International. (2012). *Standard Test Methods for Laboratory Compaction Characteristics of Soil Using Standard Effort (12 400 ft-lbf/ft^3 (600 kN-m/m^3))* (ASTM D698-12).

Bacchetta, L., Canditelli, M., Platamone, G., Procacci, S., Di Palma, P. R., Maccioni, O., Montereali, M. R., Alisi, Ch., & & Forni, C. (2024). Use of cactus pear pruning waste to improve soil properties and to produce high-quality compost. *Organic Agriculture*, *14*(3), 263–275. https://doi.org/10.1007/s13165-024-00462-9

Campos, J. (2022). *Adición del mucílago de penca del nopal para estabilizar el suelo en el jirón Manco Cápac, Pilcomayo, Huancayo, 2022* [Bachelor's thesis]. Universidad César Vallejo.

Castro-Solis, A. A., Ortiz-Hernández, E., & Macías-Sánchez, L. (2024). Analysis of the mechanical behavior of sandy silt soils, stabilized with lime and cement [Análisis del comportamiento mecánico de los suelos limo arenosos, estabilizado con cal y cemento]. *Revista Científica INGENIAR: Ingeniería, Tecnología e Investigación*, *7*(13), 69–79. https://doi.org/10.46296/ig.v7i13.0153

Cordero, Z. R. V. (2009). La investigación aplicada: una forma de conocer las realidades con evidencia científica. *Revista Educación*, *33*(1), 155–165. https://www.redalyc.org/pdf/440/44015082010.pdf

De la Cruz Vega, S. A. (2023). *Evaluación de las propiedades físico mecánicas del adobe adicionando mucílago de cactus (Opuntia spp.), Huaura, Lima, 2022* [Doctoral thesis]. Universidad Nacional del Santa. https://hdl.handle.net/20.500.14278/4374

De la Cruz Vega, S. A., & Cornelio, E. N. N. (2022). Geomechanical characteristics of controlled backfill soil for foundations, Pucallpa, Peru. *Journal of the Selva Andina Biosphere*, *10*(1), 32–45. https://doi.org/10.36610/j.jsab.2022.100100032x

Flores, I., García, J., & González, Y. (2020). Relationship between compaction and suction in earth dams with CH type soils. *Obras y Proyectos*, *27*, 15–25. https://doi.org/10.4067/S0718-28132020000100015

Guevara Lopez, I. J., & Canaza-Rojas, F. (2023). Estimation of the dry density of a granular backfill using the dynamic cone penetrometer. *Gaceta Técnica*, *24*(2), 77–91. https://doi.org/10.51372/gacetatecnica242.6

Gutiérrez Rodríguez, W. Á. G. (2023). Grain size analysis of soils by the sieve method. *Ciencia Latina Revista Científica Multidisciplinar*, *7*(2), 6908–6927. https://doi.org/10.37811/cl_rcm.v7i2.5834

Hernández Sampieri, R., Fernández Collado, C., & Baptista Lucio, P. (2014). *Metodología de la investigación* (6th ed.). McGraw Hill/Interamericana Editores.

Huamán Roca, J., & Reaño Quiespe, M. A. (2022). *Efecto del mucílago de cactus San Pedro (Echinopsis pachanoi) en estabilización de suelos. caso: carretera Huilcarpay, 2021* [Bachelor's thesis]. Universidad César Vallejo. https://hdl.handle.net/20.500.12692/76268

Huamán Rojas, J. A., Treviños Noa, L. L., & Medina Flores, W. A. (2022). Epistemología de las investigaciones cuantitativas y cualitativas. *Horizonte de la Ciencia*, *12*(23), 1–14. https://doi.org/10.26490/uncp.horizonteciencia.2022.23.1462

Kulshreshtha, Y., Vardon, P. J., Du, Y., Habert, G., Vissac, A., Morel, J-C., Rao, S. M., Paassen, L. van, Loosdrecht, M. C. M. van, Mota, N. J. A., & Jonkers, H. M. (2022). Biological stabilisers in earthen construction: A mechanistic understanding of their response to water-ingress. *Construction Technology and Architecture*, *1*, 529–539. https://doi.org/10.4028/www.scientific.net/CTA.1.529

Luna-Zapién, E. A., Zegbe, J. A., Meza-Velázquez, J. A., & Minjares-Fuentes, R. (2023). Mucílago de nopal (*Opuntia* spp.) y su aplicación como aditivo alimentario: una visión general [Cactus pear (*Opuntia* spp.) mucilage and its application as food additive: an overview]. *Revista Fitotecnia Mexicana*, *46*(1), 51–61. https://doi.org/10.35196/rfm.2023.1.51

Manterola, C., & Otzen, T. (2015). Estudios Experimentales 2ª Parte. Estudios Cuasi-Experimentales [Experimental studies. 2nd Part. Quasi-experimental studies]. *International Journal of Morphology*, *33*(1), 382–387. https://intjmorphol.com/wp-content/uploads/2015/06/art_60_331.pdf

Medina-Torres, L., Brito-De La Fuente, E., Torrestiana-Sánchez, B., & Katthain, R. (2000). Rheological properties of the mucilage gum (*Opuntia ficus indica*). *Food Hydrocolloids*, *14*(5), 417–424. https://doi.org/10.1016/S0268-005X(00)00015-1

More, N. S., & Gogate, P. R. (2019). Intensified approach for desulfurization of simulated fuel containing thiophene based on ultrasonic flow cell and oxidizing agents. *Ultrasonics Sonochemistry*, *51*, 58–68. https://doi.org/10.1016/j.ultsonch.2018.10.019

Olivera Granada, J. (2022). *Evaluación de un aditivo natural en la estabilización de un suelo fino, bajo la Norma Técnica de Estabilizadores Químicos MTC E 1109-2004* [Bachelor thesis]. Universidad Andina del Cusco. https://hdl.handle.net/20.500.12557/4740

Przybek, A. (2025). *The role of natural fibers in the building industry – The perspective of sustainable development*. *Materials*, *18*(16), 3803. https://doi.org/10.3390/ma18163803

Ramos-Galarza, C. (2021). Editorial: Diseños de investigación experimental [Editorial: Experimental investigation designs]. *CienciAmérica*, *10*(1), 1–7. https://doi.org/10.33210/ca.v10i1.356

Reyes, W., & Willians, J. (2010). Evaluación de la susceptibilidad a la compactación en cuatro series de suelo bajo uso agrícola en Venezuela [Evaluation of the compaction susceptibility in four series of soil under agricultural use in Venezuela]. *Bioagro*, *22*(1), 29–36. http://ve.scielo.org/scielo.php?script=sci_arttext&pid=S1316-33612010000100004

Sánchez Flores, F. A. (2019). Epistemic fundamentals of qualitative and quantitative research: Consensus and dissensus. *Revista Digital de Investigación en Docencia Universitaria*, *13*(1), 102–122. https://alicia.concytec.gob.pe/vufind/Record/REVUPC_abf1f335428aee0b0e2b7f-3b215eb566#details

Silva, G., Kim, S., Aguilar, R., & Nakamatsu, J. (2020). *Natural fibers as reinforcement additives for geopolymers–A review of potential eco-friendly applications to the construction industry. Sustainable Materials and Technologies*, *23*, e00132. https://doi.org/10.1016/j.susmat.2019.e00132

Soto Juscamayta, L. M. (2023). *Efectos de la adición de mucílago de nopal en las propiedades físico-mecánicas del concreto convencional f'c = 210 kg/cm² con fines de pavimento rígido, Ayacucho, 2022* [BSc thesis]. Universidad Nacional de San Cristóbal de Huamanga.

Tanta, L. (2022). *Influencia del mucílago de nopal en el mejoramiento de la subrasante de suelo arcilloso de la carretera Rosario–Sivia, Ayacucho, 2022* [BSc thesis]. Universidad Continental.

Torales, J., & Barrios, I. (2023). Research design: Classification algorithm and essential features. *Medicina Clínica y Social*, *7*(3), 210–235. https://doi.org/10.52379/mcs.v7i3.349

Vargas Mamani, J. J., Vera Vargas, G. V., & Suppé Tejada, N. A. (2019). Physical chemical characterization, microscopic sweeping and X-ray dispersion of clays mixed by *Opuntia ficus indica* in the high region of Tacna. *Revista de la Sociedad Química del Perú*, *85*(3), 305–314. https://doi.org/10.37761/rsqp.v85i3.248

Villa-Uvidia, D. N., Osorio-Rivera, M. A., & Villacis-Venegas, N. Y. (2020). Extracción, propiedades y beneficios de los mucílagos [Extraction, properties, and benefits of mucilages]. *Dominio de las Ciencias*, *6*(2), 503–524. https://doi.org/10.23857/dc.v6i2.1181

Zurita-Cruz, J. N., Márquez-González, H., Miranda-Novales, G., & Villasís-Keever, M. Á. (2018). Estudios experimentales: diseños de investigación para la evaluación de intervenciones en la clínica. *Revista Alergia México*, *65*(2), 178–186. https://doi.org/10.29262/ram.v65i2.376

Summary

Soil improvement with the addition of natural materials, such as cactus mucilage. In civil engineering, a frequent situation arises, when soils to be used in projects have little resistance or are very plastic to be used in projects, so they must be improved. The procedure of improving soils through natural stabilizers such as cactus mucilage is an ecological alternative. The objective of this work is to evaluate the properties of mucilage and the effect it has on the compaction properties of the soil from Luzuriaga Street, located in the Barranca District. Different dosages (4%, 6%, and 8%) of cactus mucilage (CM) were used on this SW (in accordance with soil sample in accordance with USCS) and A-1-b (according to AASHTO) soil sample, and the properties were evaluated by standard Proctor tests. The results of the cactus mucilage showed a humidity of 96.43% and potassium and calcium were identified as the main elements present, the viscosity was 1,087.9 cSt, the density was 0.9948 $g \cdot cm^{-3}$ and its pH was 4.61. With respect to the properties of soil with CM they indicated that 6% mucilage is the one that results in a higher dry density of 1.90 $g \cdot cm^{-3}$ and an optimal moisture content of 19.11%, which means an improvement in compaction in addition to stability. As a conclusion it was stated that the cactus mucilage modifies the structure of the soil by increasing the cohesion between the particles, resulting in a more uniform mixture. It is also indicated that a moderate dose such as 6% optimizes the properties of the soil.

Scientific Review Engineering and Environmental Sciences (2026), 35 (1), 20–39

Sci. Rev. Eng. Env. Sci. (2026), 35 (1) https://srees.sggw.edu.pl

ISSN 1732-9353 (suspended) eISSN 2543-7496 DOI 10.22630/srees.10847

Received: 03.10.2025
Accepted: 30.12.2025

Yerlan MUKHANBET[1]✉
Jarosław CHORMAŃSKI[2]
Dana TUNGATAR[1]
Mariusz Paweł BARSZCZ[2]
Ainura ALDIYAROVA[1]

[1] Kazakh National Agrarian Research University, Faculty of Water Resources and Information Technology, Kazakhstan
[2] Warsaw University of Life Sciences – SGGW, Institute of Environmental Engineering, Poland

Probabilistic assessment of annual maximum precipitation in Almaty, Kazakhstan

Keywords: urban flooding, extreme rainfall, Gumbel distribution, generalized extreme value, GEV, return period analysis

Introduction

Extreme hydrometeorological events have become a growing global concern due to their direct socio-economic and environmental impacts. Numerous studies have shown that intense rainfall events and flash floods are increasing in both frequency and severity due to climate change. These phenomena not only damage infrastructure and property but also pose significant risks to human safety, particularly in rapidly urbanizing areas with insufficient drainage systems (D'iya et al., 2014).

✉mukhanbet.yerlan@inbox.ru

Globally, urban flooding has become one of the most critical consequences of climate-induced hydrological extremes. For example, severe rainfall events in Europe, such as the 2021 floods in Germany, Belgium, and Poland, resulted in extensive infrastructural damage and loss of life (Kreienkamp et al., 2021; Pietras & Pyrc, 2025). Similar patterns are observed in South Asia, where countries like India, Pakistan, and Bangladesh experience increasingly frequent monsoon-driven floods (Latif et al., 2017; Muhammad Iskandar et al., 2025). In China and Japan, rapid urbanization combined with changing rainfall regimes has intensified flood hazards, prompting the development of advanced stormwater management systems and statistical models for rainfall prediction (Jayawardane et al., 2024; Ling et al., 2025). These international examples highlight that the challenge of managing extreme precipitation and urban flooding is not unique to a single region but represents a widespread, global issue requiring localized yet methodologically comparable approaches.

In Kazakhstan, Almaty city has recently witnessed a marked increase in the frequency and intensity of extreme precipitation events. Several episodes of intense rainfall and sudden surface runoff have caused localized flooding, especially in low-lying districts such as Almalinskiy and Bostandyk. The city's mountainous surroundings, coupled with rapid urban expansion and the loss of permeable green spaces, accelerate surface runoff and exacerbate the overload of the existing drainage infrastructure (BES Media, 2025). Furthermore, the absence of a comprehensive stormwater management system across many parts of the city leaves Almaty particularly vulnerable to the adverse effects of hydrological extremes.

These challenges are not unique to Almaty city. Similar situations have been observed in other urban centers of Kazakhstan, such as Astana city, where episodes of heavy rainfall and rapid snowmelt have overwhelmed drainage systems, resulting in urban flooding (Nakispekova, 2024). Almaty city has typical characteristics of the Central Asia urbanization processes and, in the authors' opinion, can explain similar processes in this region, where rapidly developing cities are dominant. Almaty city faces the dual challenge of adapting to intensifying climate extremes while managing the consequences of rapid urbanization. Traditional stormwater infrastructure and planning approaches, based on outdated climatic assumptions, are increasingly inadequate for modern conditions (Dong et al., 2020). This underscores the urgent need for more adaptive and data-driven methods in urban flood risk assessment and management.

International experience demonstrates that statistical modeling of extreme rainfall using probability distribution functions has become a widely accepted

approach to understanding and predicting hydrological extremes. The generalized extreme value (GEV) distribution remains the most commonly applied model in Europe, China, and Australia for estimating design rainfall and return periods of floods due to its flexibility in capturing both short-term and long-term extremes (Coles, 2001; Katz et al., 2002; Gentilucci et al., 2023).

Recent studies have shown that lognormal and gamma distributions continue to be preferred in regions where rainfall intensity exhibits moderate variability and observational records are limited, owing to their computational simplicity and stable fitting performance (Stedinger et al., 1993; Cho et al., 2004; Montes-Pajuelo et al., 2024). However, each model presents specific limitations: for instance, the GEV may overestimate rare events when sample sizes are small, while lognormal and gamma distributions tend to underestimate the upper tail of extreme rainfall (Rima et al., 2025).

Therefore, the combined application and intercomparison of multiple statistical models provide a more robust and reliable basis for assessing precipitation extremes under non-stationary climate conditions, as emphasized in recent hydrological analyses (Gentilucci et al., 2023; Rima et al., 2025).

Between 2015 and 2025, Almaty city experienced several instances of localized flooding and mudflows, primarily triggered by heavy rainfall, rapid snowmelt, and natural runoff from the surrounding mountainous terrain. Due to its geographic location at the foothills of the Trans-Ili Alatau (a subrange of the Tian Shan mountain belt), Almaty is particularly vulnerable to sudden water surges from upstream rivers and glacial sources. Each spring and summer, rising temperatures accelerate glacial melt, leading to swollen rivers and, occasionally, the formation and bursting of moraine-dammed glacial lakes (Kyrgyzbay et al., 2023; Choudhary & Kumar, 2025).

Although none of these incidents matched the scale of the 2015 glacial lake outburst flood, they collectively posed a significant challenge to the urban infrastructure. The city's peripheral districts – such as Alatau, Turksib, and Bostandyk – were the most frequently affected, often facing obstructed roads, flooded basements, and temporary evacuations (Duskayev et al., 2023; Mirlas et al., 2024). Rapid urban expansion has increased vulnerability: changes to the hydrographic network due to infrastructural development, land use patterns, and inadequate drainage have amplified local flood risks. Human activity, particularly the construction of new neighborhoods and modification of watercourses, has further complicated natural water flow, leading to more severe and recurrent urban flood events (Duskayev et al., 2023).

Despite ongoing efforts by the city and national authorities to improve early warning systems and build protective infrastructures such as mudflow barriers

and improved river channels, these events highlight the central role of sustainable urban planning and adaptation to climate change. The continued increase in average temperatures and more frequent episodes of intense precipitation intensify the risk of flash floods and mudflows in Almaty's metropolitan area (Duskayev et al., 2023; Kyrgyzbay et al., 2023; Choudhary & Kumar, 2025).

This study provides a preliminary analysis of rainfall data collected from meteorological stations in Almaty city prior to their application in urban flood modeling.

The aim of this study is to analyze trends and spatial variability of extreme precipitation and runoff potential in Almaty using ground-based meteorological data (2000–2023) through statistical analysis.

Material and methods

Study area

Almaty city is located at the foothills of the Zailiyskiy Alatau Mountains (also known as the Trans-Ili Alatau), in southeastern Kazakhstan. It serves as the administrative center of Almaty city and lies at elevations ranging from approx. 700 m to 900 m a.s.l. The city includes both lowland urbanized areas and mountainous catchments, which form the headwaters of several small rivers, such as Ulken Almaty, Kishi Almaty, Esentai, Aksay, and Kargaly (Kyrgyzbay et al., 2023).

Over the past century, Almaty has undergone rapid urban expansion, with the city's built-up area increasing from approx. 3 km² in the 19th century to over 700 km² in recent decades. This urban growth has resulted in significant transformations of the natural hydrographic network, including the channelization of streams, construction of stormwater infrastructure, and creation of artificial drainage pathways (Choudhary & Kumar, 2025). These changes have substantially altered the hydrological behavior of the area, increasing the likelihood of urban flooding. The area of Almaty city is now approx. 682 km².

The city is highly susceptible to natural hazards, including heavy rainfall, flash floods, and debris flows. These risks are exacerbated by the combination of steep mountainous topography, convective precipitation events, and reduced infiltration capacity in urbanized zones (Mirlas et al., 2024). Historical flood events, including the catastrophic mudflows of 1921 and the urban floods in 2015, have caused significant damage to infrastructure and property.

Furthermore, recent groundwater modeling studies in the northern parts of the city, particularly in the Akbulak Micro District, have identified recurring groundwater flooding events caused by poor drainage and excessive surface runoff. These issues are compounded by the obstruction of natural subsurface flows and the degradation of the historical Karasu stream system (Mirlas et al., 2024).

The combination of climate variability, increasing rainfall intensity, land-use change, and hydrological modification has created a complex and dynamic urban flood regime. Therefore, Almaty represents a critical case study for assessing the impacts of climate-induced extreme rainfall and evaluating probabilistic models for sustainable flood risk management.

Data

The rainfall data used in this study were obtained from the official website of Kazhydromet (Republic State Enterprise Kazhydromet, n.d.) covering a continuous 23–24-year period from 2000 to 2023 (from 2001 to 2023). The dataset used in the analysis in that paper consists of the total annual precipitation sums recorded at five meteorological stations within Almaty city: Almaty, Shymbulak, Mynzhylyk, Bolshoe Almatinskoe Ozero (BAL), and Kemen. The names and geographical coordinates of these stations, together with key descriptive statistics, are presented in Table 1. The 24-year data series (2000–2023) can be considered relatively short for long-term climatological analysis, when the normal analytical period for hydrometeorological characteristics should not be shorter than 30 years (World Meteorological Organization [WMO], 1989). However, this period was selected based on the availability of continuous, high-quality digital data provided by the Republican State Enterprise "Kazhydromet" Kazakhstan's official hydrometeorological service. Earlier data (prior to 2000) are mainly stored in paper archives and contain numerous gaps and inconsistencies, which reduce their homogeneity and reliability. Therefore, the 2000–2023 dataset obtained from the official Kazhydromet portal was considered optimal for ensuring completeness, calibration comparability, and statistical reliability.

To evaluate the variability of precipitation, several statistical indicators were calculated. The standard deviation (*SD*), which represents the dispersion of precipitation around the mean, ranged from 135 mm at Almaty station to 196 mm at Shymbulak, indicating moderate interannual variability. The coefficient of variation (*CV*), computed as the ratio of *SD* to the mean (*M*), varied between 0.176 and 0.202, corresponding to moderate variability (10–20%), which suggests relative stability of precipitation across the studied period.

To further describe the statistical characteristics of rainfall, skewness and kurtosis were analyzed. Positive skewness values ranging from 0.63 to 1.34 indicate a right-skewed distribution, meaning that most rainfall events are moderate, but rare extreme events occasionally occur. Kurtosis coefficients (γ_2) between 2.87 and 4.19 show that certain stations (e.g., Shymbulak) exhibit more pronounced peaks and heavier tails compared to a normal distribution (kurtosis = 3), which is typical for regions exposed to intense orographic precipitation. All descriptive parameters were calculated using the formulas presented in Wilks (2011).

TABLE 1. Geographic characteristics of meteorological stations and descriptive statistics of annual precipitation sum data series observed in the period of 2000–2023

Geographical coordinate	Meteorological station				
	Almaty	Shymbulak	Mynzhylky	BAL	Kemen
Latitude (N)	43°24′	43°12′	43°08′	43°05′	43°18′
Longitude (E)	76°93′	77°08′	77°07′	76°98′	76°96′
Descriptive statistics of annual precipitation sum					
Minimum [mm]	489	687	668	636	615
Maximum [mm]	1,010	1,480	1,240	1,320	1,360
Mean (*M*) [mm]	678	968	875	866	904
Standard deviation (*SD*) [mm]	135	196	154	165	179
Coefficient of variation (*CV*)	0.198	0.202	0.176	0.190	0.198
Skewness (γ_1)	0.995	1.34	0.739	1.12	0.632
Kurtosis coefficient (γ_2)	3.24	4.19	2.87	3.60	2.88
Data length [year]	2000–2023 (24 years)	2001–2023 (23 years)	2000–2023 (24 years)	2000–2023 (24 years)	2000–2023 (24 years)

Source: own work.

To verify the reliability and temporal consistency of the precipitation dataset, three non-parametric statistical tests were conducted for all five meteorological stations (Table 2). The Wald–Wolfowitz runs test (*U*) was used to evaluate the independence of the data series, ensuring that precipitation values are not serially correlated. The Kruskal–Wallis test (*K*) was applied to assess stationarity, confirming that there are no systematic changes or trends within the time series. The Pettitt test (*W*) was employed to check homogeneity, detecting possible abrupt shifts or inhomogeneities in the data over time.

The calculated test statistics fall within the following ranges:
- independence (U): from 1.30 to 1.83,
- stationarity (K): from 0.74 to 1.76,
- homogeneity (W): from 0.22 to 1.01.

All values are below the critical threshold of ±1.96 at a 95% confidence level, indicating that none of the null hypotheses were rejected. Therefore, the precipitation series for all stations can be considered independent, stationary, and homogeneous, providing a reliable basis for further hydrological and probabilistic modeling.

TABLE 2. Statistical characteristics of annual precipitation sum data series observed in the period of 2000–2023 by stations

Statistical test value	Meteorological station				
	Almaty	Shymbulak	Mynzhylky	BAL	Kemen
Independence	|U| = 1.5	|U| = 0.83	|U| = 0.38	|U| = 0.24	|U| = 1.23
Stationarity	|K| = 1.76	|K| = 1.32	|K| = 0.74	|K| = 0.86	|K| = 0.82
Homogeneity	|W| = 1.01	|W| = 0.22	|W| = 1.01	|W| = 0.72	|W| = 0.43

Source: own work.

The magnitude of the test statistics varies among stations, reflecting spatial differences in precipitation behavior and local influences. The Almaty station exhibits higher |U| and |K| values (1.5 and 1.76), indicating a slight upward trend likely associated with urbanization and impervious surfaces that affect local convection and moisture dynamics. In contrast, the mountain stations Shymbulak, Mynzhylky, BAL, and Kemen exhibit lower values of |U| and |K| (< 1), confirming stable and homogeneous precipitation patterns typical of natural high-altitude environments with minimal anthropogenic influence. The homogeneity test (|W| < 1.1) for all stations confirms the absence of structural breaks in the data. Overall, the precipitation records are statistically consistent, although the elevated values at Almaty suggest emerging urban–climate interactions influencing rainfall variability.

The topographic complexity of the research area requires the inclusion of meteorological data collected across the entire area. As shown in Figure 1, the network of meteorological stations covers both the urbanized areas and the surrounding mountainous part of Almaty city. Located in the southeastern part of Kazakhstan, within the Almaty Region, the city lies at the foothills of the Zailiyskiy Alatau mountains. This spatial distribution enables a more accurate representation of precipitation variability and supports the identification of potential flash-flood risk zones in Almaty city.

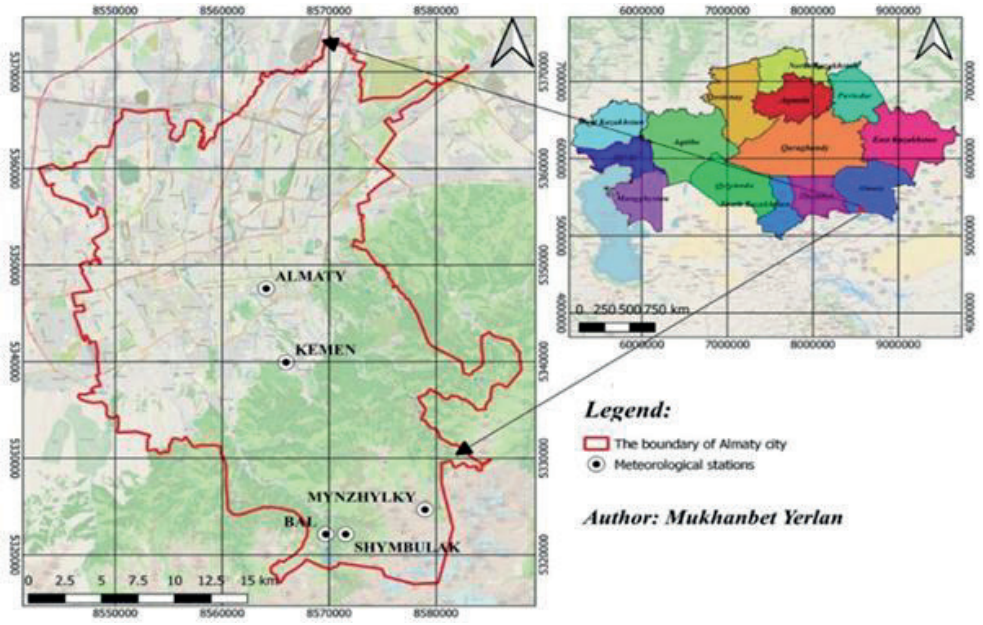

FIGURE 1. Location map of the meteorological stations in Almaty city, with a general map of Kazakhstan
Source: own work.

As illustrated in Figure 2, the spatial distribution of annual precipitation across Almaty city demonstrates a clear north-south gradient. Precipitation amounts increase significantly from the northern plains toward the foothills and mountainous zones of the Zailiyskiy Alatau. The highest annual totals, exceeding 900 mm, are observed at high-altitude stations such as Shymbulak and Mynzhylyk, while the lowest values, below 700 mm, occur in the northern and central lowland areas. This orographic influence results in substantial spatial variability of rainfall, which plays a crucial role in shaping surface runoff and the occurrence of flash floods in the city.

Given the high spatial and seasonal variability of climatic parameters, it is crucial to determine the probabilistic distributions of atmospheric precipitation. This enables:

– Assessment of the risk of extreme weather events (e.g., rare but high-impact rainfall).
– Hydrological modeling of stormwater runoff based on the statistical characteristics of precipitation.
– Development of adaptation scenarios and sustainable stormwater management measures under climate variability.

Mukhanbet, Y., Chormański, J., Tungatar, D., Barszcz, M. P., Aldiyarova, A. (2026). Probabilistic assessment of annual maximum precipitation in Almaty, Kazakhstan. *Sci. Rev. Eng. Env. Sci.*, *35* (1), 20–39. DOI 10.22630/srees.10847

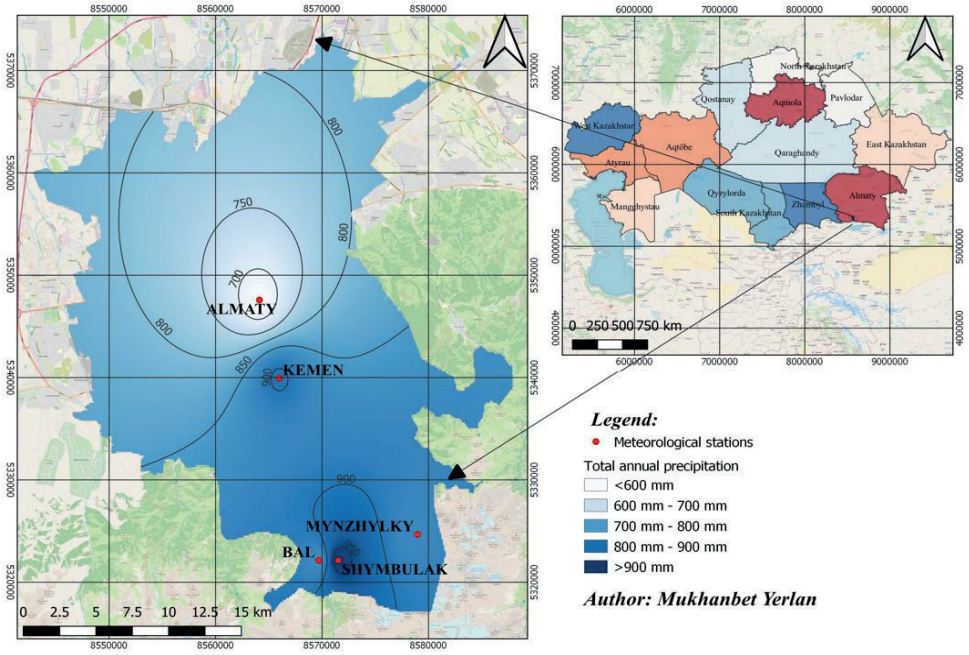

FIGURE 2. Map of annual precipitation distribution in Almaty city
Source: own work.

The application of probabilistic approaches, such as the five tested probability distributions, allows for a shift from descriptive analysis to quantitative risk assessment of pluvial flooding.

In recent decades, Almaty city has regularly faced challenges related to stormwater flooding, caused by a combination of intense precipitation events, rapid urbanization, and insufficient capacity of the existing drainage infrastructure. This problem is particularly acute during spring and summer, when short-duration but high-intensity rainfall generates substantial surface runoff that exceeds the capacity of current stormwater systems.

According to the Almaty Department for Emergency Situations, more than 50 incidents of localized flooding affecting streets, residential basements, and public infrastructure were recorded between 2010 and 2022. One of the most significant events occurred in July 2015, when over 50 mm of rainfall fell within a few hours, flooding central areas of the city. According to municipal authorities, total material damage exceeded 1.2 billion tenge, including damage to vehicles, underground utilities, and commercial facilities. One can see one of the flooding outcomes in the following link (BES Media, 2025).

Methodology

This section presents the methodology used to identify the most suitable probability distribution function for estimating design values of annual maximum precipitation. Such a model can be applied by engineers and water resource specialists for a priori assessments in frequency analysis.

During the first stage, five different probability distribution functions (PDFs) were tested on the series of annual maximum precipitation values to determine which best fit the data. These were selected due to their widespread use in contemporary hydrometeorological studies (Kundzewicz et al., 2013; Dong et al., 2020). The annual maximum precipitation series, obtained from various meteorological stations, were fitted using the HYFRAN software package (Duskayev et al., 2023), a practical tool for evaluating probability distributions. The list of applied distribution functions found in the software is presented in Table 3.

TABLE 3. Probability density functions, equations, and descriptions

Distribution	Probability formula	Typical use	Advantages	Limitations
Gumbel	$f(x)\frac{1}{\beta}\exp\left[-\frac{x-\mu}{\beta}-\exp\left(-\frac{x-\mu}{\beta}\right)\right]$	Maxima (annual peak precipitation)	Simple, widely used in hydrology	May under-estimate tail behavior (underpredict extremes)
Generalized extreme value (GEV)	$f(x)=\frac{1}{\sigma}\left(1+\xi\frac{x-\mu}{\sigma}\right)^{-\frac{1}{\xi}-1}\exp\left[-\left(1+\xi\frac{x-\mu}{\sigma}\right)^{-\frac{1}{\xi}}\right]$	Flexible for maxima with different tail behavior	Accounts for skewness and heavy tails	More complex parameter estimation
Log--Pearson Type III	$\log(X) \sim$ *Pearson Type III*	Flood and rainfall extremes	Recommended by the U.S. Water Resources Council	Sensitive to sample size and outliers
Pearson Type III	$f(x)=\frac{\beta^{\alpha}(x-x_0)^{\alpha-1}e^{-\beta(x-x_0)}}{\Gamma(\alpha)}$, where $x>x_0$	General hydrologic use	Good fit for varied data with skewness	Assumes continuous positive data
Lognormal	$f(x)=\frac{1}{x\sigma\sqrt{2\pi}}\exp\left(-\frac{(\ln x-\mu)^2}{2\sigma^2}\right), x>0$	Precipitation intensities	Suitable for moderately skewed data	Sensitive to zero and near-zero values
Normal	$f(x)=\frac{1}{\sqrt{2\pi\sigma^2}}\exp\left(-\frac{(x-\mu)^2}{2\sigma^2}\right)$	Not recommended for extremes	Easy to interpret	Poor fit for skewed and extreme event data

Source: own work.

To fit the parameters of each PDF, maximum likelihood estimation (MLE) and method of moments (MoM) approaches were used. These methods enabled the estimation of distribution parameters based on a series of annual maximum precipitation values.

In addition, it was necessary to determine the empirical exceedance probability of the observed annual maximum precipitation values. For this purpose, the following formula was used:

$$F\left(x_k\right)=\frac{k-\alpha}{n-2\alpha+1},0\le\alpha\le 0.5,$$

where: $F(x_k)$ is empirical probability corresponding to the value x_k, k is rank of the value in the ascending ordered series, n is total number of observations, α is offset parameter depending on the selected formula (cf. Table 4).

TABLE 4. Values of parameter α for estimating the empirical exceedance probability

α	Comment	Reference
0.4	Recommended for hydrometeorological data; provides a balanced estimation for both small and large sample sizes	Cunnane (1978)
0.5	Universal, but performs poorly at the tails (rare events). Frequently used in engineering calculations, but may overestimate probabilities at the distribution tails	Hazen (1914)
0	Simple and widely used, but may introduce bias	Weibull (1939)
0.3	Based on Soviet tradition, but often inadequate in mountainous regions	Chegodayev (1955)
0.375	Used in statistics; closer to the normal distribution	Blom (1958)
≈0.333	Sometimes applied in scientific publications	Tukey (1962)

Source: own work.

To calculate the empirical exceedance probability of annual maximum precipitation in Almaty city, the Cunnane formula (Cunnane, 1978) was selected. The choice of this formula is justified by the region's topographic and climatic characteristics. Almaty is situated in the foothills of the Zailiyskiy Alatau, where orographic influences result in high spatial and temporal variability in precipitation. This is particularly evident in the case of intense convective rainfall events occurring during the warm season, often associated with moisture-laden mountain air and strong atmospheric instability.

Under such conditions, the Cunnane formula provides the most balanced probability estimates, especially when dealing with a limited number of observations ($n \leq 25$ years), which is typical for meteorological stations in the city.

The Cunnane formula minimizes systematic errors at the distribution tails, offering a more accurate representation of both frequent and rare (extreme) events. This makes it particularly useful for comparing empirical data with theoretical distributions, such as the Gumbel, GEV, or log-Pearson Type III distributions, which are widely used in hydrological and climate-related studies (Kundzewicz et al., 2013; Dong et al., 2020). Moreover, the World Meteorological Organization recommends the use of the Cunnane formula for analyzing extreme hydrometeorological data in mountainous regions (WMO, 2009, 2017).

Thus, the use of the Cunnane formula is both scientifically and methodologically justified for analyzing extreme precipitation in the mountainous conditions of Almaty city. It provides a reliable foundation for estimating return periods and assessing the risks of pluvial flooding.

Results and discussion

In this study, the 24-year annual precipitation records (2000–2023) from five meteorological stations near Almaty city were analyzed. For hydrological planning and design purposes, the best available long-term precipitation data were used. The annual maximum precipitation values (in mm) were statistically processed to estimate design rainfall intensities for return periods of 10 (10%), 50 (2%), and 100 (1%) years using several PDFs, namely the exponential, GEV, normal, lognormal, and gamma distributions.

The goodness of fit of each distribution was evaluated using multiple criteria: the chi-square (χ^2) test, Akaike information criterion (AIC), Bayesian information criterion (BIC), and posterior model probability $P(M_i|x)$. Table 5 presents the comparison of empirical and theoretical precipitation quantiles (in mm) for each station.

Figures 3 and 4 show the results of fitting the GEV and lognormal distributions to the observed values of annual precipitation maxima at the Almaty weather station. The red line shows the theoretical model, the black crosses show the empirical data, and the blue lines show the 95% confidence interval. These two graphs are provided as illustrative examples.

Mukhanbet, Y., Chormański, J., Tungatar, D., Barszcz, M. P., Aldiyarova, A. (2026). Probabilistic assessment of annual maximum precipitation in Almaty, Kazakhstan. *Sci. Rev. Eng. Env. Sci.*, *35* (1), 20–39. DOI 10.22630/srees.10847

TABLE 5. Design rainfall intensities for return periods of 1%, 2% and 10% calculated by selected empirical probability functions applied to precipitation annual sum time series in meteorological stations of Almaty city

Meteorological station	Design rainfall for return periods calculated by selected probability distribution functions [mm]														
	exp.			GEV			normal			lognormal			gamma		
	10%	2%	1%	10%	2%	1%	10%	2%	1%	10%	2%	1%	10%	2%	1%
Almaty	936	1,250	1,390	851	1,020	1,090	851	955	991	849	983	1030	845	964	1,010
Shymbulak	1,350	1,820	2,030	1,210	1,480	1,590	1,220	1,370	1,420	1,210	1,400	1,470	1,210	1,380	1,440
Mynzhylky	1,160	1,500	1,650	1,070	1,260	1,330	1,070	1,190	1,230	1,070	1,230	1,280	1,070	1,200	1,250
BAL	1,180	1,570	1,730	1,080	1,310	1,410	1,080	1,200	1,250	1,070	1,230	1,290	1,070	1,210	1,270
Kemen	1,300	1,780	1,990	1,140	1,330	1,400	1,130	1,270	1,320	1,140	1,330	1,400	1,130	1,290	1,350

exp. – exponential distribution, GEV – generalized extreme value distribution, normal – normal distribution, lognormal – lognormal distribution, gamma – gamma distribution.

Source: own work.

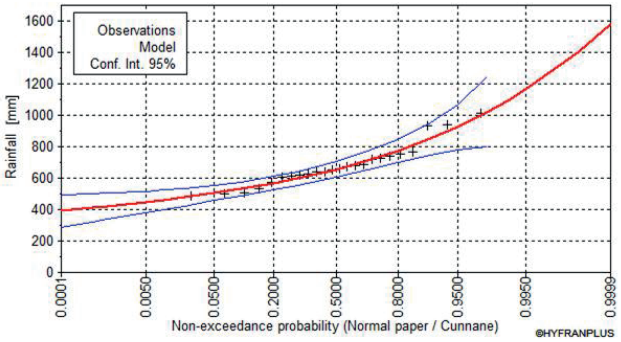

FIGURE 3. Annual maximum precipitation distribution fitted with the generalized extreme value distribution using the maximum likelihood estimation method for the Almaty meteorological station

Source: own work.

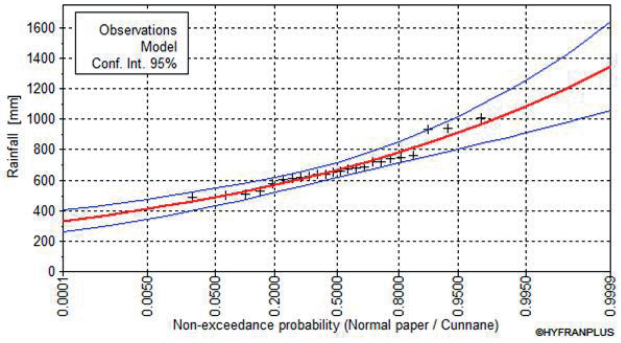

FIGURE 4. Annual maximum precipitation distribution fitted with the lognormal distribution using the maximum likelihood estimation method for the Almaty meteorological station

Source: own work.

The analysis of AIC, BIC, and $P(M_i|x)$ for the Almaty meteorological station, which serves as a representative location for an urban area in this study, shows that the lognormal distribution demonstrates superior performance, yielding the highest posterior probability $P(M_i|x) = 39.94$ along with the lowest AIC (303.2) and BIC (305.6) values (Table 6).

TABLE 6. Comparison of the analysis for the meteorological station based on AIC, BIC, $P(M_i|x)$, χ^2 test, and *p*-value criteria

Meteorological station	Parameter	Probability distribution type				
		exp.	GEV	normal	lognormal	gamma
Almaty	AIC	305.7	304.2	306.4	303.2	304.0
	BIC	308.1	307.7	308.7	305.6	306.3
	$P(M_i\|x)$	11.2	13.4	8.2	39.9	27.1
	χ^2	9.2	2.8	7.5	5.1	5.1
	p	0.05	0.41	0.11	0.27	0.27
Shymbulak	AIC	311.4	307.2	311.0	306.9	309.2
	BIC	313.7	310.6	313.3	309.2	310.2
	$P(M_i\|x)$	4.5	21.1	5.5	43.4	25.3
	χ^2	7.1	2.8	4.7	1.6	3.4
	p	0.13	0.41	0.32	0.80	0.48
Mynzhylky	AIC	310.0	312.2	312.8	310.8	311.2
	BIC	312.4	315.7	315.2	313.1	313.6
	$P(M_i\|x)$	37.4	7.1	9.2	25.8	20.4
	χ^2	8.6	4.0	2.8	4.5	4.5
	p	0.07	0.26	0.58	0.33	0.33
BAL	AIC	315.1	312.8	316.0	312.5	313.4
	BIC	317.4	316.3	318.4	314.9	315.8
	$P(M_i\|x)$	10.9	18.8	6.7	38.9	24.5
	χ^2	12.7	5.7	1.6	5.1	5.1
	p	0.01	0.12	0.79	0.27	0.27
Kemen	AIC	326.0	320.3	320.2	318.5	318.5
	BIC	328.3	323.9	322.5	320.8	320.8
	$P(M_i\|x)$	0.9	8.6	16.9	39.3	34.1
	χ^2	11.0	6.3	4.00	8.0	6.3
	p	0.02	0.09	0.40	0.08	0.17

exp. – exponential distribution, GEV – general extreme value distribution, normal – normal distribution, lognormal – lognormal distribution, gamma – gamma distribution.

Source: own work.

Although the GEV showed the best agreement with empirical data according to the χ^2 test, the lognormal distribution proved more favorable when accounting for model simplicity and goodness-of-fit through information-theoretic metrics. The gamma distribution also performed relatively well, with a posterior probability of 27.1 and competitive AIC (304.0) and BIC (306.3) values (Table 6).

The variation in the best-fit distribution across different stations and criteria underscores the complexity of hydrological modeling in a region with complex climatic conditions, such as those in Almaty city. The discrepancy between the χ^2 test (favoring the GEV) and information criteria/Bayesian probabilities (favoring lognormal/gamma) highlights the importance of using multiple goodness-of-fit measures for robust model selection. The GEV, while showing good agreement with empirical data via the χ^2 test, might be penalized by AIC and BIC if its additional parameter does not significantly improve the fit relative to its complexity.

Estimating design rainfall with different return periods (e.g., 1%, 2%, 5%, and 10%) is crucial for infrastructure planning and for mitigating risks from extreme precipitation events, such as flash floods and urban inundations, which are intensified by ongoing urbanization and climate variability in Almaty. The selection of the most appropriate PDF directly impacts the accuracy of these design values.

Similar approaches have been widely applied in other countries, where various probability distributions have been tested to model extreme rainfall events. For instance, the GEV is the most commonly used model in Europe, China, and Australia for estimating design rainfall and flood return periods due to its flexibility in capturing both short-term and long-term extremes (Coles, 2001; Burnham & Anderson, 2002; Katz et al., 2002; Gentilucci et al., 2023). In contrast, lognormal and gamma distributions are frequently applied in regions with moderate rainfall variability and limited data availability, such as parts of South Asia and Africa, owing to their computational simplicity and stable fitting performance (Stedinger et al., 1993; Cho et al., 2004; Montes-Pajuelo et al., 2024). However, these models differ in their ability to represent the upper tail of extreme precipitation: the GEV tends to perform better for rare events, whereas the lognormal and gamma distributions may underestimate extremes. Therefore, comparing multiple statistical distributions, as presented in this study, provides a more robust and comprehensive understanding of precipitation extremes under non-stationary climate conditions.

Conclusions

This study presents a comprehensive probabilistic assessment of extreme precipitation in the city of Almaty, based on 24 years of ground-based meteorological observations (2000–2023) from five stations: Almaty, Shymbulak, Mynzhylky, BAL, and Kemen. The analysis used annual maximum precipitation values and applied five theoretical probability distribution functions – exp., GEV, normal, lognormal, and gamma – to model extreme rainfall behavior.

All rainfall series were confirmed to be independent, stationary, and homogeneous, as verified by statistical tests (Wald–Wolfowitz, Kruskal–Wallis, and Pettitt). The results of the MLE showed that the GEV and lognormal distributions provided the best fit across most stations.

Quantitatively, the maximum annual precipitation during the study period ranged from 615 mm (Kemen) to 1,010 mm (Shymbulak), while the mean annual precipitation varied between 678 mm (Almaty) and 866 mm (BAL). The *CV* ranged from 0.17 to 0.20, indicating moderate interannual variability.

Based on the best-fitting probability models, the estimated rainfall quantiles showed a clear increase with longer return periods. On average across all stations, the 10-year event (10% exceedance probability) corresponded to rainfall amounts of approximately 950–1,050 mm, the 50-year event (2% exceedance) to around 1,100–1,200 mm, and the 100-year event (1% exceedance) to 1,200–1,300 mm. These values represent the expected magnitudes of extreme precipitation for the respective return periods and can serve as reference thresholds for hydrological design and risk assessment in Almaty city. The lognormal distribution demonstrated the lowest AIC and BIC values and the highest posterior probability $P(M_i|x) > 0.35$ for the Almaty and Shymbulak meteorological stations, while the GEV was slightly better for BAL and Kemen meteorological stations. The gamma model also performed reasonably well (AIC differences < 5), suggesting its potential suitability for areas with complex mountain–urban topography.

These quantitative results confirm that extreme rainfall events have intensified in Almaty city, especially during the warm season (May–September). The observed upward trend in the magnitude of extreme precipitation highlights growing risks of urban flash floods and surface runoff overload.

From a practical standpoint, the derived rainfall quantiles can be directly applied to the design of stormwater drainage networks, flood risk assessments, and climate-resilient infrastructure planning in Almaty. For instance, a 100-year design rainfall of approx. 1,250 mm can serve as a baseline parameter for the dimensioning of retention basins and flood control structures.

References

BES Media. (2025, 2 March). *Ocherednoy liven zatopil ulitsy Almaty: livnevyye kanalizatsii, kak obychno, ne spravlyayutsya s potokom vody*. BES.media. https://bes.media/news/ocherednoy-liven-zatopil-ulitsi-almati-livnyovki-kak-vsegda-ne-spravlyayutsya-696088/

Blom, G. (1958). *Statistical estimates and transformed beta-variables*. Wiley.

Burnham, K. P., & Anderson, D. R. (2002). *Model selection and multimodel inference: A practical information-theoretic approach*. Springer. https://doi.org/10.1007/b97636

Chegodayev, L. (1955). *Raspolozheniye elementov na grafike dlya raboty po teorii veroyatnostey*. Gidrometeoizdat.

Cho, H. K., Bowman, K. P., & North, G. R. (2004). A comparison of gamma and lognormal distributions for characterizing satellite rain rates from the tropical rainfall measuring mission. *Journal of Applied Meteorology*, *43*(11), 1586–1597. https://doi.org/10.1175/JAM2165.1

Choudhary, K., & Kumar, R. (2025). An analysis of stormwater management with the Internet of Things (IoT). *Nature Environment and Pollution Technology*, *24*(3), B4271. https://doi.org/10.46488/NEPT.2025.v24i03.B4271

Coles, S. (2001). *An introduction to statistical modeling of extreme values.* Springer. https://doi.org/10.1007/978-1-4471-3675-0

Cunnane, C. (1978). Unbiased plotting positions – A review. *Journal of Hydrology*, *37*(3–4), 205–222. https://doi.org/10.1016/0022-1694(78)90017-3

D'iya, S. G., Gasim, M. B., Toriman, M. E., & Abdullahi, M. G. (2014). Floods in Malaysia: Historical reviews, causes, effects and mitigations approach. *International Journal of Interdisciplinary Research and Innovations*, *2*(4), 59–65. https://www.researchpublish.com/upload/book/FLOODS%20IN%20MALAYSIA-760.pdf

Dong, X., Jiang, L., Zeng, S. H., Guo, R., & Zeng, Y. (2020). Vulnerability of urban water infrastructures to climate change at city level. *Resources, Conservation and Recycling*, *161*, 104918. https://doi.org/10.1016/j.resconrec.2020.104918

Duskayev, K., Mussina, A., Rodrigo-Ilarri, J., Zhanabayeva, Z., Tursyngali, M., & Rodrigo-Clavero, M. E. (2023). Study of temporal changes in the hydrographic network of small mountain rivers in the Ile Alatau, Kazakhstan. *Hydrology Research*, *54*(11), 1420–1431. https://doi.org/10.2166/nh.2023.305

Gentilucci, M., Rossi, A., Pelagagge, N., Aringoli, D., Barbieri, M., & Pambianchi, G. (2023). GEV analysis of extreme rainfall: Comparing different time intervals to analyse model response in terms of return levels in the study area of central Italy. *Sustainability*, *15*(15), 11656. https://doi.org/10.3390/su151511656

Hazen, A. (1914). Storage to be provided in impounding reservoirs for municipal water supply. *Transactions of the American Society of Civil Engineers*, *77*(1), 1539–1640. https://doi.org/10.1061/taceat.0002563

Jayawardane, J. M. P. M., Rajapakse, R. L. H. L., & Siriwardana, C. S. A. (2024). Urban flood assessment targeting flood risk mitigation: A case study focusing on changing environments. In H. R. Pasindu, H. Damruwan, P. Weerasinghe, L. Fernando & C. Rajapakse (Eds.),

Proceedings of Civil Engineering Research Symposium 2024 (pp. 13–14). Department of Civil Engineering, University of Moratuwa. https://doi.org/10.31705/CERS.2024.7

Katz, R. W., Parlange, M. B., & Naveau, P. (2002). Statistics of extremes in hydrology. *Advances in Water Resources*, *25*(8–12), 1287–1304. https://doi.org/10.1016/S0309-1708(02)00056-8

Kreienkamp, F., Philip, S. Y., Tradowsky, J. S., Kew, S. F., Lorenz, P., Arrighi, J., Belleflamme, A., Bettmann, T., Caluwaerts, S., Chan, S. C., Ciavarella, A., De Cruz, L., Demuth, N., Ferrone, A., Fischer, E. M., Fowler, H. J., Goergen, K., Heinrich, D., Henrichs, Y., … Wanders, N. (2021). *Rapid attribution of heavy rainfall events leading to the severe flooding in Western Europe during July 2021*. World Weather Attribution Project. https://www.worldweatherattribution.org/wp-content/uploads/Scientific-report-Western-Europe-floods-2021-attribution.pdf

Kundzewicz, Z. W., Kanae, S., Seneviratne, S. I., Handmer, J., Nicholls, N., Peduzzi, P., Mechler, R., Bouwer, L. M., Arnell, N., Mach, K., Muir-Wood, R., Brakenridge, G. R., Kron, W., Benito, G., Honda, Y., Takahashi, K., & Sherstyukov, B. (2013). Flood risk and climate change: Global and regional perspectives. *Hydrological Sciences Journal*, *59*(1), 1–28. https://doi.org/10.1080/02626667.2013.857411

Kyrgyzbay, K., Kakimzhanov, Y., & Sagin, J. (2023). Climate data verification for assessing climate change in the Almaty region of the Republic of Kazakhstan. *Climate Services*, *32*, 100423. https://doi.org/10.1016/j.cliser.2023.100423

Latif, M., Syed, F. S., & Hannachi, A. (2017). Rainfall trends in the South Asian summer monsoon and its related large-scale dynamics with focus over Pakistan. *Climate Dynamics*, *48*(11), 3565–3581. https://doi.org/10.1007/s00382-016-3284-3

Ling, Z., Jing, Y., Aqeel, M., Siddiqa, F., Yan, L., & Wenlong, M. (2025). Urban Flood Modeling and Mitigation Strategies Using Remote Sensing and GIS. Scholars *Journal of Engineering and Technology*, *13*(7), 535–551. https://doi.org/10.36347/sjet.2025.v13i07.007

Mirlas, V., Zhakyp, A., Auelkhan, Y., & Anker, Y. (2024). Assessment of urbanization-related groundwater flooding process via Visual MODFLOW modeling: A case study for the northern part of Almaty city, Kazakhstan. *Journal of Flood Risk Management*, *18*(1), e13029. https://doi.org/10.1111/jfr3.13029

MontesPajuelo, R., RodríguezPérez, Á. M., López, R., & Rodríguez, C. A. (2024). Analysis of probability distributions for modelling extreme rainfall events and detecting climate change: Insights from Mathematical and Statistical Methods. *Mathematics*, *12*(7), *1093.* https://doi.org/10.3390/math12071093

Muhammad Iskandar, M. F., Ibrahim, A., Mohtar, Z. A., Pakir Mohamed Latif, M. F., & EM Yahaya, N. K. (2025). Assessing rainfall trends and variability in a climate change. *ESTEEM Academic Journal*, *21*, 91–105. https://doi.org/10.24191/esteem.v21iMarch.4892.g3087

Nakispekova, A. (2024). *Kazakhstan unites in response to flood crisis*. The Astana Times. Bringing Kazakhstan to the World. https://astanatimes.com/2024/04/kazakhstan-unites-in-response-to-flood-crisis/

Pietras, B., & Pyrc, R. (2025). Extreme short-duration rainfall and urban flood hazard: Case studies of convective events in Warsaw and Zamość, Poland. *Water*, *17*(18), 2671. https://doi.org/10.3390/w17182671

Republic State Enterprise Kazhydromet. (2025, October 2). *Weather forecast.* https://www.kazhydromet.kz/ru/

Rima, L., Haddad, K., & Rahman, A. (2025). Generalised Additive Model-Based Regional Flood Frequency Analysis: Parameter Regression Technique Using Generalised Extreme Value Distribution. *Water*, *17*(2), 206. https://doi.org/10.3390/w17020206

Stedinger, J. R., Vogel, R. M., & Foufoula-Georgiou, E. (1993). Frequency analysis of extreme events. In D. R. Maidment (Ed.), *Handbook of Hydrology* (pp. 18.1–18.66). McGraw-Hill.

Tukey, J. W. (1962). The future of data analysis. In *Breakthroughs in Statistics: Methodology and Distribution* (pp. 408–452). Springer. https://doi.org/10.1007/978-1-4612-4380-9_31

Weibull, W. (1939). *A statistical theory of the strength of materials.* Generalstabens Litografiska Anstalts Förlag.

Wilks, D. S. (Ed.) (2011). *Statistical methods in the atmospheric sciences*. Academic Press.

World Meteorological Organization [WMO]. (1989). *Calculation of Monthly and Annual 30-year Standard Normals (WMO/TD-No. 341)*. World Meteorological Organization. https://posmet.ufv.br/wp-content/uploads/2017/04/MET-481-WMO-341.pdf

World Meteorological Organization [WMO]. (2009). *Manual on estimation of Probable Maximum Precipitation (PMP).* World Meteorological Organization. https://library.wmo.int/records/item/35708-manual-on-estimation-of-probable-maximum-precipitation-pmp?offset=2

World Meteorological Organization [WMO]. (2017). *WMO Guidelines on the Calculation of Climate Normals (WMO-No. 1203).* World Meteorological Organization. https://www.agroorbi.pt/livroagrometeorologia/DocsProg/Temas&Exerc%C3%ADciosExtraPorCap%C3%ADtulo/Cap1_Introdu%C3%A7%C3%A3o/Docs/WMO%20Guidelines%20on%20the%20Calculation%20of%20Climate%20Normals_en.pdf

Summary

Probabilistic assessment of annual maximum precipitation in Almaty, Kazakhstan. Accurate selection of a best-fit probability distribution function for rainfall data is crucial in hydrological studies and plays a fundamental role in the planning and design of infrastructure for the city of Almaty. This study presents a comprehensive statistical and probabilistic assessment of extreme precipitation in the city of Almaty, Kazakhstan, based on annual maximum precipitation data from five meteorological stations for the period 2000–2023. Given the complex mountainous terrain and distinct seasonal precipitation regimes, selecting an appropriate distribution is particularly critical for modeling design rainfall and flood risks. The reliability of the rainfall data was verified through tests for independence and stationarity. Five theoretical probability distributions – exponential, generalized extreme value, normal, lognormal, and gamma – were evaluated using the maximum likelihood estimation method. The best-fit distribution was determined using the chi-square goodness-of-fit test. The results indicate that the generalized extreme value distribution provides the best fit for most stations, followed by the lognormal and gamma

distributions, confirming its robustness in representing extreme precipitation in mountainous urban environments such as Almaty. Furthermore, spatial variability and increasing intensity of extreme rainfall events were observed, especially during the warm season. Design rainfall estimates were calculated for various exceedance probabilities (e.g., 1%, 2%, and 10%), corresponding to return periods of 100, 50, and 10 years, respectively. These findings are critical for flood risk assessment and the development of climate-resilient urban drainage systems, highlighting the broader applicability of this distribution-fitting methodology in regions exposed to hydrological extremes.

Scientific Review Engineering and Environmental Sciences (2026), 35 (1), 40–56

Sci. Rev. Eng. Env. Sci. (2026), 35 (1) https://srees.sggw.edu.pl

ISSN 1732-9353 (suspended) eISSN 2543-7496 DOI 10.22630/srees.10905

Received: 29.10.2025
Accepted: 28.01.2026

Putu SARI✉
Mohamad ANSORI
Noor Endah MOCHTAR
Laode VIZENTHE
Amanda ANNIDA
Anggoro ATMOJO
Institute Teknologi Sepuluh Nopember, Department of Civil Engineering, Indonesia

Evaluating the effectiveness of foam mortar as a lightweight fill for reducing foundation settlement on soft soils: a case study of Indonesian toll road projects

Keywords: foam mortar, lightweight fill, settlement reduction, slope stability, soft soil, ground improvement

Introduction

The issue of subsoil consolidation beneath road embankments is a primary constraint in the development of toll road infrastructure in Indonesia. The completion of consolidation is necessary before the road becomes operational to prevent premature damage to the overlying pavement structure. However, the natural consolidation process requires significant time, which often conflicts with tight project completion schedules. The need to operationalize toll roads rapidly is urgent,

✉tantrigeoteknik@gmail.com

driven by the focus on enhancing connectivity and economic considerations for investors. Consequently, several methods to accelerate soil consolidation continue to be developed. Conventional methods such as prefabricated vertical drains (PVD), sand drains, and stabilization using piles have been the cornerstone solutions. However, the application often faces the major constraint of high cost, specifically because toll road sections can extend for thousands of kilometers.

The need for a more economical alternative has led to the widespread adoption of a strategy to minimize compression magnitude by reducing embankment load. This strategy requires replacing conventional fill material with a unit weight above 18 $kN \cdot m^{-3}$ using lightweight fill. The significantly lower unit weight of the material can substantially reduce the vertical pressure on the subsoil and shorten both the duration and magnitude of settlement.

Previous studies have reported on the effectiveness of different lightweight materials. For example, Zaika et al. (2023) used expanded polystyrene (EPS) beads mixed with cement (geo-beads) – a product with a very low bulk density (10.08 $kg \cdot m^{-3}$). The application of finite element method analysis showed that the material reduced settlement by 1.8–1.9 m in clayey silt soil. Abbasi et al. (2024) also evaluated several ground improvement methods and found that lightweight foamed concrete (LWFC) was the most effective, reducing settlement by 35% due to its low density (6 $kN \cdot m^{-3}$) and high stiffness. Similar results were reported by several other studies (Marradi et al., 2012; Hao et al., 2024; Dou et al., 2025).

Innovation has led to the use of recycled materials, such as the compaction of waste tires into bales or cuboidal blocks of compressed whole tires to produce embankment material (Duda & Siwowski, 2022). The material offers advantages such as very low density (about 5 $kN \cdot m^{-3}$), high permeability, and sustainability. The results also showed that the tire bales reduced settlement by 28–33% compared to sand-filled embankments and improved slope stability in silty clay. Similarly, Ratha et al. (2018) investigated lightweight technologies and the so-called masonry arch bridge concept to reduce settlement in soft soils and to assess their environmental impact.

Several recent studies further strengthened the evidence, as observed in the report of Buathong et al. (2025), that the settlement in a conventional embankment was approximately 13.1 times greater than in a lightweight embankment on soft Bangkok clay. Ali et al. (2025) also showed that EPS particles predominantly govern the deformation process in silt-EPS mixtures by accounting for 55% to 80%. Moreover, Brouwer and Laerhoven (2024) proposed using foam glass as a lightweight fill for soft soil conditions, and initial field and laboratory results showed promising potential.

Most of these studies focus on new materials and laboratory-scale modelling, while field applications remain limited. In Indonesia, the Ministry of Public Works and Housing (PUPR) has issued a special specification for foam mortar material with a maximum dry density of 8 $kN \cdot m^{-3}$ as an embankment replacement. This is necessary to provide a regulatory foundation for the application in national road projects. This research on the use of lightweight materials was conducted not only to address settlement issues but also to consider slope stability, given that landslides have occurred in several sections of toll roads in Indonesia, both on embankments (Sari & Mochtar, 2023) and in cutting slopes (Sari et al., 2022).

Specifications are available in Indonesia, but the understanding of the performance of this material in relation to the diverse geotechnical conditions of the country requires in-depth investigation. Lastiasih and Mochtar (2022) provided initial insight by modeling two toll road sections and showed that the combination of 75% foam mortar and 25% granular soil could reduce settlement by a factor of 0.6 and increase the slope safety factor (*SF*) by 1.46 compared to a conventional embankment. However, the study was limited to soft soil at a depth of 12 m. A similar study on the use of foam mortar to analyze subsoil compression with several variations was also conducted by Efendi (2023), Jusi et al. (2024), and Jusi et al. (2025). However, that study also had certain limitations specific to its respective case study condition.

Field conditions, such as those on the Java, are highly variable in reality, both in terms of soft soil depth and embankment height. The impact of secondary consolidation settlement has also often not been adequately considered in existing studies. Therefore, this study aims to analyze the effectiveness of using foam mortar to reduce both primary and secondary settlement and enhance slope stability across three scenarios with variations in embankment height and soft soil depth in order to fill the identified gap. Another aim is to provide numerically simulated design recommendations for the application of foam mortar under specific geotechnical conditions in Indonesia for three study locations. These include Semarang–Demak 1A Sta 8+314–Sta 8+494, 1B Sta 2+850–Sta 3+010, Kediri–Kertosono (Sta 18+600–Sta 20+300), and Probolinggo–Banyuwangi Sta 45+300–Sta 46+000 sections.

The construction of toll roads on soft soil in Indonesia is associated with significant geotechnical challenges, which primarily focus on excessive and long-lasting settlement. Therefore, this study aims to evaluate the effectiveness of foam mortar as a lightweight fill to mitigate these issues across three distinct toll road projects, including Probolinggo–Banyuwangi, Kediri–Kertosono, and Semarang–Demak. The method used was comprehensive numerical analysis

with a focus on assessing the magnitude and rate of subsoil compression as well as slope stability under different scenarios of varying embankment heights, soft soil depths, and soil improvement strategies, including PVD and replacement. The results consistently showed that incorporating foam mortar significantly reduced settlement. An increase in foam mortar percentage in the embankment also led to a substantial decrease in compression magnitude. The optimal performance was observed at a mix of 75% foam mortar and 25% soil for high embankments. Furthermore, this study provided customized, efficient design solutions for each site. The trend shows that foam mortar is a viable and cost-effective alternative to conventional methods. This is because the application enhances slope stability and ensures compliance with stringent settlement rate criteria to offer a practical solution for infrastructure development on compressible soils.

Material and methods

This study analyzes the effect of lightweight fill on subsoil compression by accounting for both primary and secondary consolidation. Analyzing secondary settlement is crucial in this study, considering that several previous studies have demonstrated its influence on the stability of overlying road embankments (Chow et al., 2019; Aryandi et al., 2025). The research methodology is outlined in the accompanying flowchart (Fig. 1).

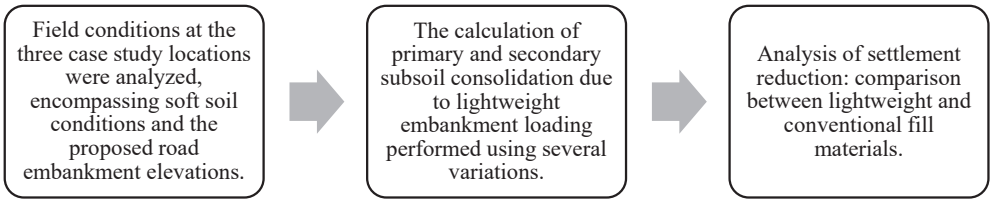

FIGURE 1. Research method
Source: own work.

The magnitude of secondary consolidation was determined and calculated using the method developed by Dhianty and Mochtar (2018). The occurrence of secondary consolidation over a relatively long period motivated Dhianty and Mochtar (2018) to recommend preloading before the operational period. This is required to eliminate the secondary consolidation (S_s) by applying a surcharge load (Δq). The magnitude of the surcharge is designed to induce an amount of settlement

equivalent to the expected secondary consolidation in addition to the primary consolidation (S_c).

The surcharge can be removed at the completion of the primary consolidation period. The completion of soil improvement through preloading stops further settlement from either primary or secondary consolidation. The determination of the magnitude of Δq and the initial embankment height (H_{init}) required to account for both S_c and S_s, presented as $H_{\text{init(p+s)}}$, requires calculating S_c, S_s, and S_c plus S_s for several iterations of load (q). The H_{init} needed to eliminate only primary consolidation is subsequently determined for all load iterations. The calculations can be used to generate the curves of H_{init} versus q_{fin} and H_{fin} versus H_{init}.

The extra surcharge load (Δq) required to eliminate S_s is further determined as follows. The Δq is removed after the soil improvement process is complete. The $H_{\text{init(p+s)}}$ represents the required initial embankment height to eliminate both primary and secondary consolidation. Therefore, it can be plotted on the curve to determine the corresponding final embankment height after settlement from both consolidation types has occurred, presented as $H_{\text{fin(p+s)}}$.

The removal of Δq from the embankment upon completion of preloading ensures the actual final embankment height in the field is less than $H_{\text{fin(p+s)}}$. The repetition of the process for all load (q) iterations leads to the generation of $H_{\text{fin(p+s)}}$ versus final embankment height ($H_{\text{fin-field}}$) and $H_{\text{init(p+s)}}$ versus $H_{\text{fin-field}}$ curves to determine $H_{\text{init(p+s)}}$ needed to eliminate both primary and secondary consolidation for any specified $H_{\text{fin-field}}$.

Several technical specifications are required for producing foam mortar, particularly regarding the cement, sand, foaming agent, and water. The parameters of common borrow material for embankment, foam mortar material, and subgrade soil are shown in Table 1.

TABLE 1. The parameters of common borrow material for embankment, foam mortar, and subgrade soil

Parameter	Common borrow material	Foam mortar	Soil subgrade
Bulk unit weight (γ) [kN·m^{-3}]	18	8	It varies in consistency from very soft to soft clay at depth, depending on the study location.
Undrained shear strength (C_u) [kN·m^{-2}]	0	0	
Internal friction angle (Φ) [°]	30	40	

Source: own work.

The lightweight embankment material was specifically designed to replace conventional soil embankments with the primary purpose of reducing the load on the supporting subsoil. This is particularly beneficial for construction on soft soil, where excessive settlement is a concern. Several key parameters lead to reduced settlement at very low density, with a maximum planned dry density of 8 kN·m^{-3}. This is significantly lighter than traditional compacted soil fills and drastically reduces the vertical stress, or overburden pressure, imposed on weak, compressible subsoils, thereby minimizing settlement. The second is the specified compressive strength (*UCS*) because the material provides structural integrity to the embankment. The two strength grades are specified as *UCS* ≥ 800 kPa (800 kN·m^{-2}) for lower foundation layers or general embankment fill, and *UCS* ≥ 2,000 kPa (2,000 kN·m^{-2}) for the main foundation layer. This ensures the embankment is stable and can distribute loads effectively without excessive internal deformation.

Case study area

The case study for geofoam application was conducted at three locations with different ground and site conditions. These locations include the Probolinggo–Banyuwangi Freeway Section Sta 45+300–Sta 46+000 (Fig. 2), the Kediri–Kertosono Freeway Section Sta 18+600–Sta 20+300 (Fig. 3), and the Semarang–Demak Freeway (Fig. 4), which comprises Section 1A (Sta 8+314–Sta 8+494) and Section 1B (Sta 2+850–Sta 3+010). The locations have different subsoil conditions and designed embankment heights, which result in the application of varying geofoam treatment methods. The focus on applying lightweight material across the three locations and conditions is based on a unified objective: reducing the impact of soil compression and enhancing the stability of the high embankments. Indonesian regulations stipulate that the rate of settlement in subsoils cannot exceed 2 cm per year. This requirement is in place to prevent cracking in the road pavement, which can pose dangers to freeway users.

The Kediri–Kertosono Toll Road, represents the second analyzed location. While this toll road is essential, it also poses a challenge for the Kediri watersheds, which are affected by its construction (Ansori et al., 2025). The section between

Sari, P., Ansori, M., Mochtar, N. E., Vizenthe, L., Annida, A., Atmojo, A. (2026). Evaluating the effectiveness of foam mortar as a lightweight fill for reducing foundation settlement on soft soils: a case study of Indonesian toll road projects. *Sci. Rev. Eng. Env. Sci.*, *35* (1), 40–56. DOI 10.22630/srees.10905

FIGURE 2. Probolinggo–Banyuwangi Toll Road project location – Section Sta 45+300– Sta 46+000
Source: own work based on Google Earth orthophoto.

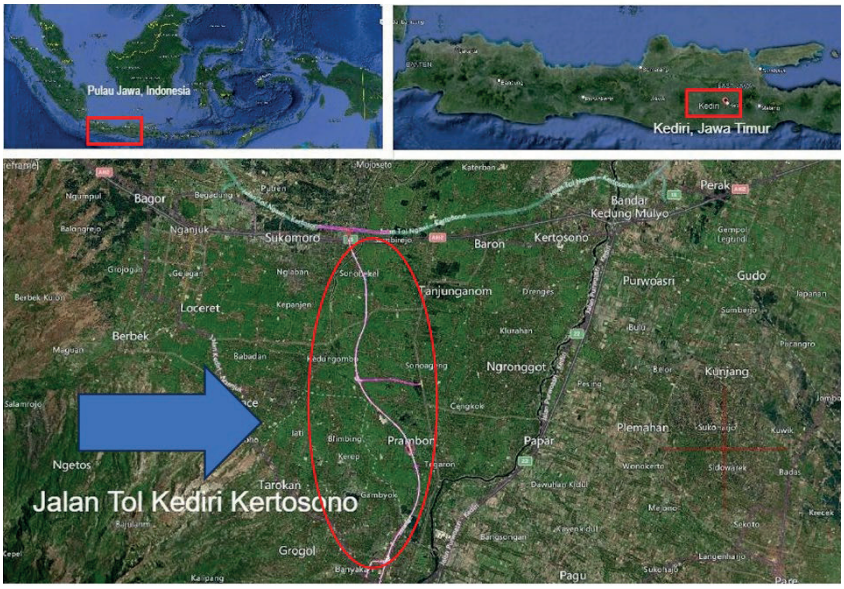

FIGURE 3. Studied the location of Kediri–Kertosono Toll Road
Source: project report.

Sta 16+900 and Sta 20+300 traverses low-lying ground and is consequently planned to be constructed on an embankment with fill height varying from 4 m to 10 m. The subsoil condition consists of soft soil with an *N*-value of the standard penetration test of less than 10, and the thickness varies from 5 m to 9 m. The description shows that the design planned in this study requires embankment construction using two methods, including the replacement of subsoil material combined with preloading, as well as the use of conventional fill soil with foam mortar. The subsoil conditions with a soft soil thickness of up to 5 m, as observed in Sta 16+900–Sta 18+600, require subsoil replacement with preloading and without PVD. The replacement depth is expected to range from 2 m to 3 m. Meanwhile, a soft soil thickness of up to 9 m, as observed in Sta 18+600–Sta 20+300, requires a combination of conventional fill soil and foam mortar.

FIGURE 4. Studied the location of Semarang–Demak Toll Road
Source: project report.

Sari, P., Ansori, M., Mochtar, N. E., Vizenthe, L., Annida, A., Atmojo, A. (2026). Evaluating the effectiveness of foam mortar as a lightweight fill for reducing foundation settlement on soft soils: a case study of Indonesian toll road projects. *Sci. Rev. Eng. Env. Sci.*, *35* (1), 40–56. DOI 10.22630/srees.10905

The Semarang–Demak Toll Road, represents the third analyzed location. Section 1A, with a total length of 2.08 km, was constructed over swamps and ponds, while Section 1B extends for 6.4 km and is located over the Java Sea. The primary challenge in the construction process is that the embankment must be placed on deep, soft subsoil extending to 25 m. The research at this location is specifically focused on locations above very high embankments, namely 10.3 m, using 100% foam mortar as a substitute for ordinary embankment materials.

Results and discussion

The focus on using lightweight material in the form of foam mortar in the Probolinggo–Banyuwangi Toll Road project represents the first location analyzed in this study, addressing three main aspects. These included the magnitude of subsoil compression, the rate of subsoil compression, and slope stability under different embankment conditions. The magnitude of subsoil compression results showed that subsoil compression increased proportionally with the thickness of the compressible soil layer. For example, the compression occurring in an eight-meter-thick soil layer using the PVD method was greater than in a six-meter-thick layer. An identical trend was observed for the replacement method, where compression under a six-meter thickness was greater than under a four-meter thickness. This comparison was conducted using an identical percentage of foam mortar. A total of five variations of foam mortar percentage were used. The results showed that an increase in the foam mortar percentage in the embankment material significantly reduced the magnitude of compression. This trend occurred consistently across all tested variations for both PVD and replacement methods, as well as all thicknesses of the soft soil layer. The comparison of the two methods with the same foam mortar percentage showed that the compression from PVD was generally greater than the replacement (Fig. 5). This direct comparison was particularly evident in the six-meter-thick soil layer.

The subsoil compression rate results showed that the planned rate of embankment compression using both PVD and replacement methods (Fig. 6) generally met the specifications set by the Directorate General of Highways. An exception was found for the embankment over a six-meter-thick soft soil layer, where the rate failed from the second year to the third year, and the deficiency continued up to the twelfth year despite implementing a three-meter-thick replacement. This showed that the replacement method was recommended for the six-meter-thick soil layer due to the failure to satisfy the required compression rate criteria.

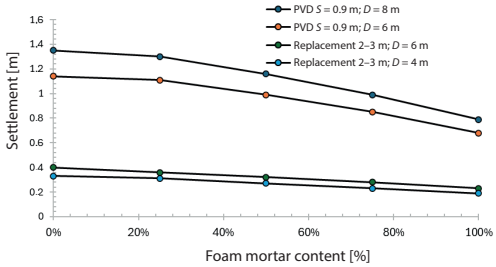

FIGURE 5. Comparison of the effect of foam mortar percentage on settlement for two improvement methods

Source: own work.

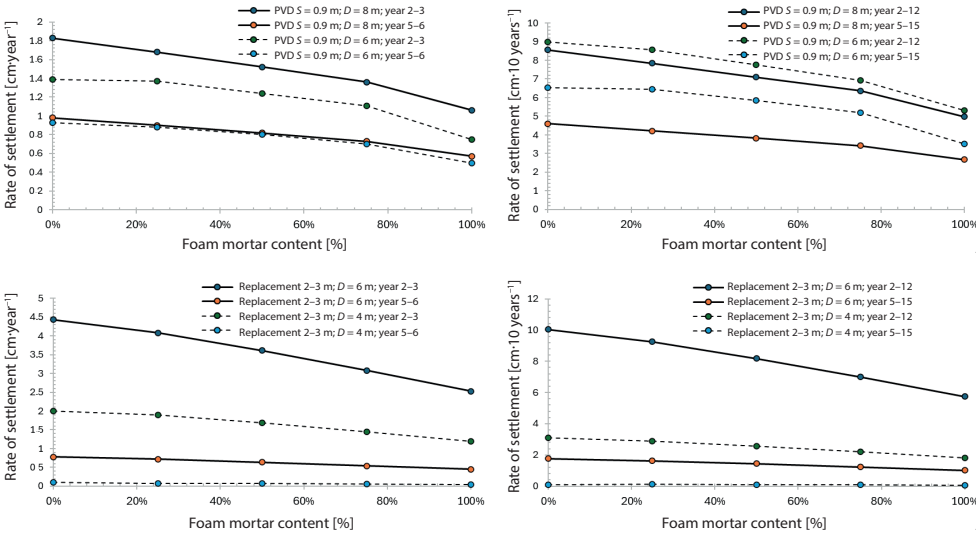

FIGURE 6. Effect of foam mortar percentage on rate of settlement for each ground improvement method for the Probolinggo–Banyuwangi Toll Road

Source: own work.

Slope stability results showed that several embankment conditions had *SF* values below 1.5. Although slope failures manifest in three dimensions, a two-dimensional analysis was employed for this study. This decision is supported by the work of Sari et al. (2020) and Sari et al. (2022), in which the amount of reinforcement required shows little variation between 2D and 3D analyses, even though the latter is substantially more labor-intensive. This reflected that the embankment did not meet safety standards and required reinforcement. The conditions were identified based on several scenarios, including embankments composed of 100% soil, 25% and 50% foam mortar mixtures, placed over six- and eight-meter-thick soft soil

Sari, P., Ansori, M., Mochtar, N. E., Vizenthe, L., Annida, A., Atmojo, A. (2026). Evaluating the effectiveness of foam mortar as a lightweight fill for reducing foundation settlement on soft soils: a case study of Indonesian toll road projects. *Sci. Rev. Eng. Env. Sci.*, *35* (1), 40–56. DOI 10.22630/srees.10905

layers, and a 100% soil embankment constructed using the replacement method on a four-meter-thick soft soil layer. The low *SF* values obtained under these conditions indicate the need to implement soil reinforcement methods to ensure embankment stability, as illustrated in Figure 7.

The significant compression observed at Section Sta 18+600–Sta 20+300 of the Kediri–Kertosono Toll Road represents the second location analyzed in this study, where the design of a composite embankment using soil and a lightweight material, in the form of foam mortar, was required. Two mix variations were considered, consisting of 50% embankment soil plus 50% foam mortar and 25% embankment soil plus 75% foam mortar. The recapitulation of the primary and secondary subsoil compression magnitudes for the different foam mortar percentages and varying embankment heights is presented in Figure 8.

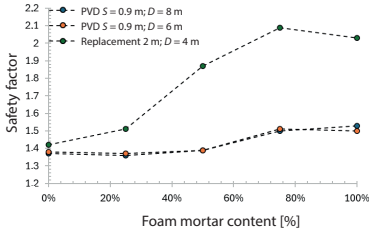

FIGURE 7. Safety factor of slope for two improvement methods with varying foam mortar percentage for the Kediri–Kertosono Toll Road

Source: own work.

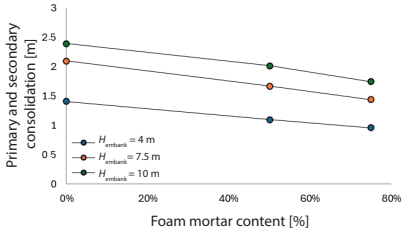

FIGURE 8. Primary and secondary consolidation of soil with various percentages of foam mortar and embankment heights (H_{embank}) for the Kediri–Kertosono Toll Road

Source: own work.

The analysis of subsoil compression beneath the embankment considered the rate of consolidation for both the untreated subsoil and that improved with PVD. The rate of settlement (*RoS*) was calculated by considering the compression per annum measured at periods of 2–3 years and 5–6 years after construction. Additional calculations were performed for decadal settlement covering the periods

of 2–12 years and 5–15 years post-construction. The recapitulation of *RoS* for different scenarios is presented in Figure 9 without PVD and Figure 10 with PVD.

The initial design of soil-foam mortar composite embankment failed to meet the requirements of the geotechnical guideline Pt T-8-2002-B (Departemen Permukiman dan Prasarana Wilayah, 2002). Consequently, a subsoil improvement method was adopted through PVD. The most efficient embankment design for all height variations at Section Sta 16+900–Sta 18+600 was determined to be a standard soil without any subsoil replacement. For Section Sta 18+600–Sta 20+300. The most efficient design varied according to the embankment height. For an embankment height of 4 m, the most effective solution was a soil embankment preloaded and improved with PVD. When the height increased to 7.5 m, the most efficient configuration changed to a composite embankment consisting of 50% soil and 50% foam mortar. At a height of 10.5 m, the optimal design shifted again, favoring a composite embankment with 75% foam mortar and 25% soil, which performed best under higher loads.

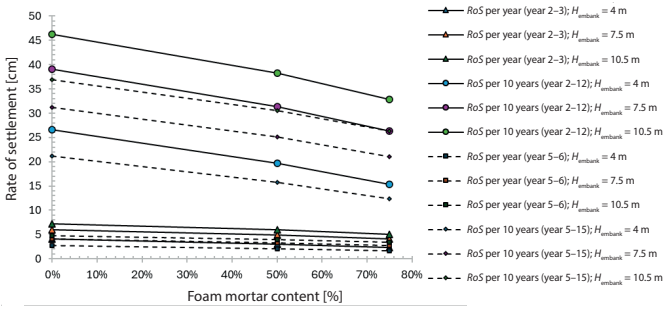

FIGURE 9. Effect of foam mortar content on settlement rate under different embankment loads (pre-PVD condition) for the Semarang–Demak Toll Road

Source: own work.

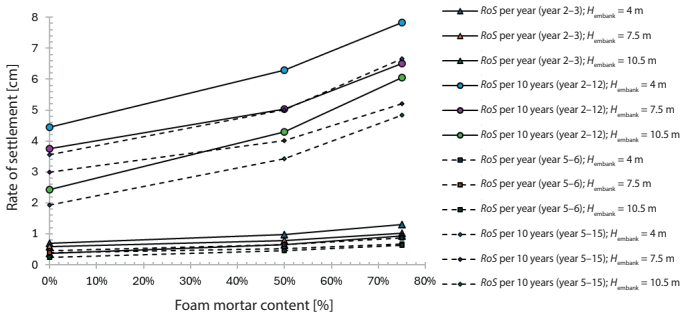

FIGURE 10. Effect of foam mortar content on settlement rate under different embankment loads (post-PVD condition) for the Semarang–Demak Toll Road

Source: own work.

Sari, P., Ansori, M., Mochtar, N. E., Vizenthe, L., Annida, A., Atmojo, A. (2026). Evaluating the effectiveness of foam mortar as a lightweight fill for reducing foundation settlement on soft soils: a case study of Indonesian toll road projects. *Sci. Rev. Eng. Env. Sci.*, *35* (1), 40–56. DOI 10.22630/srees.10905

The analysis and calculations yielded several inferences regarding the alternative design of the foam mortar light embankment for Section 1A (Sta 8+314–Sta 8+494) of the Semarang–Demak Toll Road, the third location analyzed in this study. The same was also observed for the evaluation of existing soil improvement and reinforcement designs and its steeper slope alternative for Section 1B (Sta 2+850–Sta 3+010). The light embankment foam mortar designed in Section 1A had an initial height of 12.2 m of which 1.5 m was uncompacted selected borrow material placed at the bottommost layer, 10.3 m was foam mortar in the middle, and 0.4 m was the height of the extra load placed at the top composed of compacted borrow material. Therefore, the H_{fin} of 10.3 m was maintained and composed of 100% of foam mortar after settlement and removal of the extra load at the completion of preloading. A total of 13 ϕ400 concrete micropiles with a length (L) of 14 m were used per side as reinforcements for the foam mortar light embankment. The assumption of the existing design that S_c was equal to 30% H_{fin} was found to be inaccurate and smaller by roughly 0.88 m than the calculated settlement for Zone J. It was also observed that the existing PVD design with a rectangular pattern and 1 m spacing in Section 1B could not reach consolidation of 95% at the completion of the effective age of 6 months. The situation led to improvements and corrections in the preloading and PVD design. Moreover, the existing 16 clusters of bamboo pile reinforcements for Section 1B could not assist in achieving the required slope stability at *SF* of 1.50, which led to the design of additional geotextile reinforcement and an embankment with a slope of 1 : 2 using uniaxial UW-30HL in both cases.

Conclusions

In conclusion, this study showed that using foam mortar as a lightweight embankment fill was highly effective for addressing the challenges of constructing toll roads on soft, compressible soils in Indonesia. The key results from the three case studies led to the following consolidated inferences:

– Significant settlement reduction: The incorporation of foam mortar directly and substantially reduced both the magnitude and rate of subsoil compression. The reduction in embankment load due to the low density of foam mortar was the primary mechanism, with higher foam mortar percentages producing greater settlement control.

– Enhanced slope stability: foam mortar embankments with a specific focus on those at higher mix ratios, such as 75%, improved slope stability with higher *SF* compared with conventional soil embankments by reducing the need for extensive reinforcement in several scenarios.
– Site-specific design optimization: The most efficient design was highly dependent on local conditions with a specific focus on embankment height and soft soil thickness. This was observed in several cases, including the Kediri–Kertosono route, where the optimal design transitioned from a soil embankment with PVD for a four-meter height to a 50/50 soil–foam mortar mix for 7.5 m and a 75% foam mortar mix for 10.5 m. In the Probolinggo–Banyuwangi section, the replacement method was considered unsuitable for six-meter-thick soft clay, whereas combinations of PVD and foam mortar proved effective. For the Semarang–Demak project, a 100% foam mortar embankment with micropile reinforcement was designed as a viable alternative to address construction difficulties in extremely soft soil conditions.
– Practical and economic viability: Foam mortar presented a practical and often more cost-efficient alternative to conventional ground improvement methods such as deep PVD installation or extensive soil replacement. It offered a sustainable solution by reducing embankment load at the source, thereby accelerating consolidation and minimizing long-term maintenance.

Foam mortar was a proven, versatile, and efficient material for embankment construction on soft soils. The results provided a strong technical foundation and specific design recommendations for its application in future Indonesian infrastructure projects, ensuring both structural performance and economic efficiency. Future research is critically needed to conduct real-time monitoring of foam mortar embankments under actual operational conditions. This would validate numerical predictions and assess long-term durability, settlement behavior, and environmental impacts.

Acknowledgements

The authors would like to express their deepest gratitude to Institut Teknologi Sepuluh Nopember (ITS) for the generous support and funding through the “Student Final Project Upgrading Research Grant” program in 2025. This research would not have been possible without the financial and facility assistance provided by the institution.

References

Abbasi, S. J., Weng, X., & Iqbal, M. J. (2024). Numerical analysis of differential settlement in road due to widening considering different reinforcement techniques. *Applied Sciences*, *14*(5), 1740. https://doi.org/10.3390/app14051740

Ali, S., Yong, F., Mehmood, M., Nie, W., & Jamil, F. (2025). Investigating the deformation characteristics of silt-lightweight soil with various sizes of expanded polystyrene beads. *International Journal of Geosynthetics and Ground Engineering*, *11*(4), 1–12. https://doi.org/10.1007/s40891-025-00643-w

Ansori, M. B., Lasminto, U., Jbs, I. D. B., & Sari, P. T. K. (2025). Flood modeling and inundation mapping using the HEC-RAS 2D hydrodynamic model with a meteorological rain-on-grid approach: A case study of the Banyakan Area, Kediri Regency. *IOP Conference Series: Earth and Environmental Science*, *1551*(1), 012034. https://doi.org/10.1088/1755-1315/1551/1/012034

Aryandi, S. K., Mochtar, I. B., Endah, N., & Artanto, A. A. (2025). Design of toll road embankment with secondary compression mitigation after PVD installation and solutions for The Probolinggo–Banyuwangi Toll Road Construction Project Package 2 Sta 16+300 – Sta 16+700. *Journal of Infrastructure and Facility Asset Management*, *7*(1), 57–74.

Brouwer, J. W. R., & Laerhoven, C. R. van (2024). The use of foam glass for a lightweight fill and highway foundation on soft soil conditions. In *Geotechnical engineering challenges to meet current and emerging needs of society* (pp. 2127–2131). CRC Press. https://doi.org/10.1201/9781003431749-402

Buathong, P., Jongpradist, P., & Jamsawang, P. (2025). Performance evaluation of lightweight clay-air foam embankment on soft Bangkok clay: A full-scale test and 3D numerical analysis. *Results in Engineering*, *27*, 105793. https://doi.org/10.1016/j.rineng.2025.105793

Chow, L. C., Bentler, J. G., & Lamb, R. A. (2019). Primary and post-surcharge secondary settlements of a highway embankment constructed over highly organic soils: a case history. In *Eighth International Conference on Case Histories in Geotechnical Engineering* (pp. 109–118). American Society of Civil Engineers. https://doi.org/10.1061/9780784482070.011

Departemen Permukiman dan Prasarana Wilayah (2002). *Panduan Geoteknik 1: Proses Pembentukan dan Sifat-Safat Dasar Tanah Lunak* (Pt T-8-2002-B). https://binamarga.pu.go.id/uploads/files/1744/preview_1744-1-5.pdf

Dhianty, E., & Mochtar, I. B. (2018). Method of removing secondary compression on clay using preloading. *MATEC Web of Conferences*, *195*, 03006. https://doi.org/10.1051/matecconf/201819503006

Dou, H., Xu, B., Li, F., Li, Y., Liu, H., & Zu, F. (2025). Research and application of fiber-reinforced EPS particle lightweight soil in highway engineering in cold regions. *Scientific Reports*, *15*(1), 25264. https://doi.org/10.1038/s41598-025-10866-6

Duda, A., & Siwowski, T. W. (2022). Stability and settlement analysis of a lightweight embankment filled with waste tyre bales over soft ground. *Transportation Infrastructure Geotechnology*, *9*(4), 467–491. https://doi.org/10.1007/s40515-021-00184-5

Efendi, A. W. (2023). The settlement behavior using replacement embankment with mortar foam and geofoam using LISA FEA. *Nusantara Civil Engineering Journal*, *2*(2), 75–89. https://doi.org/10.32487/nuce.v2i02.484

Hao, D., Miao, C., Fang, S., Wang, X., & Shu, Q. (2024). Experimental and numerical study on lightweight-foamed-concrete-filled widened embankment of high-speed railway. *Materials*, *17*(18), 4642. https://doi.org/10.3390/ma17184642

Jusi, U., Pratikso, & Maizir, H. (2024). Numerical model analysis of subgrade settlement with foam mortar reinforcement based on thickness variation. *Journal of Applied Engineering Science*, *22*(4), 810–818. https://doi.org/10.5937/jaes0-53365

Jusi, U., Pratikso, & Maizir, H. (2025). Numerical study of embankment on subgrade soft soil using foam mortar reinforcement. *AIP Conference Proceedings*, *3317*(1), 050003. https://doi.org/10.1063/5.0279554

Lastiasih, Y., & Mochtar, I. B. (2022). Comparison study of embankment filled with selected material and foamed mortar on toll road. *Indonesian Geotechnical Journal*, *1*(2), 12–26. https://doi.org/10.56144/igj.v1i2.1

Marradi, A., Pinori, U., & Betti, G. (2012). The use of lightweight materials in road embankment construction. *Procedia-Social and Behavioral Sciences*, *53*, 1000–1009. https://doi.org/10.1016/j.sbspro.2012.09.949

Sari, P. T. K., & Mochtar, I. B. (2023). Causes of landslides in road embankment with retaining wall and pile foundation: A case study of national road project in Porong-Sidoarjo, Indonesia. *International Journal on Advanced Science Engineering and Information Technology*, *13*(1), 42–48.

Sari, P. T. K., Lastiasih, Y., & Shoffiana, N. A. (2022). Comparison of safety factor and geosyntetic reinforcement requirement for slope stability using 2-D and 3-D analysis method. *Journal of Applied Engineering Science*, *20*(4), 1016–1026. https://doi.org/10.5937/jaes0-34051

Sari, P. T. K., Putri, Y. E., Savitri, Y. R., Amalia, A. R., Margini, N. F., & Nusantara, D. A. D. (2020). The comparison between 2-D and 3-D slope stability analysis based on reinforcement requirements. *International Journal on Advanced Science, Engineering and Information Technology*, *10*(5), 2082–2088. https://doi.org/10.18517/ijaseit.10.5.12815

Zaika, Y., Charisma, N., & Nursanti, L. L. M. (2023). Lightweight geo-bead fill to prevent soft ground deposit failure. *E3S Web of Conferences*, *464*, 08001. https://doi.org/10.1051/e3sconf/202346408001

Summary

Evaluating the effectiveness of foam mortar as a lightweight fill for reducing foundation settlement on soft soils: a case study of Indonesian toll road projects. Evaluating the effectiveness of foam mortar as a lightweight fill for reducing foundation settlement on soft soils: a case study of an Indonesian toll road. The construction of toll

Sari, P., Ansori, M., Mochtar, N. E., Vizenthe, L., Annida, A., Atmojo, A. (2026). Evaluating the effectiveness of foam mortar as a lightweight fill for reducing foundation settlement on soft soils: a case study of Indonesian toll road projects. *Sci. Rev. Eng. Env. Sci.*, *35* (1), 40–56. DOI 10.22630/srees.10905

roads on soft soil in Indonesia is associated with significant geotechnical challenges, primarily excessive and long-lasting settlement. Therefore, this study aims to evaluate the effectiveness of foam mortar as a lightweight fill to mitigate issues across three distinct toll road projects: Probolinggo–Banyuwangi, Kediri–Kertosono, and Semarang–Demak. The method used was comprehensive numerical analysis, focusing on assessing the magnitude and rate of subsoil compression and slope stability under different scenarios of varying embankment heights, soft soil depths, and soil improvement strategies, including prefabricated vertical drains and replacement. The results consistently showed that incorporating foam mortar significantly reduced settlement. An increase in foam mortar percentage in the embankment also led to a substantial decrease in compression magnitude. Optimal performance was observed with a mix of 75% foam mortar and 25% soil for high embankments. Furthermore, this study provided customized, efficient design solutions for each site. The trend indicates that foam mortar is a viable, cost-effective alternative to conventional methods. This is because the application enhances slope stability and ensures compliance with stringent settlement-rate criteria, offering a practical solution for infrastructure development on compressible soils.

Scientific Review Engineering and Environmental Sciences (2026), 35 (1), 57–74

Sci. Rev. Eng. Env. Sci. (2026), 35 (1) https://srees.sggw.edu.pl

ISSN 1732-9353 (suspended) eISSN 2543-7496 DOI 10.22630/srees.10987

Received: 11.12.2025
Accepted: 27.02.2026

Siti Nurlita FITRI✉
Niken Silmi SURJANDARI
Galuh CHRISMANINGWANG
Bambang SETIAWAN
Yusep Muslih PURWANA
Brillian Budi PRAKOSA
Raden Harya Dananjaya Hesti INDRABASKARA

Sebelas Maret University, UNS Geoscience Research Group, Civil Engineering Department, Indonesia

Nonlinear analysis for liquefaction simulation: implication of constitutive soil model

Keywords: liquefaction, DEEPSOIL, Lombok, Mandalika, strain

Introduction

Site-specific analysis of the response to seismic motion has been widely conducted using different methods. One of the approaches is nonlinear analysis, which provides the performance of the model through the dynamic loading and unloading process. During the process, several constitutive models are applied to produce dynamic properties, such as pore water pressure generation and strain–stress curves. Furthermore, one of the seismic event-induced liquefaction phenomena is also simulated from dynamic behavior output. The constitutive

✉sitinurlitafitri@staff.uns.ac.id

Fitri, S. N., Surjandari, N. S., Chrismaningwang, G., Setiawan, B., Purwana, Y. M., Prakosa, B. B., Indrabaskara, R. H. D. H. (2026). Nonlinear analysis for liquefaction simulation: implication of constitutive soil model. *Sci. Rev. Eng. Env. Sci.*, *35* (1), 57–74. DOI 10.22630/srees.10987

model plays a significant role because the large-strain shear strength is generally considered unrestricted, leading to overestimated shear stress as shear strains increase (Chiu et al., 2012). This condition leads to overestimation and unrealistic predictions for the dynamic simulation.

The general nonlinear analysis for generating soil response is the DEEPSOIL program. This approach is also applied to validate the centrifuge test for the sloping ground in a one-dimensional site (Pervaiz et al., 2021). Moreover, liquefaction simulation was also conducted to simulate the Korea liquefaction case (Lee et al., 2025), estimate the lateral spreading in Indonesia (Fitri & Sawada, 2025b), and analyze near-fault motion (Tsai & Li, 2024). Modified Kondner–Zelasko (MKZ) and General Quadratic/Hyperbolic (GQ/H) are the constitutive models embedded in this software. MKZ utilizes a hyperbolic equation to fit normalized shear modulus reduction and damping curves to simulate hysteretic soil behavior (Matasović, 1993). Meanwhile, the GQ/H model can represent the soil's shear strength and small-strain nonlinear behavior (Groholski et al., 2015). However, it demonstrates that the computed site response highly depends on the implied shear strength in the soil model, particularly for porous soil sites. The constitutive model plays a significant role because the large-strain shear strength is generally considered unrestricted, leading to overestimated shear stress as shear strains increase (Carlton & Kaynia, 2017). This condition leads to overestimation and unrealistic predictions for the dynamic simulation. The soil response is highly nonlinear, and both model outputs are strongly correlated with a limited number of critical parameters, which leads to highly sensitive output.

The Lombok area is highly vulnerable to earthquake-induced liquefaction. The Mandalika circuit, as a site project, is dominated by sand in the subgrade with a high groundwater table and is susceptible to soil liquefaction. Several studies that simulated the liquefaction in this location provide cyclic tests and empirical assessments (Fitri & Sawada, 2025a). In addition to minimizing the hazard, several countermeasures have been proposed, such as site-specific assessment from microtremor data (Fitri et al., 2018; Taruna et al., 2024) and stone column mitigation (Sunarto et al., 2024). Fitri and Sawada (2024) described liquefaction analysis in Indonesia that has not been fully explored, especially regarding appropriate parameters for liquefaction assessment. Therefore, an accurate model of liquefaction behavior at the site produces a better mitigation strategy for disaster management. The modeling of nonlinear analysis should consider the appropriate constitutive model for simulating the liquefaction behavior of a particular site.

This study aims to generate a one-dimensional nonlinear analysis for simulating liquefaction behavior through two constitutive models in DEEPSOIL. The MKZ and GQ/H models are applied to yield the soil response from seismic motion data. The dynamic behavior from the analysis, such as pore water pressure ratio, strain ratio, and shear stress, is calculated in each layer of the ground to indicate the softening and failure of the ground. Several studies examining the comparison of similar constitutive models have been conducted in Southern California (Golkarfard et al., 2024), Southern Iran (Eskandarinejad et al., 2017), and South Korea (Shamsher et al., 2025), or compared with other constitutive models such as MKZ and PDMY02 (Demir, 2021). In addition, for liquefaction analysis, examinations of total stress and effective stress approaches to generate pore water pressure ratio have been conducted through this program without considering the different constitutive models (He et al., 2025). Although the approach is the same as that used for nonlinear site response analysis, this research was applied in Indonesia and focuses on seismic-induced liquefaction. This research is expected to provide an accurate constitutive model for the Lombok region to assess disaster mitigation actions comprehensively.

Material and methods

Research location

This research is located on Lombok Island, especially in the Mandalika circuit project. The detailed location is presented in Figure 1.

a

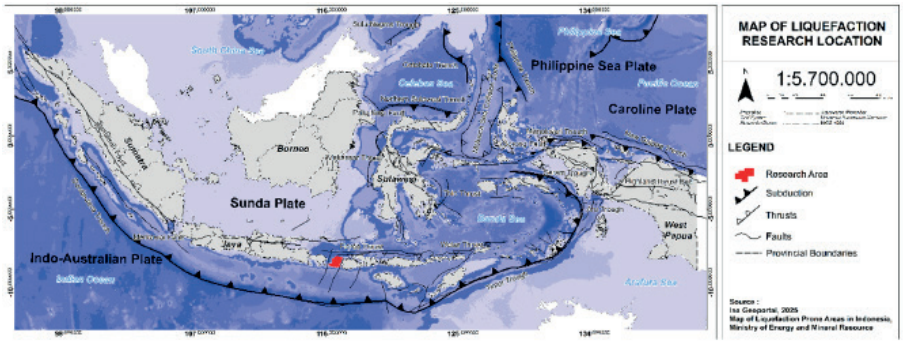

FIGURE 1. Research location in macroscale (a) and microscale (b)
Source: own work based on Ina-Geoportal maps (2025).

Fitri, S. N., Surjandari, N. S., Chrismaningwang, G., Setiawan, B., Purwana, Y. M., Prakosa, B. B., Indrabaskara, R. H. D. H. (2026). Nonlinear analysis for liquefaction simulation: implication of constitutive soil model. *Sci. Rev. Eng. Env. Sci.*, *35* (1), 57–74. DOI 10.22630/srees.10987

b

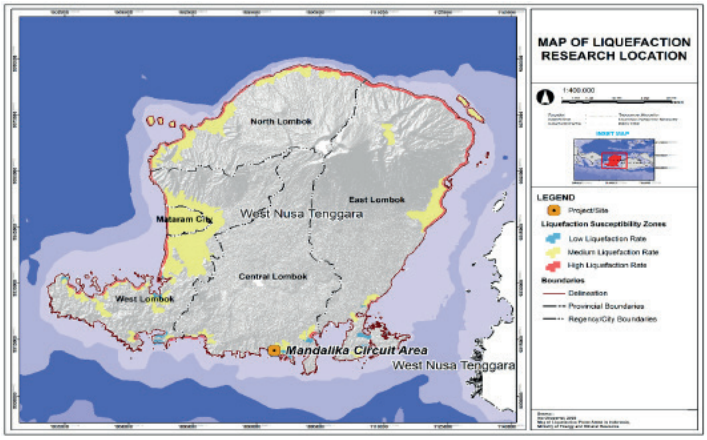

FIGURE 1. (cont.)

Regarding liquefaction susceptibility, the area is in the medium liquefaction risk zone based on the Indonesian liquefaction hazard map, which is layered in Figure 1. The site investigation was conducted using a standard penetration test (N-SPT) with five boreholes.

Soil properties

Sandy soil with a shallow groundwater table dominates the ground. Based on the site investigation, the five boreholes have different bedrock conditions, although all the properties are mixed with clay or silt. The groundwater level is generally 1.5 m, but in this analysis, the groundwater level is assumed to be 1 m deep for all boreholes. The bedrock condition is simulated at 20 m for BH1, BH2, and BH3, while at 10 m for BH4 and 17 m for BH5. To avoid misunderstanding, the unit weight of the soil is described as γ_S. Detailed information is presented in Table 1.

The soil properties that apply for the simulation are unit weight, shear wave velocity corresponding to the N-SPT value, and friction angle (ϕ). The relationship between shear wave velocity (V_s) and the SPT value (N_{60}) and initial effective vertical stress of the ground (σ'_{v0}) is described in Equation 1 (Brandenberg et al., 2010; Amalia et al., 2023):

$$\ln(V_s) = 4.045 + 0.096 \ln(N_{60}) + 0.236 \ln(\sigma'_{v0}). \quad (1)$$

This analysis computes the same layer consistency for the similar shear wave velocity values. Detailed N-values of SPT and V_s are also depicted in Figure 2.

TABLE 1. Soil properties for all borehole

BH1							
Depth	0–1 m	1–3 m	3–7 m	7–11 m	11–14 m	14–17 m	17–20 m
Soil type	sand		silty sand		sand	clayey sand	
γ_s [kN·m^{-3}]	16.2	16.2	16	17	18	18	18
V_s [m·s^{-1}]	196	260	264	300	326	346	356
ϕ [°]	27	24	29	32	35	38	38
BH2							
Depth	0–1 m	1–4 m	4–6 m	6–9 m	9–14 m	14–18 m	18–20 m
Soil type	sand		silty sand			sand	
γ_s [kN·m^{-3}]	17	17	18	18	16	16.8	17.8
V_s [m·s^{-1}]	197	270	289	313	287	296	340
ϕ [°]	29.1	39.81	38	39	37	38.5	38.5
BH3							
Depth	0–1 m	1–2 m	2–4 m	4–5 m	5–7 m	7–17 m	17–20 m
Soil type	sand					silty sand	
γ_s [kN·m^{-3}]	16	16.2	17.2	16	16	16	17.8
V_s [m·s^{-1}]	216	222	270	252	234	248	355
ϕ [°]	22	22	32	35	35	38	39
BH4							
Depth	silty sand			sand		×	×
Soil type	0–1 m	1–3 m	3–5 m	×	8–10 m	×	×
γ_s [kN·m^{-3}]	16	16.5	17	×	17.8	×	×
V_s [m·s^{-1}]	208	210	251	×	340	×	×
ϕ [°]	27	28	31	×	35	×	×
BH5							
Depth	sand					gravelly sand	
Soil type	0–1 m	1–7 m	7–8 m	8–12 m	12–13 m	13–14 m	14–17 m
γ_s [kN·m^{-3}]	16	17.5	16.2	16.2	17.5	17.5	18
V_s [m·s^{-1}]	195	276	261	255	292	313	330
ϕ [°]	28	30	32	32	35	38	38

Source: own work.

Fitri, S. N., Surjandari, N. S., Chrismaningwang, G., Setiawan, B., Purwana, Y. M., Prakosa, B. B., Indrabaskara, R. H. D. H. (2026). Nonlinear analysis for liquefaction simulation: implication of constitutive soil model. *Sci. Rev. Eng. Env. Sci.*, *35* (1), 57–74. DOI 10.22630/srees.10987

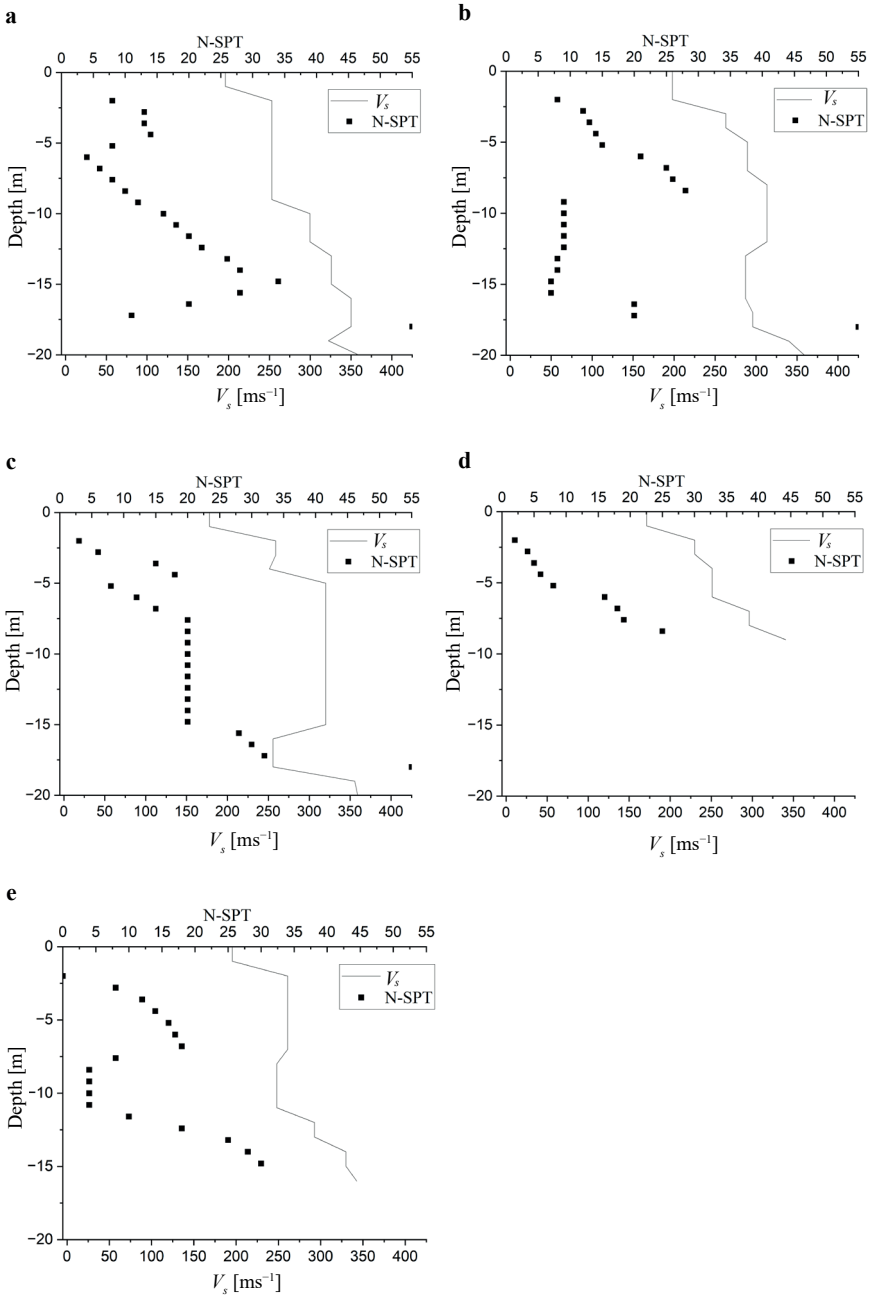

FIGURE 2. Results of standard penetration test (N-SPT) and shear wave velocity (V_s) test in designated boreholes: a – BH1, b – BH2, c – BH3, d – BH4, e – BH5

Source: own work.

DEEPSOIL model and assumption

In this study, the analysis of seismic behavior is based on site-specific response analysis through DEEPSOIL. This nonlinear calculation is applied to a one-dimensional model with input from the soil properties, using the seismic load from the Kobe earthquake ground motion. This is due to lack of real ground motion recorded at the location, although the area is highly impacted as a seismically prone site. The Kobe earthquake is embedded in DEEPSOIL and has been applied in several liquefaction cases in Indonesia, such as the 2018 Palu earthquake (Jalil et al., 2021; Hori et al., 2023) and the Yogyakarta airport project (Fitri & Pramana, 2025).

The dynamic properties of sand, such as soil properties, are estimated from Darendeli's empirical model (Stokoe et al., 2004). This approach is calculated to simulate cyclic loading behavior, such as loading and unloading, and yields the stress–strain loop connection. Moreover, Phillips and Hashash (2009) employed the damping factor (D) and modulus reduction ($G/G_{\max}$) for calibration and minimizing discrepancies between the targeted and resulting curves.

In general, numerous soil constitutive models for dynamic analysis have been proposed to account for the solid–liquid coupling phenomena in saturated sandy soils exposed to intense shaking, such as applying the effective stress method (Chiaradonna et al., 2018; Wang et al., 2014, 2021; Boccieri et al., 2024; Chen et al., 2024). Moreover, several constitutive models are available in DEEPSOIL for assessing the dynamic behavior of the ground. However, this research will apply two constitutive models for liquefaction analysis: General Quadratic/Hyperbolic (GQ/H) and Modified Kondner–Zelasko (MKZ). The detailed analysis, which focuses on shear strain and stress, is distinguished by the following approach.

Modified Kondner–Zelasko (MKZ)

The MKZ model is an upgrade from the hyperbolic approach model provided by Matasović and Vucetic (1993). This analysis applies β and s for fitting the shape of the curve where G_0 is the initial shear modulus, shear strength is τ, and shear strain is γ. The process ensures a stress–strain curve that complies with a user-specified shear strength at a specified strain while matching the analysis goal modulus-reduction (and related damping) curve over a selected strain range:

Fitri, S. N., Surjandari, N. S., Chrismaningwang, G., Setiawan, B., Purwana, Y. M., Prakosa, B. B., Indrabaskara, R. H. D. H. (2026). Nonlinear analysis for liquefaction simulation: implication of constitutive soil model. *Sci. Rev. Eng. Env. Sci.*, *35* (1), 57–74. DOI 10.22630/srees.10987

$$\tau = \frac{G_0 \gamma}{1 + \beta \left(\frac{\gamma}{\gamma_r} \right)^S}. \tag{2}$$

While in DEEPSOIL, the model is augmented by γ_r as confining pressure according to Hashash's and Park's theory (2001). The value is calculated by dividing the vertical effective stress (σ'_v) by the reference stress (σ_{ref}):

$$\gamma_r = \left(\frac{\sigma'_v}{\sigma_{\text{ref}}} \right)^b. \tag{3}$$

General Quadratic/Hyperbolic (GQ/H)

As an extended method from MKZ, the GQ/H method is a further approach that combines ultimate shear strength and modulus reduction factor with θ_τ as a parameter for fitting the curve, and maximum shear stress ($\tau_{\max}$):

$$\tau = \tau_{\max} \left[\frac{1}{\theta_\tau} \left\{ 1 + \left(\frac{\gamma}{\gamma_r} \right) - \sqrt{\left\{ 1 + \frac{\gamma}{\gamma_r} \right\}^2 - 4\theta_\tau \frac{\gamma}{\gamma_r}} \right\} \right], \tag{4}$$

where θ_τ is calculated by the equation:

$$\theta_\tau = \theta_1 + \theta_2 x \frac{\theta_4 x \left(\frac{\gamma}{\gamma_r} \right)^{\theta_5}}{\theta_3^{\theta_5} \theta_4 x \left(\frac{\gamma}{\gamma_r} \right)^{\theta_5}}. \tag{5}$$

DEEPSOIL utilizes the MRDF (Phillips & Hashash, 2009) technique that improves the fit to damping behavior and modulus reduction. The correction factor is calculated as Equation 5. Parameters θ_1, θ_4, and θ_τ are employed to alter the large strain values according to the designated large strain shear strength and to maintain the modulus reduction curves derived from reference studies as much as possible. After generating the layered domain, the GQ/H curve fitting procedure generates the shear strength correction for the soil shear strength–shear strain graph and delivers the parameters θ_1 through θ_5. All further detailed descriptions are provided in the DEEPSOIL user manual (DEEPSOIL, 2024).

Behavior reversal and hysteresis

In order to improve the simulation of cyclic strain calculation, the GQ/H model further specifies a thorough hysteresis formulation for including unloading and reloading approaches. The reaction to hysteretic stress is provided by Equation 6. The τ_{rev} and γ_{rev} are the point of reversal at stress and strain point, and τ acts as a reduction factor, and $G\gamma_{\max}$ is the tangent modulus that associated with the particular $\gamma_{\max}$:

$$\tau = F\left(\gamma_{\max}\right)\left[-\frac{\tau_{\max}}{\theta_{\tau}}\left\{1+\frac{\gamma-\gamma_{\text{rev}}}{2\gamma_r}\right\}-\right.$$

$$\left.-\sqrt{1+\left(\frac{\gamma-\gamma_{\text{rev}}}{2\gamma_r}\right)^2-4\theta_r\left(\frac{\gamma-\gamma_{\text{rev}}}{2\gamma_r}\right)-G\gamma_{\max}\left(\gamma-\gamma_{\text{rev}}\right)}\right]+G\gamma_{\max}\left(\gamma-\gamma_{\text{rev}}\right)+\tau_{\text{rev}}. \quad (6)$$

Pore water pressure generation

The pore water pressure generation is calculated by Equation 7 and considers the Dobry–Matasovic (Dobry et al., 1982) model approaches when it is called normalized excess pore pressure (r_u) as u_n, a parameter for fitting the curve (p, s, and F), f is the dimensionality factor, N_c is the number of cycles, the shear strain reversal value is γ_c, and γ_{tvp} is the threshold for shear strain:

$$u_n = \frac{pfN_C F\left(\gamma_C-\gamma_{tvp}\right)^S}{1+fN_C F\left(\gamma_C-\gamma_{tvp}\right)^S}. \quad (7)$$

The normalized excess pore water pressure ratio is also defined as the u_n parameter in the following equation:

$$r_u = \frac{u'}{\sigma'_v}, \quad (8)$$

where r_u is the pore water pressure ratio, u' is excess pore water pressure, and σ'_v is the effective vertical stress.

Fitri, S. N., Surjandari, N. S., Chrismaningwang, G., Setiawan, B., Purwana, Y. M., Prakosa, B. B., Indrabaskara, R. H. D. H. (2026). Nonlinear analysis for liquefaction simulation: implication of constitutive soil model. *Sci. Rev. Eng. Env. Sci.*, *35* (1), 57–74. DOI 10.22630/srees.10987

Results and discussion

Pore water pressure output

The output for r_u from each layer is presented in Figure 3 for all layers. All the results are included in two constitutive models, the MKZ and GQ/H models. The Darendeli model (Stokoe et al., n.d.) was employed to evaluate the modulus reduction and damping contours in this investigation for each layer, with the coefficient at rest (K_0) applied from Jacky's formula (Diaz-Segura, 2016). Different behaviors are depicted in all grounds since the model is on layered ground with varying soil properties. The r_u value occurs after 1 m depth because the modeling of the groundwater table is below 1 m depth.

In general, the MKZ and GQ/H results describe almost similar values in the several maximum ranges of r_u (BH1, BH2, BH3, BH5), although they have differences around the r_u under 0.5 (BH2, BH3, BH5). In addition, all the boreholes depict the deeper layer of the ground, and the values of the two constitutive models tend to be similar but have slight differences. The maximum value of r_u is in BH1 at 18 m, BH2 at 16 m, BH3 at 12 m, BH4 at 4 m, and BH5 at 10 m.

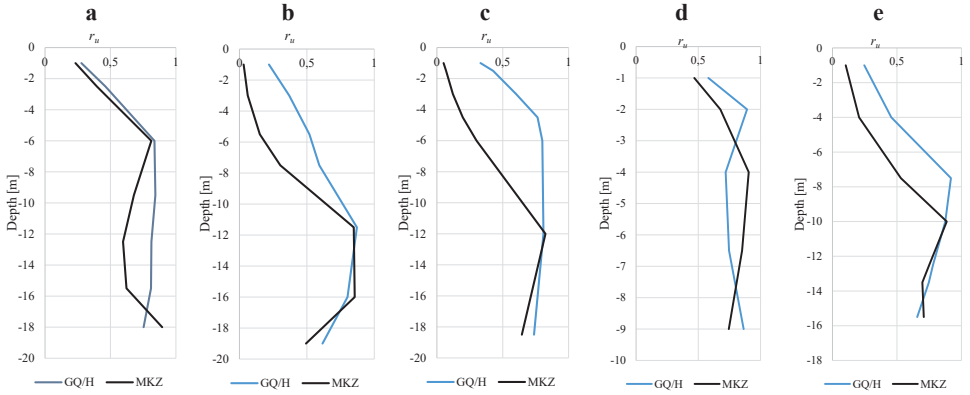

FIGURE 3. Pore water pressure generation from DEEPSOIL analysis: a – BH1, b – BH2, c – BH3, d – BH4, e – BH5

Source: own work.

This study only focuses on modeling liquefaction simulation based on pore water pressure (r_u) generation without any supporting data from the physical laboratory tests. Based on the centrifuge analysis (Groholski et al., 2016), the MKZ typically generates the r_u effectively at a moderate level of liquefaction but lacks prediction accuracy under full liquefaction conditions. Furthermore, Raza and Ahmad implied

that $r_u \geq 0.9$ indicates complete liquefaction condition while marginal liquefaction is $0.8 \leq r_u \leq 0.9$ (Raza & Ahmad, 2024). Based on the results, the smaller the value of r_u from the MKZ approach, the larger the gap between the two constitutive models. This means that in the no liquefaction to marginal liquefaction conditions, the MKZ predicts less safe results than GQ/H. This threshold also combines with the strain value to predict the real phase of the liquefied soil layer more accurately.

GQ/H ignores the multiple, occasionally subjective processes frequently required to calibrate MKZ for strength under high stresses in cyclic loading. This condition leads to a more straightforward and transparent model calibration and more dependable output for crucial liquefaction situations. In addition, some studies also declare that similar degradation indicators for modulus and strength are included in the GQ/H model, which can more accurately represent large-strain shear strength than MKZ (Mei, 2018; Di Buccio & Pagliaroli, 2020).

Shear stress and strain relation

Due to the large gap between the two constitutive models in the r_u output, especially at shallow depths, the hysteresis loops (relation between stress and strain) are focused on the −5 m depth in all boreholes. This depth is chosen because the r_u value tends to be under 0.8 at this particular depth except in BH4, which means it is not in the full liquefaction condition. All the results are shown in Figure 4.

All the boreholes present a similar behavior in that strain results from MKZ tend to be smaller than GQ/H, although the values were reversed under conditions of full liquefaction (BH4). This output is appropriate for the study that proved MKZ underestimates the rate of shear strength degradation at high pore water pressures and the loss of cyclic stiffness, but it may be overestimated at large strains. Meanwhile, the GQ/H approach improves estimates of how soil deteriorates before and after the first phase of liquefaction by providing more realistic hysteresis that appropriately represents the significant decrease in cyclic resistance and energy dissipation (Shamsher et al., 2025).

The liquefaction analysis is not only about predicting the behavior of the excess pore water pressure ratio (r_u), but also the output for shear and strain of the modeling. The combination of the failure process in the soil due to strain stress, especially in shear force, is considered. The maximum r_u value in each borehole with the MKZ model is described in Figure 5.

Fitri, S. N., Surjandari, N. S., Chrismaningwang, G., Setiawan, B., Purwana, Y. M., Prakosa, B. B., Indrabaskara, R. H. D. H. (2026). Nonlinear analysis for liquefaction simulation: implication of constitutive soil model. *Sci. Rev. Eng. Env. Sci.*, *35* (1), 57–74. DOI 10.22630/srees.10987

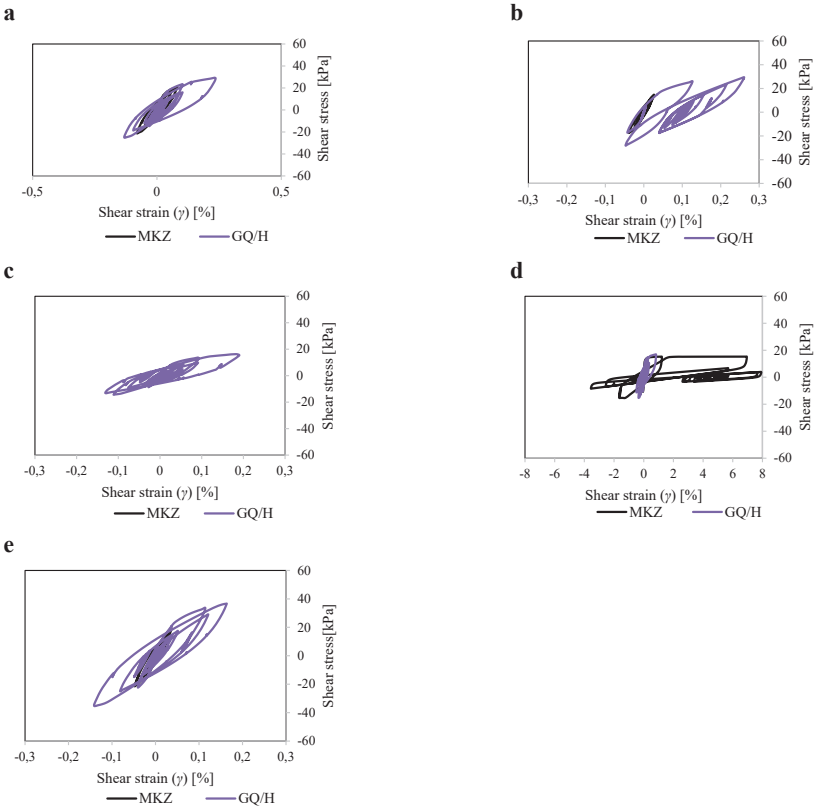

FIGURE 4. Shear stress and shear strain relation output in depth of −5 m: a – BH1, b – BH2, c – BH3, d – BH4, e – BH5

Source: own work.

The strain output shows that the peak of r_u does not always produce the maximum strain ratio. However, the pore water pressure of the MKZ model is lower than of GQ/H because the degradation model considers a reduction in soil material stiffness at each time step. For a more accurate simulation, Chiaradonna et al. (2015) suggested that the recalculation of stiffness and soil strength during the post-cyclic consolidation phase should be considered, as should the dissipation and redistribution of excess pore pressure inside a soil deposit.

The study covers the numerical analysis through modeling soil properties in Indonesia to obtain the liquefaction behavior of the ground. Although the cyclic load does not fully represent the actual seismic motion, the behavior of the softening soil is expected to be the basic threshold for disaster management in the Lombok region. The two constitutive models offer benefits and drawbacks

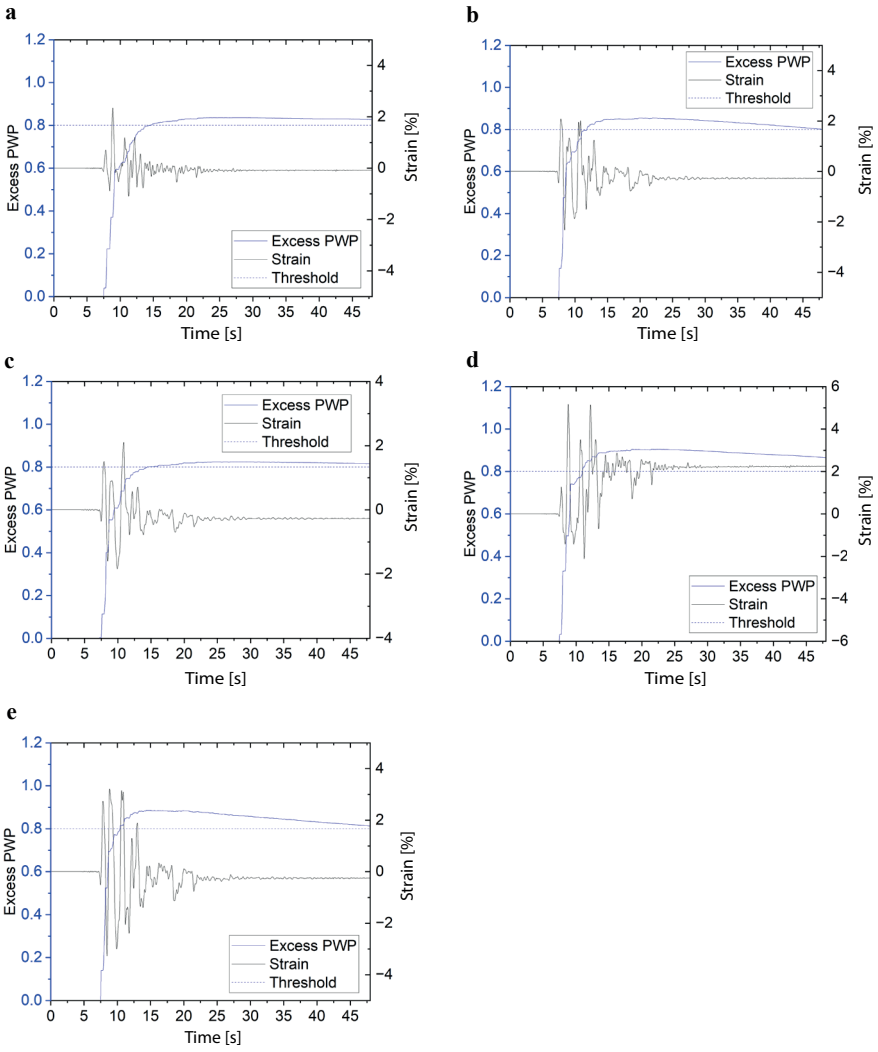

FIGURE 5. Relationship among excess pore water pressure ratio (r_u) and strain in the DEEPSOIL model: a – BH1, b – BH2, c – BH3, d – BH4, e – BH5

Source: own work.

to the output that a geotechnical expert should consider in engineering practices. In addition, laboratory physical testing, such as centrifuge and 1 g shaking table tests, is necessary for future study because these tests can replicate the soil model and specific site profiles, allowing for advanced validation of the MKZ and GQ/H constitutive models.

Conclusions

This research conducted the liquefaction behavior analysis through two constitutive models, namely the MKZ and GQ/H models. The pore water pressure ratio, shear stress, and strain ratio under seismic conditions were simulated based on DEEPSOIL. The major conclusion is the following:

1. From the investigation of pore water pressure ratio (r_u) from each borehole, the similar data shows that in the condition of full liquefaction, the MKZ tends to simulate the smaller value rather than the GQ/H model but has the opposite output when in a state of marginal liquefaction. Although at the maximum point, two models offer almost the same value in every borehole.
2. The output of shear strain ratio and shear stress in marginal liquefaction is the main reason MKZ underestimates the stress-strain value. All boreholes indicate that the GQ/H simulates a better estimation of the middle liquefaction situation for both the r_u and strain approaches. The realistic hysteresis as a dynamic property effect is investigated by GQ/H, which appropriately represents the significant decrease in cyclic loading.
3. The relationship between the shear strain ratio, pore water pressure ratio (r_u), and seismic time leads to a pattern in which the maximum r_u does not always provide the most significant strain ratio at a particular time. The combination of dynamic properties should be considered to assess liquefaction behavior comprehensively.

Acknowledgments

This research is funded by a Research Group Grant from Sebelas Maret University with contract 371/UN27.22/PT.01.03/2025. All the authors express their gratitude for this program.

References

Amalia, K. P., Ismanti, S., & Saputra, A. (2023). Liquefaction potential evaluation in Toba crater Indonesia. *International Journal of GEOMATE*, *25*(110), 123–131. https://doi.org/10.21660/2023.110.3990

Boccieri, G., Gaudio, D., & Conti, R. (2024). An uncoupled approach for estimating seismic-induced pore water pressures in liquefiable sandy soils. *Computers and Geotechnics*, *170*, 106266. https://doi.org/https://doi.org/10.1016/j.compgeo.2024.106266

Brandenberg, S. J., Bellana, N., & Shantz, T. (2010). Shear wave velocity as function of standard penetration test resistance and vertical effective stress at California bridge sites. *Soil Dynamics and Earthquake Engineering*, *30*(10), 1026–1035. https://doi.org/10.1016/j.soildyn.2010.04.014

Carlton, B., & Kaynia, A. M. (2017). Nonlinear site response model with improved damping and strain softening. In *Proceedings of 16th World Conference on Earthquake Engineering, Santiago, Chile*. Paper 0721. http://wcee.nicee.org/wcee/article/16WCEE/WCEE2017-721.pdf

Chen, G., Qin, Y., Wu, Q., Gu, X., & Juang, C. H. (2024). A Unified Model of Cyclic Shear–Volume Coupling and Excess Pore Water Pressure Generation for Sandy Soils under Various Cyclic Loading Patterns. *Journal of Geotechnical and Geoenvironmental Engineering*, *150*(9), 4024075. https://doi.org/10.1061/JGGEFK.GTENG-12247

Chiaradonna, A., Tropeano, G., d'Onofrio, A., & Silvestri, F. (2018). Development of a simplified model for pore water pressure build-up induced by cyclic loading. *Bulletin of Earthquake Engineering*, *16*(9), 3627–3652. https://doi.org/10.1007/s10518-018-0354-4

Chiaradonna, A., Tropeano, G., d'Onofrio, A., Silvestri, F., & Park, D. (2015, November 1-4). *Application of a simplified model for the prediction of pore pressure build-up in sandy soils subjected to seismic loading*. 6th International Conference on Earthquake Geotechnical Engineering, Christchurch, New Zealand. https://secure.tcc.co.nz/ei/images/ICEGE15%20Papers/Chiaradonna%20189.00_.pdf

Chiu, P., Pradel, D. E., Kwok, A. O. L., & Stewart, J. P. (2008). Seismic response analyses for the silicon valley rapid transit project. In *Geotechnical Earthquake Engineering and Soil Dynamics IV* (pp. 1–10). ASCE Library. https://doi.org/10.1061/40975(318)210

DEEPSOIL (2024). *A nonlinear and equivalent linear seismic site response of 1-D soil columns*. User manual. Board of Trustees of University of Illinois at Urbana. https://deepsoil.cee.illinois.edu/Files/DEEPSOIL_User_Manual_v7.pdf

Demir, S. (2021). Numerical assessment of the performance of different constitutive models used to predict liquefiable soil behavior. *International Advanced Researches and Engineering Journal*, *5*(2), 260–267. https://doi.org/10.35860/iarej.871429

Di Buccio, F., & Pagliaroli, A. (2020). Numerical modelling of seismic site response at large strains: a parametric study. *American Journal of Civil Engineering*, *8*(5), 117–127. https://hdl.handle.net/11564/736424

Diaz-Segura, E. G. (2016). The coefficient of earth pressure at rest. *Electronic Journal of Geotechnical Engineering*, *21*(5). https://doi.org/10.1016/0148-9062(94)90690-4

Dobry, R., Ladd, R. S., Yokel, F. Y., Chung, R. M., & Powell, D. (1982). *Prediction of pore water pressure buildup and liquefaction of sands during earthquakes by the cyclic strain method: Building science series*. National Bureau of Standards, US Department of Commerce, US Governmental Printing Office.

Eskandarinejad, A., Jahanandish, M., & Zafarani, H. (2017). Divergence between nonlinear and equivalent-linear 1D site response analyses for different V_S realizations of typical clay sites. *Pure and Applied Geophysics*, *174*(10), 3955–3978. https://doi.org/10.1007/s00024-017-1586-y

Fitri, S. N., & Pramana, I. M. W. (2025). Non-linear seismic response for liquefaction analysis: pore water pressure and strain ratio approach. *Scientific Review Engineering and Environmental Sciences*, *34*(3). https://doi.org/10.22630/srees.10426

Fitri, S. N., & Sawada, K. (2024). Evaluation and opportunities for soil liquefaction vulnerability research: Lesson learned from Japan for Indonesia-A bibliometric analysis. In *Proceedings of the 2024 11th International Conference on Geomatics in Civil Engineering* (pp. 14–29). Springer Nature Singapore. https://doi.org/10.1007/978-3-031-68624-5_2

Fitri, S. N., & Sawada, K. (2025a). Comprehensive assessment for liquefaction vulnerability in Indonesia: empirical and element simulation approaches. *Civil Engineering Journal*, *11*(1), 326-345. https://doi.org/10.28991/CEJ-2025-011-01-019

Fitri, S. N., & Sawada, K. (2025b). Soil liquefaction induces lateral spreading estimation based on site-specific response analysis. In S. A. Kristiawan, K. C. Tsai, M. Shahin, A. R. M. Sam & P. D. Hai (Eds.), *Proceedings of the 6th International Conference on Rehabilitation and Maintenance in Civil Engineering* (Vol. 2, pp. 255–266). Springer Nature Singapore. https://doi.org/10.1007/978-981-96-4694-4_26

Fitri, S. N., Soemitro, R. A. A., Warnana, D. D., & Sutra, N. (2018). Application of microtremor HVSR method for preliminary assessment of seismic site effect in Ngipik landfill, Gresik. *MATEC Web of Conferences*, *195*, 03017. https://doi.org/10.1051/matecconf/201819503017

Golkarfard, H., Ravichandran, N., Sedaghat, A., Saketh Jella, V., & Andrus, R. (2024, February 25-28). *Effects of different soil constitutive models on nonlinear seismic site response analysis using DEEPSOIL for the Blue Ridge and Piedmont Regions, South Carolina*. Geo-Congress 2024, Vancouver, British Columbia, Canada. https://doi.org/10.1061/9780784485316.028

Groholski, D. R., Hashash, Y. M., Kim, B., Musgrove, M., Harmon, J., & Stewart, J. P. (2016). Simplified model for small-strain nonlinearity and strength in 1D seismic site response analysis. *Journal of Geotechnical and Geoenvironmental Engineering*, *142*(9), 04016042. https://doi.org/10.1061/(ASCE)GT.1943-5606.0001496

Groholski, D. R., Hashash, Y. M. A., Musgrove, M., Harmon, J., & Kim, B. (2015, November 1-4). *Evaluation of 1-D non-linear site response analysis using a general quadratic/hyperbolic strength-controlled constitutive model*. 6th International Conference on Earthquake Geotechnical Engineering, Christchurch, New Zealand. https://secure.tcc.co.nz/ei/images/ICEGE15%20Papers/Hashash%20269.00.pdf

Hashash, Y. M. A., Park, D. (2001). Non-linear one-dimensional seismic ground motion propagation in the Mississippi Embayment. *Engineering Geology*, *62*(1–3), 185-206.

He, H., Miao, Y., & Wang, S. (2025). Reproducing nonlinear ground response and pore pressure variations using in-situ soil properties. *Soil Dynamics and Earthquake Engineering*, *194*, 109380. https://doi.org/https://doi.org/10.1016/j.soildyn.2025.109380

Hori, R., Inoue, K., Ikeda, T., & Kiyota, T. (2023). Analytical study on ground behavior during the 2018 Sulawesi earthquake, Indonesia. *IOP Conference Series: Earth and Environmental Science*, *1244*(1), 012035. https://doi.org/10.1088/1755-1315/1244/1/012035

Jalil, A., Fathani, T. F., Satyarno, I., & Wilopo, W. (2021). Nonlinear site response analysis approach to investigate the effect of pore water pressure on liquefaction in Palu. *IOP Conference Series: Earth and Environmental Science*, *871*(1), 012053. https://doi.org/10.1088/1755-1315/871/1/012053

Lee, Y. G., Pervaiz, U., Park, D., Kim, B., & Han, J. T. (2025). Assessment of liquefaction potential using simplified method and one-dimensional effective stress ground response analysis during 2017 Pohang earthquake in South Korea: A case study. *Soil Dynamics and Earthquake Engineering*, *196*, 109463. https://doi.org/https://doi.org/10.1016/j.soildyn.2025.109463

Matasović, N. (1993). *Seismic response of composite horizontally-layered soil deposits* (doctoral dissertation). University of California. https://www.researchgate.net/publication/34090029

Matasović, N., & Vucetic, M. (1993). Cyclic characterization of liquefiable sands. *Journal of Geotechnical Engineering*, *119*(11), 1805–1822. https://doi.org/10.1061/(ASCE)0733-9410(1993)119:11(1805)

Mei, X. (2018). *Pore pressure generation and liquefaction analysis using nonlinear, effective stress-based site response analysis* (doctoral dissertation). University of Illinois at Urbana-Champaign. http://hdl.handle.net/2142/102927

Pervaiz, U., Park, D., Hashash, Y., & Xing, G. (2021). Testing performance of pore pressure models implemented in one-dimensional site response analysis program against centrifuge test data measured in mildly sloping ground. *Soil Dynamics and Earthquake Engineering*, *149*, 106867. https://doi.org/10.1016/j.soildyn.2021.106867

Phillips, C., & Hashash, Y. M. (2009). Damping formulation for nonlinear 1D site response analyses. *Soil Dynamics and Earthquake Engineering*, *29*(7), 1143–1158. https://doi.org/10.1016/j.soildyn.2009.01.004

Raza, H., & Ahmad, N. (2024). Assessment of seismic liquefaction hazard and ground response in subduction zone: a 1D non-linear effective stress approach. *Engineering Research Express*, *6*(4), 045121. https://doi.org/10.1088/2631-8695/ad980a

Shamsher, S., Won, M. S., Park, Y. C., Park, Y. H., & Sayed, M. A. (2025). Effect of nonlinear constitutive Models on seismic site response of soft reclaimed soil deposits. *Journal of Marine Science and Engineering*, *13*(7), 1333. https://doi.org/10.3390/jmse13071333

Stokoe, K. H., Darendeli, M. B., Gilbert, R. B., Menq, F. Y., & Choi, W. K. (n.d.). *Development of a new family of normalized modulus reduction and material damping curves*. https://apps.peer.berkeley.edu/lifelines/Workshop304/pdf/Stokoe_PlenaryPaper.pdf

Sunarto, S., Setyono, E., Darmawan, A. A., & Ondang, K. K. (2024). Liquefaction potential and soil bearing capacity improvement with stone column case study. *AIP Conference Proceedings*, *2927*(1), 030009. https://doi.org/10.1063/5.0193689

Taruna, R. M., Septiadhi, A., Sungkono, Mase, L. Z., & Mashuri. (2024). Preliminary assessment of liquefaction vulnerability using microtremor analysis in North Lombok. *Journal of Physics: Conference Series*, *2866*(1), 012061. https://doi.org/10.1088/1742-6596/2866/1/012061

Tsai, C. C., & Li, P. C. (2024). Quantifying near-fault motion effects on soil liquefaction through effective stress site response analysis. *Soil Dynamics and Earthquake Engineering*, *183*, 108779. https://doi.org/10.1016/j.soildyn.2024.108779

Wang, R., Cao, W., Xue, L., & Zhang, J. M. (2021). An anisotropic plasticity model incorporating fabric evolution for monotonic and cyclic behavior of sand. *Acta Geotechnica*, *16*(1), 43–65. https://doi.org/10.1007/s11440-020-00984-y

Wang, R., Zhang, J. M., & Wang, G. (2014). A unified plasticity model for large post-liquefaction shear deformation of sand. *Computers and Geotechnics*, *59*, 54–66. https://doi.org/10.1016/j.compgeo.2014.02.008

Summary

Nonlinear analysis for liquefaction simulation: implication of constitutive soil model. The nonlinear analysis for assessing the cyclic behavior of a specific location is widely applied to minimize geohazards, especially soil liquefaction. The Mandalika circuit project in the Lombok area is highly prone to earthquakes and is located on sand as the subgrade. The high soil liquefaction susceptibility leads to a comprehensive assessment by implementing the appropriate soil constitutive model. One-dimensional nonlinear analysis with two constitutive models, Modified Kondner–Zelasko (MKZ) and General Quadratic/Hyperbolic (GQ/H), provided by the DEEPSOIL program, is examined to generate the dynamic behavior aimed at by this research. Five boreholes from SPT data are conducted as part of the soil investigation data. Based on the pore water pressure, the MKZ and GQ/H in the maximum value (full liquefaction condition) are almost similar in output. However, in other situations, they show the opposite result. The GQ/H predicts a more realistic simulation in the low and medium liquefaction cases, which presents the most significant correlation between strain ratio and shear stress results in all sites. For an accurate evaluation of liquefaction behavior, the combination of dynamic features from an appropriate constitutive model should be considered to simulate the liquefaction behavior of sand.

Scientific Review Engineering and Environmental Sciences (2026), 35 (1), 75–94

Sci. Rev. Eng. Env. Sci. (2026), 35 (1) https://srees.sggw.edu.pl

ISSN 1732-9353 (suspended) eISSN 2543-7496 DOI 10.22630/srees.10715

Received: 01.10.2025
Accepted: 10.02.2026

Weam Abdulwahhab MOHAMMED
Teba SAADI HUSSEIN✉
Noor SAADI HUSSEIN
Ministry of Education, Iraq

Recovered poly manganese chloride ($PMnCl_2$) from industrial waste sludge to decolorize and detoxify textile dyes and comparison with alum

Keywords: coagulant recovery, characterization, decolorization and detoxification, poly manganese chloride, textile dyes

Introduction

Agriculture, forestry, fishing, hydropower generation, industry, and other innovative endeavors all depend heavily on water as a resource. Most industrial effluents are treated, and their properties are determined by the manufacturing methods and raw material types used (Tyagi et al., 2013).

To create, enhance, and put into practice suitable techniques for treatment to eliminate pollutants, a lot of research has been encouraged due to the production of massive output polluted wastewater (Ahmed et al., 2020). To remove color and other organic pollutants wastewater requires a post-treatment process (Hossain et al., 2019). Ion exchange, filtration, chemical precipitation, and the application

✉teba.saadi.ts@gmail.com

of membrane technology are all well-established traditional methods for wastewater treatment (Vasudevan et al., 2010; Sher et al., 2013). These include the production of sludge and heavy metal residues that may be harmful to the ecology, as well as the end-of-life nanomaterials and enhanced color of wastewater (Zhao et al., 2014; Tetteh & Rathilal, 2020). High wastewater treatment system costs and other technological problems are caused by the issues listed above (Holkar et al., 2016).

Effectively reduce the organic burden before moving on to other methods of treatment. It is now important to pre-treat industrial wastewater utilizing coagulation and flocculation techniques (Saifuddin & Dinara, 2011). A crucial process that involves the addition of coagulants, coagulation destabilizes and neutralizes suspended particles, causing them to form big flocs or aggregates. Because of ion adsorption and surface group ionization, negatively charged suspended particles typically clump together when combined with positively charged coagulants. Filtration, flotation, or sedimentation processes are used to get rid of these aggregates (Sánchez-Martin et al., 2012; Sahu & Chaudhari, 2013; Balls, 2014; Bodlund, 2020). Since methods for managing industrial discharges containing toxic compounds are costly and a significant burden for most businesses in underdeveloped nations, these discharges represent major issues for rural communities worldwide (Hung & Kaya, 2020).

Due to the fast expansion of industrialization sectors, wastewater treatment plants are likely depleted and unable to provide granular discharge regulations. Industrial discharge of untreated wastewater into water bodies has an impact on aquatic diversity and human health (Jamali & Moradnia, 2018). Chemical phenolic pollutants are widely used, as demonstrated by materials such as reactive dyes, which are frequently used as synthetic dyes in apparel, paper, and leather sectors. These harmful pollutants are a serious concern to aquatic ecosystems because they seriously damage aquatic life and have a negative impact on human health as well as the larger ecological system (Mohammed & M-Ridha, 2024).

Industrial dyes are utilized all over the world today, and a lot of research is being done to create new synthetic processes that will enhance their application properties. However, textile dyes can provide serious wastewater issues for the dyeing industry because of their high solubility. Interest in decolorization techniques has grown as a result of growing ecological consciousness and public concern, as well as more stringent laws governing wastewater discharge in recent years. Analyzing and cleaning up industrial wastewater effluents contaminated with dyes are crucial procedures. Current cleaning methods are either expensive or harmful to human health because some colors are known to be particularly harmful to the environment, cancer, and mutagenicity (Mohammed & M-Ridha, 2025).

Coagulation has been the sole economically viable technique for color removal over the years. This approach still has a lot of benefits today and is still utilized both alone and in conjunction with other approaches. It was discovered that this combination treatment was highly successful. It was demonstrated that effluent had been completely decolored (Ghaly et al., 2014).

The purpose of this study has two purposes: utilizing environmentally polluting industrial sludge to recover manganese metal and transform it from an environmental burden into an effective coagulant applicable in the treatment of industrial dyes (1); and comparing the synthetic coagulant with a traditional coagulant (alum) and selecting the most efficient coagulant in the process of removing organic textile dyes (2).

Material and methods

The study was carried out in two experimental steps. In the first step, manganese chloride recovery is conducted to produce poly manganese chloride ($PMnCl_2$). Hydrochloric acid (HCl) and sodium hydroxide (NaOH) solutions from Sigma were used. A jar test is first conducted to determine the optimal recovered coagulant based on its effectiveness in pollutant removal. In the second step, to evaluate the effectiveness of recovered coagulants against traditional alum coagulants, an additional test is carried out. Figure 1 illustrates the whole procedure of purification of industrial water and recovery of $PMnCl_2$ of used in this study.

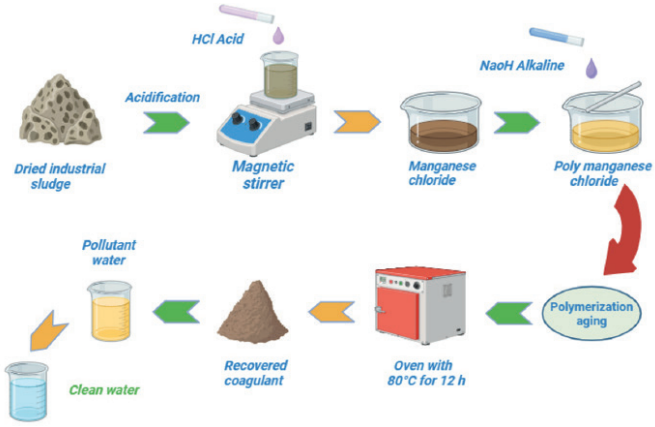

FIGURE 1. Study procedure

Source: own work.

Mohammed, W. A., Saadi Hussein, T., Saadi Hussein, N. (2026). Recovered poly manganese chloride ($PMnCl_2$) from industrial waste sludge to decolorize and detoxify textile dyes and comparison with alum. *Sci. Rev. Eng. Env. Sci.*, *35* (1), 75–94. DOI 10.22630/srees.10715

Textile dyes, namely reactive yellow (RY17) and direct blue (DB53), were used provided by an Iraqi textile factory made in Switzerland. According to the material safety data sheet for RY17 and DB53, these dyes have a negative consequences since they can irritate the respiratory system when inhaled. Furthermore, consumption may result in nausea, vomiting, diarrhea, and gastrointestinal irritation. To prepare a solution of 40 $mg \cdot l^{-1}$ of textile dyes, deionized water was used in laboratory experiments. Table 1 presents the characteristic details and structures of these pollutants.

The wastewater treatment plant in Al-Tajiat (a region in Baghdad, Iraq), which is part of the organized industrial area, supplied the industrial sludge. The sludge samples were dried for 48 h. The main characteristics of the industrial sludge sample were as follows: 300 $g \cdot l^{-1}$ of total solids (TS), 135 $g \cdot l^{-1}$ of total volatile solids (TVS), and 165 $g \cdot l^{-1}$ of fixed solids (FS) with 75.13 $g \cdot l^{-1}$ of chemical oxygen demand (COD).

All these characteristics were determined according to the procedure described in the standard methods (American Public Health Association [APHA], 2005), and the elemental composition is illustrated in Table 2.

TABLE 1. Dyes chemical properties

Pollutant	MWt [g·mol]	λ_{max} [nm]	Chemical structure
Reactive yellow 17	452.79	530	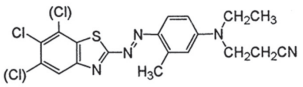
Direct blue 53	1,418.94	545	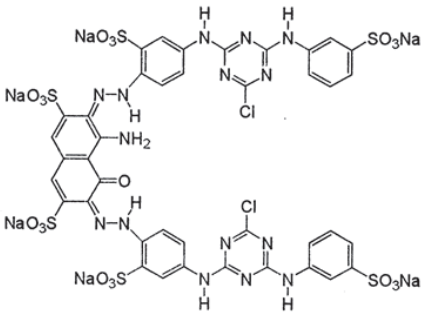

M_{wt} – weight-average molecular weight, λ_{max} – wavelength of maximum absorption.
Source: Safety data sheet.

TABLE 2. Elemental composition of the industrial sludge samples

Parameter	Unit	Value
Si concentration	$mg \cdot kg^{-1}$	13,600
Zn concentration	$mg \cdot kg^{-1}$	2,300
Cu concentration	$mg \cdot kg^{-1}$	1,100
Mn concentration	$mg \cdot kg^{-1}$	9,200
Fe concentration	$mg \cdot kg^{-1}$	7,850
Hg concentration	$mg \cdot kg^{-1}$	n.d.
Ni concentration	$mg \cdot kg^{-1}$	720
Cd, Cr concentration	$mg \cdot kg^{-1}$	b.d.
Pb concentration	$mg \cdot kg^{-1}$	680
Moisture	%	70
pH	–	6.6

n.d. – not determined, b.d. – below detection limit.

Source: own work.

Poly manganese chloride recovery

This step involves drying the industrial sludge then mixing the sample with hydrochloric acid at a pH of 2 in a glass beaker. For 30 min, the composite sample was agitated using a magnetic stirrer at different acidification stirring speeds. After combining, the composite sample is allowed to settle for 30 min. To create the $PMnCl_2$, NaOH is added progressively as a base material until the compound is homogeneous. After that, the polymerization process is carried out to improve the performance of the coagulant, then dried in an electric oven at 80°C for 12 h and ground. It is obtained within limits of 30 g of powder per 1 kg of sludge sample.

Factors effecting recovered poly manganese chloride

Solutions of HCl at varying concentrations are applied to the sludge. The factors that influencing on $MnCl_2$ coagulation are investigated such as:

– The acid concentration effect: at different concentrations 5%, 10%, 15%, 20%, 25%, 30%, and 35%; with parameters stirrer speed 100 rpm; pH of 2; reaction period 20 min; and temperature 40°C.
– The stirrer force effect: stirring at 100 rpm, 200 rpm, 300 rpm, 400 rpm, 500 rpm, and 600 rpm; 20 min reaction time; and a 30% acid concentration.

– The contact time effect: the chosen time intervals are 20 min, 40 min, 60 min, 80 min, 100 min, and 120 min, with a constant flow rate; 30% HCl concentration; 300 rpm stirring speed.
– The temperature effect: 40°C, 60°C, 80°C, and 100°C; 300 rpm of stirring; 100 min of reaction duration; and 30% acid concentration were applied.

Decolorization by recovered coagulant process

Using a jar test (JTL6) with four paddles, the recovered coagulation experiment was conducted with 500 ml of a solution containing 40 mg of dyes per 1 l was used for all tests, and each was assessed independently in beakers (Zhang et al., 2021). First, to obtain the required dosages of recovered coagulant, a dosage range of 10–60 $mg \cdot l^{-1}$ was examined. Equation 1 was used to determine the percentage of removal after samples were stirred with rapid mixing (150 rpm) for 2 min and slow mixing (30 rpm) for 15 min at moderate pH and room temperature, then the necessary coagulant dosage was added (Tetteh & Rathilal, 2021):

$$C_n = \frac{C_i - C_f}{C_i} 100\%, \tag{1}$$

where C_n is the removal efficiency (response parameter), C_i is the initial value of the contaminant, and C_f is the final value of the contaminant.

Characterization of recovered poly manganese chloride

By scanning electron microscopy (SEM), surface morphological analysis of $PMnCl_2$ and alum was conducted to define their elemental distributions and particle shapes. A scanning electron microscope, Nova Nano SEM, was employed to examine the morphological structure of the samples obtained. This was operated at an acceleration voltage under the scale of 20 μm with a landing energy capacity of 15 kV. Additionally, utilizing the Jasco FTIR 460 plus spectrometer, Fourier transform infrared (FTIR) in the 500–4,000 cm^{-1} range, the recovered poly manganese chloride and alum were characterized.

Decoloization by alum coagulant process

The traditional coagulation with alum was experimented by using a jar test (JTL6). All experiments were conducted using 500 ml of a solution containing dye at a concentration of 40 $mg \cdot l^{-1}$, tested individually in separate beakers. Alum

dosages ranging from 10 $mg \cdot l^{-1}$ to 60 $mg \cdot l^{-1}$ were examined under identical conditions to determine the optimal dosage. Dye removal efficiency was estimated using Equation 1.

The kinetics of agglomeration

Coagulation is driven by Brownian motion of the suspended particles coagulation is ejected (Nnaji et al., 2014). When colloidal particles destabilize and agglomerate to a diameter greater than 1 μm Brownian motion becomes less effective (Sun et al., 2019). Equation 2 describes the kinetics of the coagulation rate process (Kumar et al., 2016; Zahrim et al., 2017). Additionally, kinetics determine the floc formation rate and help terminate the critical period prior to floc destabilization. Because kinetic parameters (*n* and *k*) determine how quickly contaminant rates are removed from effluent, kinetic study is crucial. Kinetic parameters, a dependent variable (*C*), and an independent variable (*t*) make up the rate equation:

$$\frac{dC}{Dt} = -KC^n. \tag{2}$$

where *C* is the concentration of particles, *t* is the coagulation time, *k* is the *n*-th order coagulation rate constant, and *n* is the order of the coagulation process.

The particle concentration and time have an indirect relationship. The amount of pollutant concentration absorbed by the coagulant can be directly correlated with the rate of contaminant removal. Equation 3 yields the rate constant for a fast coagulation process (K_{RC}) by multiplying Smoluchowski's rate constant by the collision efficiency (*E*) (Daud et al., 2015):

$$K = EK_{RC}, \tag{3}$$

where K_{RC} is given by Equation 4:

$$K_{RC} = \frac{4KBT}{3\mu}, \tag{4}$$

where μ is the fluid viscosity.

By Equation 5, the Brownian diffusion coefficient (D_B) is given:

$$D_B = \frac{k_B T}{\beta}, \tag{5}$$

Mohammed, W. A., Saadi Hussein, T., Saadi Hussein, N. (2026). Recovered poly manganese chloride ($PMnCl_2$) from industrial waste sludge to decolorize and detoxify textile dyes and comparison with alum. *Sci. Rev. Eng. Env. Sci.*, *35* (1), 75–94. DOI 10.22630/srees.10715

$$\beta = 2k. \tag{6}$$

Equation 2 becomes Equation 7 when integrated for the first order reaction ($n = 1$):

$$\ln\left(\frac{C}{C_0}\right) = K_1 t, \tag{7}$$

where C_0 is the initial concentration, C is the final concentration, and k_1 is the first-order rate constant in $1 \cdot min^{-1}$.

A plot of $\ln\left(\frac{C}{C_0}\right)$ versus t will yield a straight line passing through the origin with a slope of K_1 using Equation 7 (Othman et al., 2011). However, if line does not pass through origin but intersects Y-axis at a different point, process is better represented by a second-order coagulation model ($n = 2$), in which case Equation 2 transforms into Equation 8:

$$\frac{dC}{dt} = -KC^2. \tag{8}$$

Then, Equation 3 yields Equation 4 after integration:

$$\frac{1}{C} = K_2 t + \frac{1}{C_0}, \tag{9}$$

where k_2 is the second-order rate constant expressed in $l \cdot mg^{-1} \cdot min^{-1}$.

Quality of water

Water quality parameters were applied to both untreated and treated solutions using $PMnCl_2$. Chemical oxygen demand (COD) meters were used to measure the total amount of oxygen required to chemically oxidize both organic and inorganic pollutants in water. For total organic carbon (TOC), 1.0 ml of 2N potassium dichromate ($K_2Cr_2O_7$), 1.6 ml of sulfuric acid (H_2SO_4), and 4.0 ml of pollutant samples were added to a digestion flask. The mixture was allowed to digest for 90 min at 110°C before being cooled to room temperature, and optical density at 590 nm was recorded. The toxicity of the untreated and treated water

was evaluated. The samples were examined in the Iranian Ministry of Environment laboratories. The means and standard errors of the means (mean ±*SE*) were calculated for each experiment, which was carried out in triplicate.

The findings and discussions

Factors influencing the efficiency of manganese chloride coagulation:

– The acid concentration effect: Figure 2 shows the relationship between the amount of HCl present and the amount of $MnCl_2$ generated. The results show that $MnCl_2$ generation increases as acid concentration increases up to a limit of 30% HCl content.
– The agitation forces effect: Figure 3 shows that the stirring velocity is a crucial factor in completing the reaction and achieving the best results. The results indicated that the maximum concentration of $MnCl_2$ was formed at a stirring velocity of 300 rpm.
– The contact time effect: Figure 4 illustrates the impact of contact time on the amount of $MnCl_2$ created. The results indicated that the synthesis of $MnCl_2$ increased with the length of contact between the reagents until the time limit; 100 min was the optimum time.
– The reaction temperature effect: Figure 5 illustrates that the production of $MnCl_2$ increases with temperature until a limit degree. The results showed the percentage of $MnCl_2$ produced rises with temperature. At 80°C, production conditions are ideal.

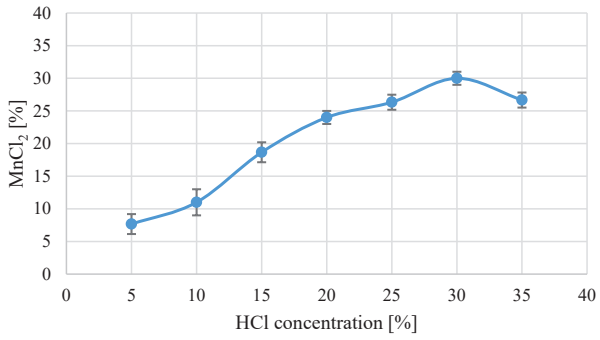

FIGURE 2. Effect of hydrochloric acid concentration on manganese chloride productivity
Source: own work.

Mohammed, W. A., Saadi Hussein, T., Saadi Hussein, N. (2026). Recovered poly manganese chloride ($PMnCl_2$) from industrial waste sludge to decolorize and detoxify textile dyes and comparison with alum. *Sci. Rev. Eng. Env. Sci.*, *35* (1), 75–94. DOI 10.22630/srees.10715

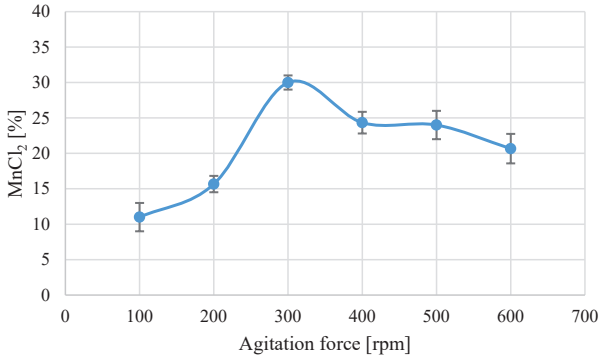

FIGURE 3. Effect of agitation forces on manganese chloride productivity
Source: own work.

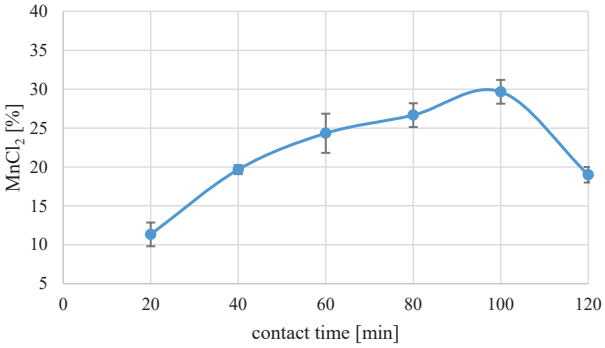

FIGURE 4. Effect of contact time on manganese chloride productivity
Source: own work.

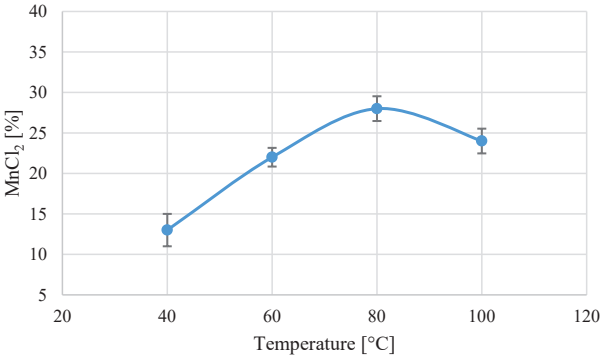

FIGURE 5. Effect of temperature on manganese chloride productivity
Source: own work.

Comparative decolorization between recovered and alum coagulant

Table 3 and Figure 6 illustrate the comparison of color removal efficiency for two coagulants at the variable dosages. The order of coagulant performance was as follows: recovered poly manganese chloride coagulant with an optimum dosage of 30 mg·l^{-1} achieved removal efficiencies of 90.33% and 86.11% for RY17 and DB53, respectively, while pure alum coagulant at the same dosage (30 mg·l^{-1}) achieved removal efficiencies of 85.42% and 80.34% for RY17 and DB53, respectively, which gives the recovered coagulant an advantage in removing the dyes over the alum coagulant.

Table 3. Summary of coagulant dosage and removal efficiency results

Coagulant	Dose of coagulants[mg·l^{-1}]	RY17 pollutant		Removal efficiency [%]	DB53 pollutant		Removal efficiency [%]
		initial turbidity [NTU]	final turbidity [NTU]		initial turbidity [NTU]	final turbidity [NTU]	
Recovered	30	24.93	2.41	90.33	26.82	3.71	86.11
Alum	30	24.93	3.63	85.42	26.82	5.27	80.34

Source: own work.

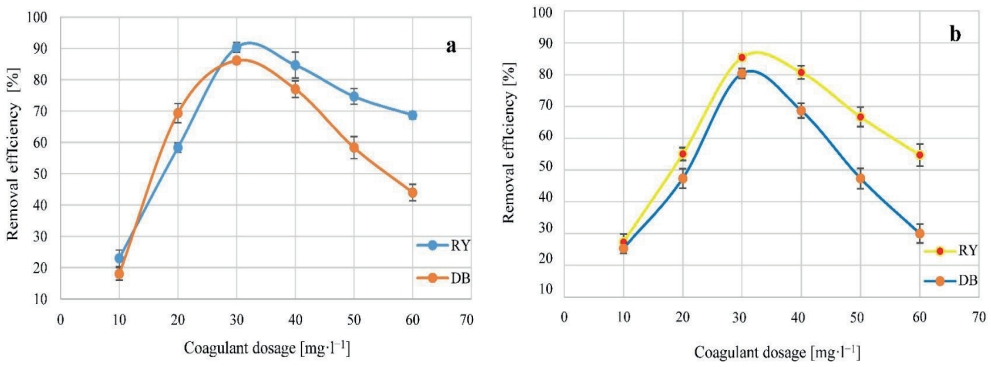

FIGURE 6. Effect of coagulant dosage on RY77 and DB53 removal efficiency by using poly manganese chloride (a) and alum (b)

Source: own work.

This supports findings from prior research showing that treatability performance increases with increasing coagulant dosage until agglomeration saturation is reached, at which point performance begins to stabilize or decline (Bressane et al., 2023). Because of the inverted net charge on suspended solids in wastewater, this resulted in a notable decrease in contaminant removal (Daud et al., 2015).

Mohammed, W. A., Saadi Hussein, T., Saadi Hussein, N. (2026). Recovered poly manganese chloride ($PMnCl_2$) from industrial waste sludge to decolorize and detoxify textile dyes and comparison with alum. *Sci. Rev. Eng. Env. Sci.*, *35* (1), 75–94. DOI 10.22630/srees.10715

Additionally, because an overdose would have prevented a polymeric chain reaction and allowed contaminants to find vacant places for adsorption bridging with a higher possibility of sweeping, it might have resulted in re-stabilization (Abreu et al., 2020). Furthermore, either too much or too little dosage might have a detrimental effect on the coagulation treatment procedure, increasing the expense of using chemicals (Kukić et al., 2018; Maurya & Daverey, 2018).

Scanning electron microscope test results

Figure 7 shows the SEM images of the coagulant grains at a scale of 20 μm with landing energy capacity of 15 kV. The crystal shape in the SEM micrograph indicates the poly manganese chloride in the sample. The manganese oxide could be the black spots, also explaining the ratios of manganese and chlorine which are compatible with the elemental analysis of poly manganese chloride. The agglomeration of the large flocs was facilitated by rough surfaces with vast heterogeneity, inconsistent form, and mesoporosity (Dos Santos et al., 2018). Recovered coagulant macromolecules showed highly selective, high-affinity manganese ions that improved precipitation. This indicates that morphological surfaces are strongly bonded to manganese ions, facilitating both adsorption and agglomeration. Furthermore, in the case of alum as a coagulant, the surface charge of colloidal particles in solution contributes to their destabilization, particularly when their settling process is slow, resulting in a state of apparent stability within the dispersion. A slight decrease in zeta potential combined with an increase in ionic strength can cause colloidal stability and destabilization (Tisti & Ghawi, 2020).

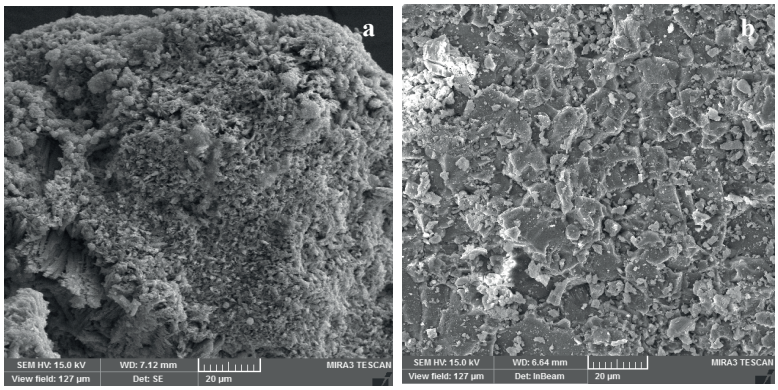

FIGURE 7. SEM images of poly manganese chloride (a) and alum (b)
Source: own work.

The energy dispersive spectrometer (EDS) was employed to analyze the alterations in support characteristics for poly manganese chloride. Figure 8a illustrates the energy dispersive spectrometer EDS techniques. The findings indicated that there was approximately 38.45 wt% of element Mn, followed by a 33.15 wt% of element O, and elements C, Si, Fe, Cl, and Zn at about 9.01 wt%, 11.93 wt%, 3.62 wt%, 2.16 wt%, and 1.68 wt%, respectively. In alum, the elements Al and O were about 26.20 wt% and 48.77 wt%, respectively, while C and S were about 9.17 wt%, and 15.86 wt%, respectively, as shown in Figure 8b.

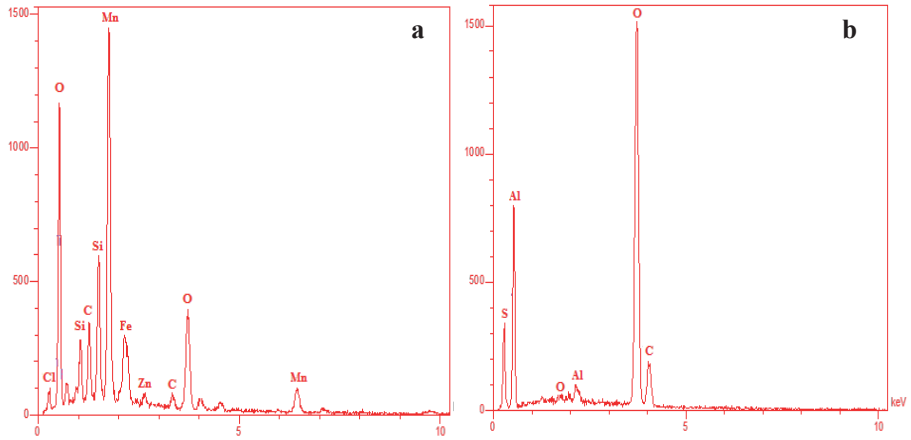

FIGURE 8. EDS analysis of poly manganese chloride (a) and alum (b)
Source: own work.

Fourier transform infrared test results

FTIR analysis of poly manganese chloride is shown in Figure 9a, where the hydroxyl vibration bands at 2,890 cm^{-1} are stretched. At 1,627 cm^{-1}, the absorption band is assigned to the OH bending vibration and the C–O stretching vibration. The asymmetric stretching vibration of Mn–OH–Mn and the Si–O bending and stretching vibrations are associated with the bands at 1,150 cm^{-1} and 1,210 cm^{-1}. Furthermore, three peaks for poly manganese chloride were identified at 1,270 cm^{-1}, 1,330 cm^{-1}, and 1,400 cm^{-1}; they were explained as bending vibrations of Mn–OH (Zhou et al., 2014).

Mohammed, W. A., Saadi Hussein, T., Saadi Hussein, N. (2026). Recovered poly manganese chloride ($PMnCl_2$) from industrial waste sludge to decolorize and detoxify textile dyes and comparison with alum. *Sci. Rev. Eng. Env. Sci.*, *35* (1), 75–94. DOI 10.22630/srees.10715

Alum's FTIR spectra, as shown in Figure 9b, showed a large peak at 3,442 cm^{-1} because of the presence of O–H groups in the material (Rong et al., 2013). A peak at 1,632 cm^{-1} indicates H–O–H stretching, which may have been caused by the hydroxyl group in the alum. Additionally, a peak at 531 cm^{-1} indicates Al–O stretching vibrations. Possible explanations for the other peaks at 1,060 cm^{-1} and 980 cm^{-1} include SO_4 stretching and the likely HOO matrix, respectively (Singh et al., 2012). The presence of OH and HOO groups may result from hydrogen bonds that occur within alum as it forms a variety of hydrates, the most prevalent of which are the octadecahydrate $Al_2(SO_4)_3 \cdot 18H_2O$ and the hexadecahydrate $Al_2(SO_4)_3 \cdot 16H_2O$.

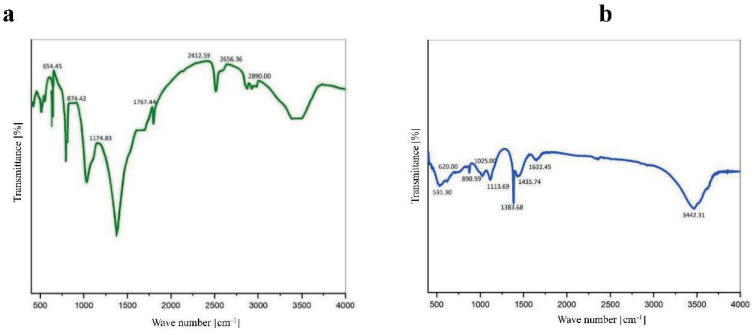

FIGURE 9. FTIR spectra of poly manganese chloride (a) and alum (b)
Source: own work.

Quality water evaluation of dye samples

COD and TOC were used to evaluate how well recovered poly manganese chloride reduced the organic pollutant in the tested colors. According to Figure 10, the COD values of RY17 and DB53 were calculated to be 788 $mg \cdot l^{-1}$ and 895 $mg \cdot l^{-1}$, respectively, before treatment. However, following poly manganese chloride treatment, the COD significantly decreased to 150 $mg \cdot l^{-1}$ and 210 $mg \cdot l^{-1}$, respectively. Observed percentage reductions in COD values were 80.96% for RY17, and 76.53% for DB53. The TOC values for RY17 and DB53 were estimated to be 680 $mg \cdot l^{-1}$ and 710 $mg \cdot l^{-1}$, respectively, before to treatment. However, following poly manganese chloride treatment, the TOC drastically decreased by 83.82% and 80.28%, respectively, as seen in Figure 11.

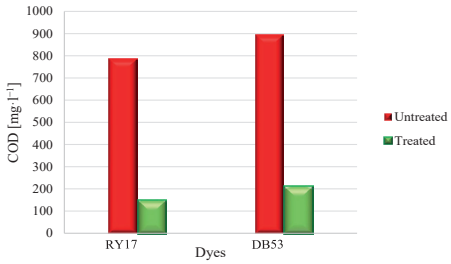

FIGURE 10. COD values of textile dyes before and after

Source: own work.

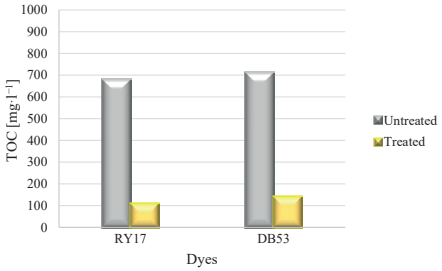

FIGURE 11. TOC values of textile dyes before and after

Source: own work.

Another study examined the use of sequential ozonation and an up-flow biological aerated filter method to remove color and COD from wastewater containing reactive dyes; the color and COD removal efficiencies were 97% and 90%, respectively (Lu et al., 2009). Another study used polyurethane foam (PUF) immobilized microbial consortia to reduce the COD and TOC levels of a carcinogenic azo dye, Congo red (CR), by 85% and 83%, respectively (Lade et al., 2015).

Conclusions

Among the available dye removal techniques, coagulation is extensively applied because of its simplicity and high efficacy. Recovered poly manganese chloride and alum are the coagulants applied to remove this pollutant. Manganese chloride can be recovered from industrial sludge to produce poly manganese chloride, which is an effective coagulant for treating textile dyes. The best recovery efficiency

in the recovered coagulant is achieved with a 30% HCl concentration, 300 rpm stirring speed, 100 min of reaction time, and 80°C reaction temperature according to the current analysis of lab experiments. The optimum dose for the recovered coagulant was 30 $mg \cdot l^{-1}$. The decolorization and reduction of the organic pollutant by poly manganese chloride are better than those by alum at the same dose, which shows the clear superiority of poly manganese chloride over alum in removal. In summary, our study has found an economical and effective way to create environmentally friendly wastewater treatment solutions. Additionally, money will be saved and industrial sludge, one of the most valuable resources given the global situation, will be safely reused by implementing this technique at the application level.

Acknowledgments

The authors are thankful to the Iraqi textile factory and University of Baghdad, College of Engineering, Environmental Engineering Department for Their cooperation. Our sincere gratitude to the Research and Development Laboratories at the College.

References

Abreu, M., Montel, A. L., & Scapin, E. (2020). *Use of natural coagulants/flocculants in the treatment of hospital laundry effluents.* ChemRxiv. https://doi.org/10.26434/chemrxiv.12982574.v2

Ahmed, S. N., Ali, S. J., Al-Zubaidi, H. A. M., Ali, A. H., & Ajeel, M. A. (2020). Improvement of organic matter removal in water produced of oilfields using low cost Moringa peels as a new green environmental adsorbent. *Global Nest Journal*, *22*, 268–274. https://doi.org/10.30955/gnj.003098

American Public Health Association [APHA]. (2005). *Standard methods for the examination of water and wastewater. 21st Edition*. American Public Health Association, American Water Works Association and Water Environment Federation.

Balls, M. (2014). *Relationships between floc properties and NOM removal using a moorland water source.* University College London. https://discovery.ucl.ac.uk/id/eprint/1417138/1/Balls_M_Thesis.pdf

Bodlund, I. (2020). *Coagulants Protein from plant materials: Potential Water Treatment Agent.* Royal Institute of Technology. https://www.diva-portal.org/smash/get/diva2:575557/FULLTEXT01.pdf

Bressane, A., Goulart, A. P. G., Melo, C. P., Gomes, I. G., Loureiro, A. I. S., Negri, R. G., Moruzzi, R., Reis, A. G. dos, Formiga, J. K. S., Silva, G. H. R. da, & Thomé, R. F. (2023).

A non-hybrid data-driven fuzzy inference system for coagulant dosage in drinking water treatment plant: machine-learning for accurate real-time prediction. *Water*, *15*(6), 1126. https://doi.org/10.3390/w15061126

Daud, Z., Awang, H., Nasir, N., Ridzuan, M. B., & Ahmad, Z. (2015). Suspended solid, color, COD and oil and grease removal from biodiesel wastewater by coagulation and flocculation processes. *Procedia-Social and Behavioral Sciences*, *195*, 2407–2411. https://doi.org/10.1016/j.sbspro.2015.06.234

Dos Santos, T. R. T., Mateus, G. A. P., Silva, M. F., Miyashiro, C. S., Nishi, L., Andrade, M. B. de, Fagundes-Klen, M. R., Gomes, R. G., & Bergamasco, R. (2018). Evaluation of magnetic coagulant (α-Fe_2O_3-MO) and its reuse in textile wastewater treatment. *Water, Air, & Soil Pollution*, *229*(3), 92. https://doi.org/10.1007/s11270-018-3747-8

Holkar, C. R., Jadhav, A. J., Pinjari, D. V., Mahamuni, N. M., & Pandit, A. B. (2016). A critical review on textile wastewater treatments: possible approaches. *Journal of Environmental Management*, *182*, 351–366. https://doi.org/10.1016/j.jenvman.2016.07.090

Hossain, M. S., Omar, F., Asis, A. J., Bachmann, R. T., Sarker, M. Z. I., & Ab Kadir, M. O. (2019). Effective treatment of palm oil mill effluent using FeSO4. 7H2O waste from titanium oxide industry: Coagulation adsorption isotherm and kinetics studies. *Journal of Cleaner Production*, *219*, 86–98. https://doi.org/10.1016/j.jclepro.2019.02.069

Hung, Y.-T., & Kaya, D. (2020). *Treatment of vegetable oil refining wastes*. Civil and Environmental Engineering Faculty Publications. https://engagedscholarship.csuohio.edu/cgi/viewcontent.cgi?params=/context/encee_facpub/article/1400/&path_info=vegetable_oil_refining_waste_treatment.pdf.pdf

Ghaly, A. E., Ananthashankar, R., Alhattab, M. V. V. R., & Ramakrishnan, V. V. (2014). Production, characterization and treatment of textile effluents: a critical review. *Journal of Chemical Engineering & Process Technology*, *5*(1), 1–19. http://dx.doi.org/10.4172/2157-7048.1000182

Jamali, H. A., & Moradnia, M. (2018). Optimizing functions of coagulants in treatment of wastewater from metalworking fluids: Prediction by RSM method. *Environmental Health Engineering and Management Journal*, *5*(1), 15–21. https://doi.org/10.15171/EHEM.2018.03

Kukić, D., Šćiban, M., Prodanović, J., Vasić, V., Antov, M., & Nastić, N. (2018). Application of natural coagulants extracted from common beans for wastewater treatment. *Advances in Civil and Architectural Engineering*, *9*(16), 77–84. https://doi.org/10.13167/2018.16.7

Kumar, M. M., Karthikeyan, R., Anbalagan, K., & Bhanushali, M. N. (2016). Coagulation process for tannery industry effluent treatment using Moringa oleifera seeds protein: Kinetic study, pH effect on floc characteristics and design of a thickener unit. *Separation Science and Technology*, *51*(12), 2028–2037. https://doi.org/10.1080/01496395.2016.1190378

Lade, H., Kadam, A., Paul, D., & Govindwar, S. (2015). Biodegradation and detoxification of textile azo dyes by bacterial consortium under sequential microaerophilic/aerobic processes. *EXCLI Journal*, *14*, 158–174.

Lu, X., Yang, B., Chen, J., & Sun, R. (2009). Treatment of wastewater containing azo dye reactive brilliant red X-3B using sequential ozonation and upflow biological aerated filter

process. *Journal of Hazardous Materials*, *161*(1), 241–245. https://doi.org/10.1016/j.jhazmat.2008.03.077

Maurya, S., & Daverey, A. (2018). Evaluation of plant-based natural coagulants for municipal wastewater treatment. *3 Biotech*, *8*(1), 77. https://doi.org/10.1007/s13205-018-1103-8

Mohammed, W. A., & M-Ridha, M. J. (2024). Extraction and purification techniques of the bio-catalyst cabbage peroxidase enzyme to remove reactive dyes and bisphenol-A pollutants. *Results in Engineering*, *21*, 101961. https://doi.org/10.1016/j.rineng.2024.101961

Mohammed, W. A., & M-Ridha, M. J. (2025). Removal of textile dyes by cross linking immobilized bio-catalyst enzyme on quartz particles: An experimental batch and mathematical model. *Mathematical Modelling of Engineering Problems*, *12*(3), p1013. https://doi.org/10.18280/mmep.120328

Nnaji, N. J. N., Ani, J. U., Aneke, L. E., Onukwuli, O. D., Okoro, U. C., & Ume, J. I. (2014). Modelling the coag-flocculation kinetics of cashew nut testa tannins in an industrial effluent. *Journal of Industrial and Engineering Chemistry*, *20*(4), 1930–1935. https://doi.org/10.1016/j.jiec.2013.09.013

Othman, Z., Bhatia, S., & Ahmad, A. L. (2011). Influence of the Settleability Parameters for Palm Oil Mill Effluent (POME) pretreatment by using Moringa Oleifera seeds as an Environmental Friendly Coagulant. *Journal of Materials Science and Engineering*, *5*(3), 332–340.

Rong, H., Gao, B., Dong, M., Zhao, Y., Sun, S., Yue, Q., & Li, Q. (2013). Characterization of size, strength and structure of aluminum-polymer dual-coagulant flocs under different pH and hydraulic conditions. *Journal of Hazardous Materials*, *252*, 330–337. https://doi.org/10.1016/j.jhazmat.2013.03.011

Sahu, O. P., & Chaudhari, P. K. (2013). Review on chemical treatment of industrial waste water. *Journal of Applied Sciences and Environmental Management*, *17*(2), 241–257. http://dx.doi.org/10.4314/jasem.v17i2.8

Saifuddin, N., & Dinara, S. (2011). Pretreatment of palm oil mill effluent (POME) using magnetic chitosan. *Journal of Chemistry*, *8*, S67–S78. https://doi.org/10.1155/2011/427532

Sánchez-Martín, J., Beltrán-Heredia, J., & Peres, J. A. (2012). Improvement of the flocculation process in water treatment by using Moringa oleifera seeds extract. *Brazilian Journal of Chemical Engineering*, *29*, 495–502. https://doi.org/10.1590/S0104-66322012000300006

Sher, F., Malik, A., & Liu, H. (2013). Industrial polymer effluent treatment by chemical coagulation and flocculation. *Journal of Environmental Chemical Engineering*, *1*(4), 684–689. https://doi.org/10.1016/j.jece.2013.07.003

Singh, P. K., Kumar, P., Seth, T., Rhee, H. W., & Bhattacharya, B. (2012). Preparation, characterization and application of Nano CdS doped with alum composite electrolyte. *Journal of Physics and Chemistry of Solids*, *73*(9), 1159–1163. https://doi.org/10.1016/j.jpcs.2012.05.008

Sun, Y., Zhou, S., Chiang, P. C., & Shah, K. J. (2019). Evaluation and optimization of enhanced coagulation process: Water and energy nexus. *Water-Energy Nexus*, *2*(1), 25–36. https://doi.org/10.1016/j.wen.2020.01.001

Tetteh, E. K., & Rathilal, S. (2020). Application of organic coagulants in water and wastewater treatment. In A. Sand & E. Zaki (Eds.), *Organic Polymers.* Intech Open.

Tetteh, E. K., & Rathilal, S. (2021). Application of magnetized nanomaterial for textile effluent remediation using response surface methodology. *Materials Today: Proceedings*, *38*, 700–711. https://doi.org/10.1016/j.matpr.2020.03.827

Tisti, H. J., & Ghawi, A. H. (2020). Performance improvement of package water treatment plant by using static mixer and natural coagulant. *Journal of Green Engineering*, *10*(7), 3717–3744.

Tyagi, S., Sharma, B., Singh, P., & Dobhal, R. (2013). Water quality assessment in terms of water quality index. *American Journal of Water Resources*, *1*(3), 34–38. https://doi.org/10.12691/ajwr-1-3-3

Vasudevan, S., Lakshmi, J., & Sozhan, G. (2010). Studies relating to removal of arsenate by electrochemical coagulation: optimization, kinetics, coagulant characterization. *Separation Science and Technology*, *45*(9), 1313–1325. https://doi.org/10.1080/01496391003775949

Zahrim, A. Y., Dexter, Z. D., Joseph, C. G., & Hilal, N. (2017). Effective coagulation-flocculation treatment of highly polluted palm oil mill biogas plant wastewater using dual coagulants: Decolourisation, kinetics and phytotoxicity studies. *Journal of Water Process Engineering*, *16*, 258–269. https://doi.org/10.1016/j.jwpe.2017.02.005

Zhang, H., Lin, H., Li, Q., Cheng, C., Shen, H., Zhang, Z., Zhang, Z., & & Wang, H. (2021). Removal of refractory organics in wastewater by coagulation/flocculation with green chlorine-free coagulants. *Science of the Total Environment*, *787*, 147654. https://doi.org/10.1016/j.scitotenv.2021.147654

Zhao, S., Gao, B., Yue, Q., & Wang, Y. (2014). Effect of Enteromorpha polysaccharides on coagulation performance and kinetics for dye removal. *Colloids and Surfaces A: Physicochemical and Engineering Aspects*, *456*, 253–260. https://doi.org/10.1016/j.colsurfa.2014.05.035

Zhou, F. S., Hu, B., Cui, B. L., Liu, F. B., Liu, F., Wang, W. H., Liu, Y., Lu, R. R., Hu, Y. M., Zhang, Y. H., & Wu, J. G. (2014). Preparation and characteristics of polyaluminium chloride by utilizing fluorine-containing waste acidic mother liquid from clay-brine synthetic cryolite process. *Journal of Chemistry*, 2014(1), 274126. https://doi.org/10.1155/2014/274126

Summary

Recovered poly manganese chloride ($PMnCl_2$) from industrial waste sludge to decolorize and detoxify textile dyes and comparison with alum. Th coagulation process for treating wastewater pollutants, due to its simplicity and safety, has received growing attention for a while. In this research, manganese chloride in industrial wastewater sludge can be recovered to produce poly manganese chloride as an effective and low-cost coagulant for the treatment of industrial pollutants. However, in recovering manganese chloride, there are some factors that affect efficiency, such as hydrochloric acid concentration, agitation force during acidification, contact time, and temperature. To describe the coagulant's morphological and elemental structure, scanning electron microscopy (coupled with energy dispersive spectroscopy) and Fourier transform infrared

Mohammed, W. A., Saadi Hussein, T., Saadi Hussein, N. (2026). Recovered poly manganese chloride ($PMnCl_2$) from industrial waste sludge to decolorize and detoxify textile dyes and comparison with alum. *Sci. Rev. Eng. Env. Sci.*, *35* (1), 75–94. DOI 10.22630/srees.10715

spectroscopy were used. The purpose of this research is to determine the ideal recovery coagulant conditions and assess this coagulant's efficacy in comparison to a conventional coagulant, alum, to treat textile dyes reactive yellow (RY17) and direct blue (DB53). In this paper, the results show that the optimum acidification concentration was 30% with a stirring speed of 300 rpm for 100 min at 80°C. Using a jar test, the optimum dose for the recovered coagulant was 30 $mg \cdot l^{-1}$. The decolorization of RY17 and DB53 was found to be 90.33% and 86.11%, respectively. The chemical oxygen demand and total organic carbon were reduced by 80.96% and 83.82%, respectively, for RY17, while for DB53 were reduced by 76.53% and 80.28%, respectively. At the same dose of alum, the decolorization of RY17 and DB53 was 85.42% and 80.34%, respectively. The decolorization performance illustrated that at the same dosage the recovered coagulant has slightly higher quality than the alum coagulant.

Scientific Review Engineering and Environmental Sciences (2026), 35 (1), 95–114

Sci. Rev. Eng. Env. Sci. (2026), 35 (1) https://srees.sggw.edu.pl

ISSN 1732-9353 (suspended) eISSN 2543-7496 DOI 10.22630/srees.10914

Received: 02.11.2025
Accepted: 03.03.2026

Zainab Adel Mohammed NUMAN✉
Abeer Mohammed HUMAD
University of Babylon, Civil Engineering Department, Iraq

Utilization of recycled concrete powder in the production of geopolymer mortars based on fly ash

Keywords: fly ash, FA, cement, OPC, recycled concrete powder, RCP, geopolymer mortars

Introduction

Concrete is the second most utilized material on earth, just after water, and it comprises about 20% portland cement (PC). Aa amount of 1 ton of PC produces approximately 1 ton of carbon dioxide (CO_2) emissions into the atmosphere (Davidovits, 1991). Consequently, researchers continue to study more viable and eco-friendly building materials that can lead to a diminished energy consumption and also minimize environmental effects. Geopolymers are a new binder that has the potential to substitute portland cement in concrete works (Ababneh et al., 2020). Geopolymers are synthetic alkali aluminosilicate materials formed through the reaction of aluminosilicate substances with aqueous alkaline solutions, such as sodium hydroxide or silicate solutions (Davidovits, 2020). Geopolymer concrete (GPC) is an innovative, sustainable, and eco-friendly binding agent derived from geological raw materials or by-products containing aluminosilicates, such as calcined kaolin clay (CKC), fly ash (FA), red mud,

✉zainab.numan.moren218@student.uobabylon.edu.iqa

Numan, Z. A. M., Humad, A. M. (2026). Utilization of recycled concrete powder in the production of geopolymer mortars based on fly ash. *Sci. Rev. Eng. Env. Sci.*, *35* (1), 95–114. DOI 10.22630/srees.10914

and ground granulated blast furnace slag (GGBFS), which entirely substitute cement in concrete (Kumar, 2015).

Wan et al. (2023) examined the mechanical and microstructural characteristics of cement-based products using recycled powder (RP) with high replacement rates (70–100%). It was found that compressive strength decreased significantly with the increase in the RP content, but alkali activation showed significant enhancement. Compressive strength also increased by more than 100% at 70% replacement of RP under optimum sodium silicate modulus conditions. At full replacement, the alkali-activated mixes exhibited a high proportion of strength recovery relative to the unactivated ones; therefore, these results showed that alkali-activated RP would be a viable, sustainable binder in cementitious systems.

Midhin et al. (2023) study included a systematic review of ultra-high-performance geopolymer concrete (UHP-GC), addressing its mechanical, microstructural, and physical aspects. It was found that when slag was partially replaced with 2,535% silica fume, the optimal ratio of Na_2SiO_3 to NaOH was 35, and the molarity of NaOH was 16M, resulting in better compressive and tensile strength. The paper has highlighted that an optimized mix design improves the formation of geopolymeric gel and porosity, which makes UHP-GC a high-strength and sustainable substitute in current concrete technology.

The current improvements in geopolymer sturdiness were discovered by Alahmari et al. (2023). They are water absorption, temperature resistance, sulfuric, sulfate, chloride ion penetration, and freeze-thaw resistance. The analysis screen has implications for a great life of geopolymer concrete compared with conventional cement-majority-based concrete. Moreover, this analysis presents suggestions and highlights the capacities of research on the geopolymer concrete that is closely related.

Razak et al. (2020) evaluated the compressive strength of geopolymer paste with FA and ordinary portland cement (OPC) paste under the effects of porosity and water absorption. Using the Brunauer–Emmett–Teller technique, the researchers found that geopolymer paste exhibited lower surface area, pore volume, and pore length compared with OPC. The geopolymer was based on micropores as its main microstructure, while OPC used mesopores. The decreased pore length and water absorption, therefore, enhanced the compressive strength of geopolymer to 76.7 MPa after 28 days. The authors concluded that geopolymers based primarily on FA show great resistance to wear and the environment and superior to the conventional OPC paste.

Sharma et al. (2022) explored the potential of the recycled fine powder (RFP) being used as an activator and partial alternative for FA within the production

of geopolymer mortar. The test involved unique alternative ranges (10–50%) and kept the combination parameters consistent, including an alkali-to-binder ratio of 0.45, a 12M sodium hydroxide molarity, a sodium silicate-to-sodium hydroxide ratio of 2, and a water-stable ratio of 0.35. The study compared workability (slump flow, setting time), mechanical strength, and durability based on the tests of compressive strength, water absorption, porosity, and drying shrinkage under ambient and heat-curing conditions. It was found that a 30% replacement of FA with RFP gave optimal strength and durability-enhancing results. Microstructural analysis revealed the presence of calcium-rich compounds and an additional Na_2O-Al_2O_3-SiO_2-H_2O gel phase, which provided a denser structure and improved the overall performance of the geopolymer mortar.

Zhang et al. (2023) studied the mechanical, durability, and microstructural properties of geopolymer recycled aggregate concrete (GPRAC). The researchers have found that the performance metrics, including compressive and flexural strength, elastic modulus, and freeze-thaw resistance, could be significantly enhanced through the optimization of curing temperature, precursor combinations, and mix proportions. Recycled aggregates increased the use of better recycled aggregates, which minimized porosity and water absorption by about 19% and 25%, respectively, with no reduction in density. In general, the research proved that GPRAC can be used to address the needs of the engineering profession, minimize carbon emissions, and establish low-carbon and sustainable construction methods.

Purpose and goals of research

This paper will examine the possibility of using concrete waste powder as a partial replacement material in FA-based geopolymer mortars, and more specifically, its ability to improve sustainability while maintaining acceptable mechanical and durability properties.

The targeted objectives of the research are to:

– Assess how the addition of concrete waste powder would alter the compressive and flexural strength of the FA-based geopolymer mortars.
– Measure the performance of the developed geopolymer mortars in terms of acid resistance by mass loss and strength retention.
– Examine the microstructure of the geopolymer mortars with scanning electron microscopy (SEM) and correlate it with mechanical and durability behavior.
– Determine the appropriate amount of replaced concrete powder that would compromise between mechanical performance, durability, and micro-structural integrity.

Numan, Z. A. M., Humad, A. M. (2026). Utilization of recycled concrete powder in the production of geopolymer mortars based on fly ash. *Sci. Rev. Eng. Env. Sci.*, *35* (1), 95–114. DOI 10.22630/srees.10914

– Enhance the creation of low-carbon and sustainable construction materials by fostering the valorization of concrete waste in geopolymer systems.

Scientific novelty and contribution

The novelty of this research lies in the systematic use of the recycled concrete powder (RCP) in FA-based geopolymer mortar systems, whereby RCP was experimentally explored both as a partial substitution of the binder and the fine aggregate, with the latter studies within the same research. Contrary to the majority of the earlier conducted studies that considered one specific replacement position or low rates, this study assessed high replacement ratios (up to 75%) and emphasized the unique effects of RCP, given the functional role in the mix design.

Furthermore, this paper offers a comparative evaluation of the OPC-based mortars and alkali-activated FA mortars with RCP, providing a complete insight into strength progression, durability, and microstructural transformation of these mortars under the same curing conditions. Another innovation made is the finding that compressive strength retention is a more credible indicator of acid resistance than mass loss, as evidenced by the SEM results that distinguish internal microstructural degradation processes (gel dissolution and micro-cracking) and surface erosion.

The results not only provide definite levels of performance for sustainable use of RCP in geopolymer mortars but also suggest the most optimal mix strategies to balance mechanical performance, durability, and environmental performance, which adds new knowledge on designing eco-effective cementitious materials to work in aggressive exposure conditions.

Experimental work

Material

The materials that were used in this study were OPC with the brand Almas, following the Iraqi standard IQS 5/2019 (Central Organization for Standardization and Quality Control [COSQC], 2019), and FA type F obtained from Eurobuild Constructions Chemicals and examined according to the ASTM C618-22 standard (ASTM International, 2022). The alkali activator was liquid sodium silicate with alkali modulus ($Ms = SiO_2/Na_2O$) equal to 3.3, with silicon dioxide (SiO_2) content of 43.25% and sodium oxide (Na_2O) content of 13.1%. The alkalinity was adjusted

to 1.5 by adding sodium hydroxide (NaOH) flakes with 99% purity to the sodium silicate solution to adjust the total alkalinity within the desired range for alkaline polymerization. The activator was used in 15% (as solid content) of the binder. The chemical and physical properties of the binders are shown in Table 1.

TABLE 1. The physical and chemical properties of cement and fly ash used in this study

Specification	Cement	Fly ash
Silica (SiO_2) content [%]	20.90	48.15
Alumina (Al_2O_3) content [%]	6.20	18.87
Iron oxide (Fe_2O_3) content [%]	3.10	4.59
$SiO_2 + Al_2O_3 + Fe_2O_3$ content [%]	–	–
Sulfate (SO_3) content [%]	1.75	1.53
Lime (CaO) content [%]	62.30	14.52
Magnesia (MgO) content [%]	2.70	2.48
Loss on ignition (LOI) [%]	3.3	6.0
Specific gravity [-]	3.15	2.32

Source: own work.

Moreover, aluminum foil was used to increase the solubility and reactivity of FA. Aluminum foil was incorporated into very small amounts as an auxiliary aluminum source to enhance the geopolymerization process. Under highly alkaline conditions, metallic aluminum reacts with hydroxide ions and contributes to the formation of soluble aluminate species ($Al(OH)_4^-$), which increase the availability of reactive aluminum necessary for aluminosilicate gel formation (Duxson et al., 2007; Davidovits, 2020). Previous studies have demonstrated that the introduction of additional aluminum sources, such as metallic aluminum powder or soluble aluminate compounds, can accelerate geopolymerization kinetics and promote matrix densification, particularly in FA-based geopolymer systems cured under ambient conditions (Provis & van Deventer, 2014; Ariffin et al., 2021). The dosage of aluminum foil was carefully controlled to avoid excessive gas formation associated with aluminum–alkali reactions and was kept constant across all mixtures to ensure consistency and comparability of results. RCP obtained from different types of demolished cubes was ground into fine materials that were thoroughly mixed and passed through a 600-micron sieve and used as a partial replacement for binder, as shown in the mix details presented in Table 2 and Figure 1. The water-to-binder ratio was 0.45 for all mortars, whereas the binder-to-sand ratio was 1 : 2.75.

Numan, Z. A. M., Humad, A. M. (2026). Utilization of recycled concrete powder in the production of geopolymer mortars based on fly ash. *Sci. Rev. Eng. Env. Sci.*, *35* (1), 95–114. DOI 10.22630/srees.10914

TABLE 2. Mix proportions

Mix ID[a]	Fly ash [kg]	Portland cement [kg]	Fine aggregates [kg]	Water [kg]	Sodium silicate[b] [kg]	Aluminum [g]	Recycled concrete powder [kg]	Super-plasticizer [%]
P100 (S100) ref1	–	4.6	9.2	2	–	–	–	1
P100 (S75W25)ref2	–	4.6	6.9	2	–	–	2.3	1
P100 (S50W50)ref3	–	4.6	4.6	2	–	–	4.6	1
F100 (S100)	4.6	–	9.2	2	1.5	2.5	–	–
F100 (S75W25)	4.6	–	6.9	2	1.5	2.5	2.3	–
F100 (S50W50)	4.6	–	4.6	2	1.5	2.5	4.6	–
F75 W25(S100)	3.45	–	9.2	2	1.5	2.5	1.15	–
F75 W25(S75W25)	3.45	–	6.9	2	1.5	2.5	3.45	–
F75W25(S50W50)	3.45	–	4.6	2	1.5	2.5	5.75	–

[a]Mix ID code: P – portland cement, S – sand, W – concrete waste powder, F – fly ash, ref1–3 mix – reference samples, P100(S50W50) means 100% of OPC + (50% of sand + 50% of recycled concrete powder).

[b]Ms = 1.5.

Source: own work.

FIGURE 1. Materials used in this study: a – ordinary portland cement, b – fly ash, c – recycled concrete powder; d – sodium silicate (activator solution)

Source: own work.

Curing conditions

After casting, all specimens were placed in an oven and cured inside the molds at a temperature of 80°C for 24 h to promote geopolymerization. Following heat curing, the specimens were removed from the oven and demolded after 24 h. The samples were then stored under ambient laboratory conditions at a temperature of 25 ±2°C until the designated testing ages. This combined curing regime (initial heat curing followed by ambient curing) was adopted to ensure adequate geopolymer gel formation at early ages while allowing subsequent strength development under realistic service conditions.

Mix proportions

The alkaline solution used in this study was prepared by mixing sodium silicate liquid with NaOH to adjust the alkali modulus (Ms = SiO_2/Na_2O) from 3.3 to 1.5, followed by the addition of mixing water and aluminum foil. The components were thoroughly stirred for 10–15 min using a continuous mixer under constant heating conditions, then left to rest for 24 h before casting mortar to obtain a homogeneous alkaline activator.

The silicate modulus of the alkaline activator (Ms = SiO_2/Na_2O) was adjusted to 1.5 to provide a balanced ratio between soluble silica and alkalinity. This value is widely reported as favorable for FA-based geopolymer systems, as it enhances dissolution of aluminosilicate species while facilitating the formation of a compact and stable geopolymeric gel under ambient curing conditions. A high Ms could cause a high viscosity ratio and restrict reaction kinetics, and a low Ms could cause inadequate silica supply and gel connectivity.

In the current paper, the concentration of the NaOH was chosen at range of 12–16M, as this has been commonly reported in the literature to be effective when it comes to using FA-based geopolymer binders, especially when allowed to cure under ambient conditions. An increase in molarity increases the dissolution of aluminosilicate species and the geopolymerization rate, whereas decreasing it can lead to aluminosilicate species not being fully activated and becoming weak. In this study, NaOH molarity was kept constant to limit the number of variables and to focus on the influence of concrete waste powder content and replacement strategy.

The dry ingredients (cement, sand, and RCP) were first mixed for 3 min using an eight-liter batch mixer. Separately, FA was blended with the prepared alkaline solution and mixed for 3 min for consistency. Then this mixture was combined

with the dry ingredients and mixed for at least 5 min. Fresh properties were then tested accordingly.

For the hardened properties, molds were washed and oiled, and the mortar was cast and compacted on a vibrating table, and the ASTM C109/C109 M-16a standard on compressive strength (ASTM International, 2016) and ASTM C348-98 standard on flexural strength (ASTM International, 1998) were followed. The specimens were then wrapped with nylon to avoid evaporation (Al-Bayati et al., 2022). The samples were kept at room temperature in covered plastic bags until the predetermined ages of 7 days and 28 days.

The mix proportions were selected to ensure consistency and allow direct comparison between different replacement strategies. The water-to-binder ratio (0.45) and binder-to-sand ratio (1 : 2.75) were maintained constant for all mixtures to minimize the influence of workability variations. The alkaline activator content was fixed at 15% of binder with an alkali modulus of 1.5, based on reported optimal ranges for FA-based geopolymer mortars under ambient curing.

Concrete waste powder replacement levels of 25%, 50%, and 75% were chosen to represent incremental substitution scenarios, enabling the evaluation of both physical (packing and filler effects) and chemical (reactivity and geopolymerization) contributions. This approach allows the identification of performance limits and durability implications associated with increasing RCP content.

Tests

Hardened properties

The mortars' mechanical properties, such as compressive and flexural strengths, were determined. Cube specimens with dimensions of 50 × 50 × 50 mm were used to determine compressive strength according to the ASTM C109/C109M-16a standard (ASTM International, 2016). The tests were conducted at 7 days and 28 days, with the average value of three specimens reported for each age. The loading rate was maintained constant at 900 $N \cdot s^{-1}$. Additionally, prism specimens measuring 40 × 40 × 160 mm were cast to evaluate the flexural strength of the cement mortars at 28 days, following the ASTM C348-98 standard (ASTM International, 1998) by using the one-point bending load. Beyond mechanical properties, durability-related characteristics such as porosity and water absorption were also assessed following the ASTM C642-13 standard (ASTM International, 2013).

Fresh tests

Fresh properties like workability, flow ability, and setting time are essential to cement mortars that include FA and RCP, as they directly determine the quality of the casts, compaction, and finally the longevity of hardened mortar. It has been found that FA is more effective in enhancing the flow and spreading behavior, whereas RCP tends to decline workability because of the smaller particle size and greater water retention capacity (Cunha et al., 2025). In the same vein, alkali-activated mortar with concrete sludge was studied, and it was shown that the level of fineness of binders, chemical composition, and activator dosage have a significant influence on viscosity and flow performance, with the consequent implication being that the formulation of mixtures must be considered in ensuring the best fresh properties are attained (Kesikidou et al., 2021). Additionally, rheological studies of mortars prove that zeta potential and packing density, which determine plastic viscosity and yield stress, change with the addition of FA, affecting the compaction efficiency and the number of voids in the mortar (Ma et al., 2022; Delihowski et al., 2024). Consequently, the fresh behavior of FA- and RCP-based mortars should be evaluated in order to provide sufficient workability, allow proper placement, and increase the durability behavior in the conditions of service.

Scanning electron microscopy test

Microstructural analysis of the hardened mortar was performed using a SEM in accordance with ASTM C1723-10 standard (ASTM International, 2010). Small fragments were carefully extracted from the broken specimens after the completion of the compressive strength test at 28 days, ensuring that the observed microstructure accurately represents the post-failure condition of the mortar. The SEM analysis was conducted at the College of Materials Engineering, University of Babylon, using a TESCAN MIRA3 field-emission scanning electron microscope (FE-SEM), model number MIRA3-XMU, operating at an accelerating voltage of 15 kV. High-magnification images were obtained to evaluate the morphological changes, pore distribution, and the bonding characteristics between the reaction products and the aggregates.

Numan, Z. A. M., Humad, A. M. (2026). Utilization of recycled concrete powder in the production of geopolymer mortars based on fly ash. *Sci. Rev. Eng. Env. Sci.*, *35* (1), 95–114. DOI 10.22630/srees.10914

Results and discussion

Compressive strength test results

The compressive strength data presented in Figure 2 clearly indicate that the combination of binder chemistry, reactivity of the precursors, and the time taken to cure the resin are controlling factors in the development of strength. The reference OPC-based mixes (P100 series) demonstrated a gradual augmentation of compressive strength between 7 days and 28 days, and this is typical of the gradual hydration process and the constant development of calcium silicate hydrate (C–S–H) gel. Out of these blends, P100 (S50W50) had the best compressive strength (49 MPa at 28 days), which means that even partial substitution of cement with waste powder enhances packing of particles and increases microstructural densification without majorly affecting cement hydration.

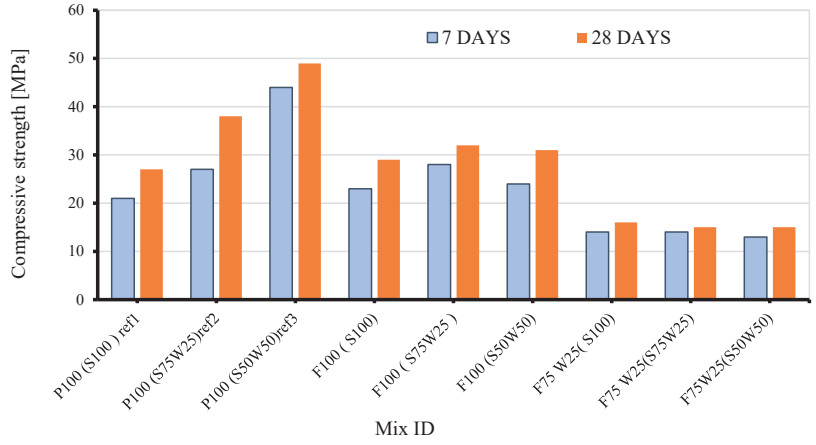

FIGURE 2. Compressive strength test results of mortar mixes at 7 days and 28 days
Source: own work.

The higher performance of P100 (S75W25) and P100 (S50W50) than P100 (S100) indicates that the addition of the optimal quantity of waste powder enhances the availability of fine reactive particles, which causes refinement of pores and enhances the transfer of loads in the hardened matrix. This observation indicates the importance of optimized solid packing and more sites of nucleation in speeding up hydration and strength gain.

Contrary to this, the FA-based systems showed slower strength development, which could be explained by the fact that a different reaction mechanism determines geopolymerization. The homogeneous compressive strength attained by F100 (S75W25) and F100 (S50W50) after 28 days (28–31 MPa) corresponds to the gradual dissolution of an aluminosilicate over time and formation of sodium aluminosilicate hydrate (N 50W50 50W50) gel. These findings permit to conclude that the partial inclusion of waste powder results in higher efficiency of geopolymerization because it provides reactive silica and alumina and thus, consolidation of the matrix.

Nevertheless, higher replacement levels, as was the case with the F75W25 (S75W25) and F75W25 (S50W50) mixes led to much lower compressive strength values (13–16 MPa at 28 days). The loss is mechanistically attributed to a lack of sufficient content of reactive binder, incomplete polymerization, and porosity, which together contribute to the weakening of the geopolymeric network. To this extent to which this behavior proves that the disproportion of the precursors constrains the network of gel connectivity and impairs the structural integrity.

In general, the findings show that compressive strength is very sensitive to the composition of the precursors and the balance of reactivity. Whereas OPC-based systems have the advantage of optimized particle packing, FA-based binders need a minimum ratio of reactive content in the form of aluminosilicate and enough curing time to result in good geopolymerization. The results are in accordance with earlier research on the significance of precursor optimization and curing conditions in the creation of dense and mechanically robust binder systems (Sajedi & Razak, 2011; Matos Riscado et al., 2025; Shamsah et al., 2025).

Flexural strength test results

The findings of the flexural strength results, as illustrated in Figure 3, point to the high reliance of the tensile performance on the binder composition, the continuity of the microstructure, and interfacial bonding. The flexural strength of the reference OPC-based mixes was shown to improve conspicuously with the waste powder content peaking at 10 MPa, with P100 (S50W50) having the best flexural strength value at S50W50. Mechanically, this can be explained by the fact that the particle packing is better and that a denser and more uniform gel network of calcium silicate hydrate (C1050) forms, which effectively seals the microcracks and makes the substance resistant to tensile stresses. The same has been extensively observed in cementitious systems with a well-established C–S–H phase, which is the major contributor to flexural capacity (Mehta & Monteiro, 2006).

Numan, Z. A. M., Humad, A. M. (2026). Utilization of recycled concrete powder in the production of geopolymer mortars based on fly ash. *Sci. Rev. Eng. Env. Sci.*, *35* (1), 95–114. DOI 10.22630/srees.10914

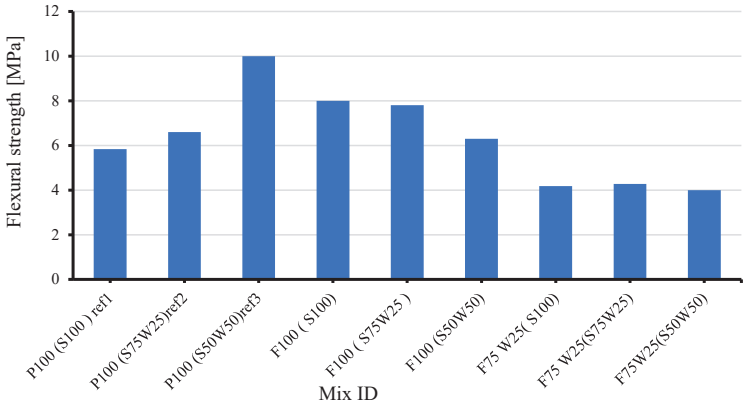

FIGURE 3. Flexural strength test results of mortar mixes at 28 day
Source: own work.

The gradual growth of flexural strength between P100 (S100) and P100 (S75W25) is another indication of partial replacement of waste powder, contributing to the refinement of microstructures and eliminating stress concentrations at weak interfaces. The relationship between flexural and compressive strength trends is confirmed to be close; that is, both the increase of hydration and the increase of matrix densification lead to an increase in both, load-bearing and crack-resisting capacity.

The F100 (S100) and F100 (S75W25) mixes had competitive flexural strengths of 8.0 MPa and 7.8 MPa, respectively, among the other alternative binders. This indicates that geopolymerization of such mixes resulted in a fine enough interconnected aluminosilicate gel (N–A–S–H), an ability to transfer stress throughout the matrix, and enhanced interfacial bonding. F100 performance of moderate (S50W50) (6.3 MPa) shows that, although waste powder contributes to the formation of gels, the over-replacement could interfere with gel continuity and tensile resistance.

Incomplete geopolymerization and weak interfacial transition zones can be attributed to significantly lower flexural strengths in the F75W25 series (4.0–4.28 MPa). Weak reactive levels of aluminosilicate and weak gel development contribute to a more uniform and porous structure, which is very disadvantageous during flexural loading; the crack starts and spreads as controlled by microstructural flaws.

These results are in agreement with recent research that has pointed out that the flexural performance of geopolymer mortars is very sensitive to the precursor chemistry, concentration of activators, and curing regime. Optimized proportions

of activators have been presented to bring a significant increase in the flexural response of FA-based geopolymers (Altawil & Olgun, 2025), whereas the use of micro-reinforcing or fine reactive additives enhances tensile bridging and matrix adhesion (Naenudon et al., 2022; Paramban & Gavindarajulu, 2024). Moreover, the fact that the improvement is reported by Ebrahim et al. (2024), supports the idea that a proper curing environment is a significant factor in the ability of geopolymer to obtain a compact and mechanically efficient matrix.

In general, all the findings show that P100 (S50W50) offers the best ratio of microstructural integrity and tensile resistance, whereas F100 (S100) and F100 (S75W25) are promising in terms of the flexural behavior of geopolymer systems, with the flexural behavior comparable to that of OPC-based systems. The subpar performance of the F75W25 series underscores the need to optimize precursor ratios, activator molarity, and curing conditions in a bid to realize higher flexural capacity in blended binder systems.

Acid resistance test

The influence of acid exposure on the mechanical properties of the examined mixes is shown by the correlation between mass loss and compressive strength loss, as depicted in Figure 4. The acid resistance findings show that the relationship between the loss of mass and compressive strength degradation is not linear or direct, which also confirms that the processes of the acid attack on cementitious and geopolymer systems are complex and multi-scale.

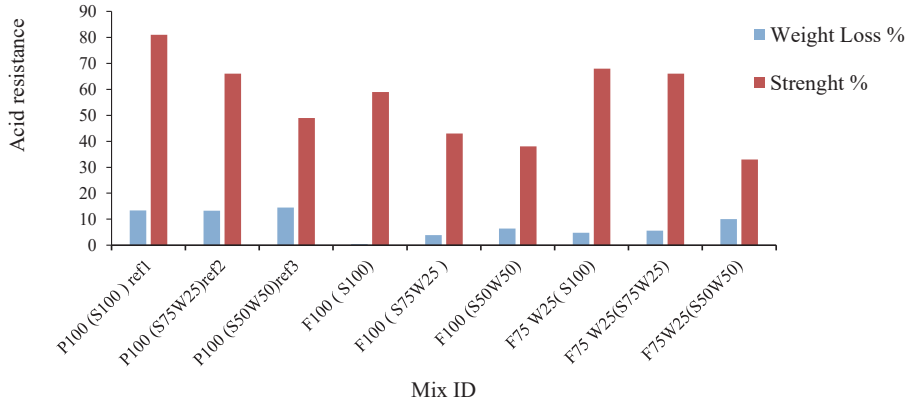

FIGURE 4. Acid resistance test results of mortar mixes at 28 day
Source: own work.

Numan, Z. A. M., Humad, A. M. (2026). Utilization of recycled concrete powder in the production of geopolymer mortars based on fly ash. *Sci. Rev. Eng. Env. Sci.*, *35* (1), 95–114. DOI 10.22630/srees.10914

As an example, the P100 (S100) mix had a small decrease in compressive strength (13.35), although it had a drastic mass loss (about 81) (Fig. 4). Such behavior implies that not only surface dissolution but also internal microstructural integrity is important in retaining the load-bearing capacity. On the contrary, the P100 (S50W50) mix experienced a considerable reduction in compressive strength (49%) but experienced a comparatively low mass loss (14.5%). It implies that weakening of the binding phases and the interfacial transition zones under the influence of acids can be disastrous to the mechanical strength, even when the loss of material is hardly visible.

The mechanistic explanation of this behavior is the preferential dissolution of calcium-rich hydration products when exposed to acidic conditions. During the decalcification process of the C–S–H gel in OPC-based systems, microcracking and a decrease in cohesion and internal damage occur, directly causing the reduction in compressive strength irrespective of the extent of surface erosion (de Siqueira & Cordeiro, 2022). This effect determines the loss of compressive strength that can be independent of the loss of mass.

On the other hand, it was observed that the FA-based geopolymer mixes (F100 series) exhibited significantly reduced mass losses (0.46–6.39%) and a gradual loss of compressive strength with increasing waste replacement, reduced by approximately 59% in F100 (S100) to 38% in F100 (S50W50), as shown in Figure 4. This has been possible because of the perfection of the pore structure and greater production of chemically stable aluminosilicate gels (N3A3S3H), which are much less prone to acidic dissolution compared with calcium-based hydration products.

The same situation could be noted with the F75W25 series, where the compressive strength loss was reduced to about 33.0% with increasing waste replacement, albeit with moderate values of mass loss between 4.76% and 10.0% (Fig. 4). This observation suggests that waste addition enhances chemical stability and decreases permeability, thereby restricting internal degradation and acid intrusion. The overall impact of the decreased calcium content, microstructural densification, and the existence of acid-resistant binding phases leads to enhanced resistance to the effects of acid on the mechanical deterioration.

On the whole, the findings indicate that compressive strength retention is a more effective predictor of acid durability compared with mass loss only; the trends in Figure 4 also support this point of view. The addition of complementary materials or waste powders to cementitious components and partial replacement is a good approach toward improvements in long-term mechanical performance in hostile acidic conditions. This finding is consistent with other researchers who have identified the key functions of gel chemistry and microstructural densification to enhance durability (Bayapureddy et al., 2023; Abdalla et al., 2024).

Scanning electron microscopy

The SEM analysis also helped to provide a crucial insight into the microstructural characteristics that controlled the mechanical and durability performance of the mortars that were under study. It was found in the micrographs that there are pores and voids of different shapes and sizes that exist in the entire matrix, and that the reaction products and packing density are heterogeneous as presented in Figure 5. Such gaps may be explained by a lack of full geopolymerization, a lack of dissolution of the aluminosilicate precursors, and localized excess water or trapped air during mixing and casting.

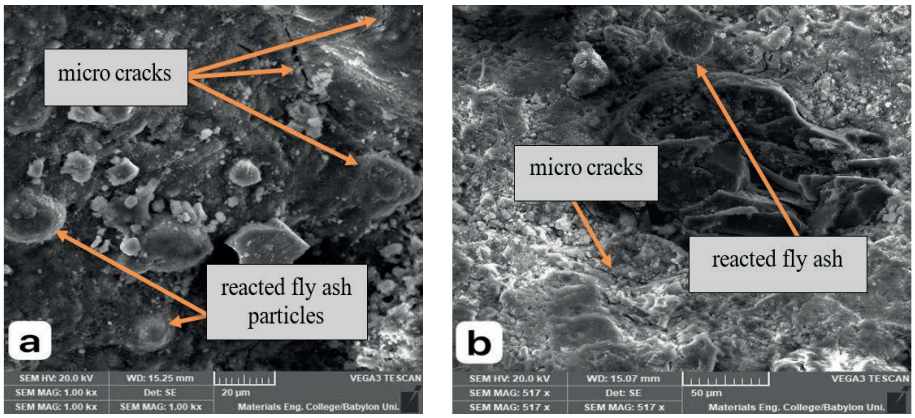

FIGURE 5. The SEM images of geopolymer mortar-based on F75W25(S50W50) (a), and geopolymer mortar-based on F100 (S100) (b)

Source: own work.

In the FA-geopolymer mortars, the unreacted FA particles that were partially spherical and partially sub-rounded were evidently encased in the hardened matrix with no major dissolution occurring on the surface. The fact that such unreacted particles persist indicates a low extent of alkali activation efficiency, which can be related to inappropriate proportions of the reactants toward the activators, ambient curing conditions, or inadequate curing times. Consequently, these particles become inert inclusions but do not bear geopolymeric gels.

The presence of unreacted FA particles together with interconnected voids compromises the continuity of the binding phase and interferes with stress transfer through the matrix. This microstructural discontinuity explains the lower compressive and flexural strengths of the mixes that have a greater composition of concrete waste powder and lower geopolymer reactivity. Further, these defects

Numan, Z. A. M., Humad, A. M. (2026). Utilization of recycled concrete powder in the production of geopolymer mortars based on fly ash. *Sci. Rev. Eng. Env. Sci.*, *35* (1), 95–114. DOI 10.22630/srees.10914

provide favorable access to fluid ingress and thus enhance vulnerability to chemical attack, adding to the loss of strength seen during the acid exposure experiments.

Conversely, mixes with increased mechanical performance were characterized by relatively denser matrices with lower amounts of unreacted particle content and lesser porosity, suggesting superior geopolymer gel formation and enhanced particle packing. The result of this densification is an increase in interfacial bonding between the products of exchanges and aggregates, which results in better distribution of loads and high resistance to environmental degradation.

In general, the results of mechanical and durability tests are effectively supported by the SEM observations, which prove that the level of precursor activation, polymer continuity, and refinement of pore structure control the behavior of geopolymer mortars. The results show that the composition of the activators, the curing regime, and the incorporation level of waste to be used are important in order to produce a compact microstructure and a durable geopolymer matrix.

Conclusions

This paper proved that FA and RCP can be used as alternatives to OPC or even as partial replacements of sand when making mortar. Mortars were made with various replacements (25%, 50%, and 75%) were made. Their mechanical and durability performances were tested using compressive strength, flexural strength, and acid resistance tests. The findings showed that alkaline activation had a considerable effect on enhancing strength and microstructural compactness.

The compressive strength findings showed that the reference OPC mortars showed the best overall performance, and the mixes with FA showed average strength depending on the concentration of the activators. Comparatively, the mixes containing a higher RCP content exhibited significantly less strength, which was mainly explained by a lack of material reactivity and an increase in porosity. On the whole, the results indicate the potential sustainability of FA-based mixes as an alternative, but there is a risk of overusing RCP at the cost of mechanical performance.

Similar tendencies were observed in flexural strength results, with FA-based mortars at approximately 8 MPa, which is close to the reference value of 10 MPa, and RCP-rich mixes at a significantly lower level of approximately 4 MPa, which is explained by a lack of complete geopolymerization and weak interfacial bonding.

The acid resistance tests showed that the mass loss/strength degradation relationship was not linear. Gel dissolution and micro-cracking, which were internal damages, had a greater effect on the loss of strength compared with erosion on the surface. Blends with an optimum ratio of FA and partial replacement of sand with fine waste powder showed optimum durability, whereas over-replacement of the binder with RCP performed poorly.

All in all, it can be inferred that using FA mortars with the right amount of activation and proper curing, it is possible to achieve similar strength and better durability than with OPC. It was found that the best combination was achieved when the sand was partly substituted with ground waste materials, but the substitution of the binder with RCP led to a significant decrease in strength. These findings indicate that a balanced mix design, controlled dosage of activators, and proper curing conditions are key to the creation of eco-efficient and long-lasting cementitious systems.

References

Ababneh, A., Matalkah, F., & Aqel, R. (2020). Synthesis of kaolin-based alkali-activated cement: carbon footprint, cost and energy assessment. *Journal of Materials Research and Technology*, *9*(4), 8367–8378. https://doi.org/10.1016/j.jmrt.2020.05.116

Abdalla, T. A., Shitote, S. M., Matallah, M., & Koteng, D. O. (2024). Effect on sulfuric acid resistance and shrinkage of concrete incorporating processed bagasse ash and silica fume. *Advances in Civil Engineering*, *2024*(1), 5534536. https://doi.org/10.1155/2024/5534536

Al-Bayati, M. A., Abdulrahman, M. B., Alzeebaree, R., & Arbili, M. M. (2022). The effect of materials and curing system on the behavior of self-compacting geopolymer concrete. *Journal of Mechanical Behavior of Materials*, *31*(1), 710–718. https://doi.org/10.1515/jmbm-2022-0206

Alahmari, T. S., Abdalla, T. A., & Rihan, M. A. M. (2023). Review of recent developments regarding the durability performance of eco-friendly geopolymer concrete. *Buildings*, *13*(12), 3033. https://doi.org/10.3390/buildings13123033

Altawil, H., & Olgun, M. (2025). Optimization of mechanical properties of geopolymer mortar based on Class C fly ash and silica fume: A Taguchi method approach. *Case Studies in Construction Materials*, *22*, e04332. https://doi.org/10.1016/j.cscm.2025.e04332

Ariffin, N., Abdullah, M. M. A. B., Postawa, P., Zamree Abd Rahim, S., Mohd Arif Zainol, M. R. R., Putra Jaya, R., Śliwa, J., Omar M. F., Wysłocki, J. J., Błoch, K., & Nabiałek, M. (2021). Effect of aluminium powder on kaolin-based geopolymer characteristic and removal of Cu^{2+}. *Materials*, *14*(4), 814. https://doi.org/10.3390/ma14040814

ASTM International. (1998). *Standard test method for flexural strength of hydraulic-cement mortars* (ASTM C348-98). ASTM International. https://doi.org/10.1520/C0348-98

ASTM International. (2011). *Standard Guide for Examination of Hardened Concrete Using Scanning Electron Microscopy* (ASTM C1723-10). ASTM International.

ASTM International. (2013). S*tandard test method for density, absorption, and voids in hardened concrete* (ASTM C642-13). ASTM International.

ASTM International. (2016). *Standard test method for compressive strength of hydraulic cement mortars (using 2-in. or [50-mm] cube specimens)* (C109/C109M-16a). ASTM International. https://doi.org/10.1520/C0109_C0109M-16A

ASTM International. (2022). *Standard specification for coal fly ash and raw or calcined natural pozzolan for use in concrete* (ASTM C618-22). ASTM International. https://doi.org/10.1520/C0618-22

Bayapureddy, Y., Muniraj, K., & Gangireddy, M. M. (2023). Characteristic evaluation of concrete containing sugarcane bagasse ash as pozzolanic admixture. *Research on Engineering Structures and Materials*, *9*(4), 1287–1307. https://doi.org/10.17515/resm2023.819ma0712

Central Organization for Standardization and Quality Control [COSQC]. (2019). *Portland cement* (IQS 5/2019). Central Organization for Standardization and Quality Control.

Cunha, S., Kaptan, K., Hardy, E., & Aguiar, J. (2025). Physical, mechanical, and durability behavior of sustainable mortars with construction and demolition waste as supplementary cementitious material. *Buildings*, *15*(15), 2757. https://doi.org/10.3390/buildings15152757

Davidovits, J. (1991). Geopolymers: Inorganic polymeric new materials. *Journal of Thermal Analysis and Calorimetry*, *37*(8), 1633–1656. https://doi.org/10.1007/bf01912193

Davidovits, J. (2020). *Geopolymer chemistry and applications* (5th ed.). Geopolymer Institute.

Delihowski, J., Izak, P., Wojcik, Ł., Stempkowska, A., & Jarosz, M. (2024). The influence of selected grain size fractions of coal fly ash on properties of clay-cement mortars used for the flood levees construction. *Scientific Reports*, *14*(1), 21485. https://doi.org/10.1038/s41598-024-72315-0

Duxson, P., Fernández-Jiménez, A., Provis, J. L., Lukey, G. C., Palomo, A., & Deventer, J. S., van (2007). Geopolymer technology: the current state of the art. *Journal of Materials Science*, *42*(9), 2917–2933. https://doi.org/10.1007/s10853-006-0637-z

Ebrahim, A. A. M., Ahmed, D. A., & Abu-Elwafa, R. (2024). Development of an eco-friendly geopolymer mortar using slag and fly ash with high bentonite content for thermal and environmental applications. *Scientific Reports*, *14*(1), 26727. https://doi.org/10.1038/s41598-024-76780-5

Kesikidou, F., Konopisi, S., & Anastasiou, E. K. (2021). Influence of concrete sludge addition in the properties of alkali-activated and non-alkali-activated fly ash-based mortars. *Advances in Civil Engineering*, *2021*(1), 5534002. https://doi.org/10.1155/2021/5534002

Kumar, M. (2015). Geopolymer concrete: Leading the world towards a sustainable future. *International Journal of Engineering Research & Technology (IJERT)*, *4*(9), 302–306.

Ma, J., Zhang, H., Wang, D., Wang, H., & Chen, G. (2022). Rheological properties of cement paste containing ground fly ash based on particle morphology analysis. *Crystals*, *12*(4), 524. https://doi.org/10.3390/cryst12040524

Matos Riscado, A. L. L. de, Vieira, C. M. F., Monteiro, S. N., Azevedo, A. R. G. de, & Marvila, M. T. (2025). Parameter optimization for fly ash geopolymer mixtures: molarity, silica modulus, and solution/binder influence. *Scientific Reports*, *15*(1), 20355. https://doi.org/10.1038/s41598-025-06076-9

Mehta, P. K., & Monteiro, P. J. M. (2006). *Concrete microstructure, properties, and materials*. McGraw-Hill.

Midhin, M. A. K., Wong, L. S., Ahmed, A. N., Jasim, A. M. D. A., & Paul, S. C. (2023). Strength and chemical characterization of Ultra High-Performance Geopolymer concrete: a coherent evaluation. *Civil Engineering Journal*, *9*(12), 3254–3277. https://doi.org/10.28991/CEJ-2023-09-12-020

Naenudon, S., Vilaivong, A., Zaetang, Y., Tangchirapat, W., Wongsa, A., Sata, V., & Chindaprasirt, P. (2022). High flexural strength lightweight fly ash geopolymer mortar containing waste fiber cement. *Case Studies in Construction Materials*, *16*, e01121. https://doi.org/10.1016/j.cscm.2022.e01121

Paramban, R. K., & Govindarajulu, K. V. (2024). Characteristic study of geopolymer fly ash fine aggregate and its influence on partial replacement of M-sand in the strength properties of mortar. *Structures*, *68*, 107141. https://doi.org/10.1016/j.istruc.2024.107141

Provis, J. L., & Deventer, J. S. L. van (2014). *Alkali-Activated Materials. State of the Art Report* (RILEM TC 224-AAM). Springer. https://doi.org/10.1007/978-94-007-7672-2

Razak, S., Zainal, F. F., & Shamsudin, S. R. (2020). Effect of porosity and water absorption on compressive strength of fly ash based geopolymer and OPC paste. *IOP Conference Series: Materials Science and Engineering*, *957*(1), 012035. https://doi.org/10.1088/1757-899X/957/1/012035

Sajedi, F., & Razak, H. A. (2011). Effects of curing regimes and cement fineness on the compressive strength of ordinary Portland cement mortars. *Construction and Building Materials*, *25*(4), 2036–2045. https://doi.org/10.1016/j.conbuildmat.2010.11.043

Shamsah, M., Kalfat, R., Subramaniam, K. V., & Hanumananaik, M. (2025). Calcium enhanced ambient cured fly ash based geopolymer binders. *Scientific Reports*, *15*(1), 25603. https://doi.org/10.1038/s41598-025-07854-1

Sharma, A., Singh, P., & Kapoor, K. (2022). Utilization of recycled fine powder as an activator in fly ash based geopolymer mortar. *Construction and Building Materials*, *323*, 126581. https://doi.org/10.1016/j.conbuildmat.2022.126581

Siqueira, A. A. de, & Cordeiro, G. C. (2022). Sustainable cements containing sugarcane bagasse ash and limestone: Effects on compressive strength and acid attack of mortar. *Sustainability*, *14*(9), 5683. https://doi.org/10.3390/su14095683

Wan, X., Li, H., Che, X., Xu, P., Li, C., & Yu, Q. (2023). A study on the application of recycled concrete powder in an alkali-activated cementitious system. *Processes*, *11*(1), 203. https://doi.org/10.3390/pr11010203

Zhang, Y., Wu, D., Wang, Y., Zhou, Y., Wang, S., & Zhao, Y. (2023). Influence of fly ash content on the durability of mortar specimens under dry/wet sulfate attack. *Materials*, *17*(1), 113. https://doi.org/10.3390/ma17010113

Numan, Z. A. M., Humad, A. M. (2026). Utilization of recycled concrete powder in the production of geopolymer mortars based on fly ash. *Sci. Rev. Eng. Env. Sci.*, *35* (1), 95–114. DOI 10.22630/srees.10914

Summary

Utilization of recycled concrete powder in the production of geopolymer mortars based on fly ash. This research examined the performance and durability of geopolymer mortars with fly ash (FA) and fly ash with recycled concrete powder (RCP) as a partial replacement for fly ash and/or the fine aggregate in the production of sustainable alternative mortars when compared with references based on ordinary portland cement (OPC). Mortar mixes were made by substituting binder and sand with RCP at varying ratios (25%, 50%, and 75%), and the mechanical and durability properties of the mortar mixtures were evaluated. The findings demonstrated that OPC-based mortars exhibited the highest performance, whereas the FA-based system activated with sodium silicate also presented significant strength with improved compactness and long-term stability. In contrast, high RCP content reduced reactivity, which highlights the importance of maintaining balanced binder proportions. There was also the use of geopolymer binders with the replacement of manufactured sand with FA fine aggregate (GFFA), 10–20% of manufactured sand, which resulted in enhanced mechanical performance and sustainability, as well as improved recycling of industrial by-products. Acid resistance tests confirmed the presence of stronger microstructural deterioration, such as gel dissolution and micro-cracking, compared with surface erosion, in influencing the reduction in strength. Furthermore, FA and RCP improved acid resistance capacity by refining microstructure and stabilizing binders. Overall, compressive strength retention proved to be a more reliable indicator of acid durability than mass loss. Therefore, properly designed FA-based mortars provide an effective, durable, and eco-friendly alternative to OPC, suitable for construction applications exposed to aggressive or challenging environments.

Instruction for Authors

The journal publishes in English languages, peer-reviewed original research, critical reviews and short communications, which have not been and will not be published elsewhere in substantially the same form. Author of an article is required to transfer the copyright to the journal publisher, however authors retain significant rights to use and share their own published papers. The published papers are available under the terms of the principles of Open Access Creative Commons CC BY-NC license. The submitting author must agree to pay the publication charge (see Charges).

The author of submitted materials (e.g. text, figures, tables etc.) is obligated to restricts the publishing rights. All contributors who do not meet the criteria for authorship should be listed in an Acknowledgements section of the manuscript. Authors should, therefore, add a statement on the type of assistance, if any, received from the sponsor or the sponsor's representative and include the names of any person who provided technical help, writing assistance, editorial support or any type of participation in writing the manuscript.

Uniform requirements for manuscripts

The manuscript should be submitted by the Open Journal System (OJS) at https://srees.sggw.edu.pl/about/submissions. All figures and tables should be placed near their reference in the main text and additionally sent in a form of data files (e.g. Excel, Visio, Adobe Illustrator, Adobe Photoshop, CorelDRAW). Figures are printed in black and white on paper version of the journal (color printing is combined with an additional fee calculated on a case-by-case basis), while on the website are published in color.

The size of the manuscript should be limited up to 10 pages including overview, summary, references and figures (the manuscript more than 13 pages is unacceptable); Please set the text format in single column with paragraphs (A4 paper format), all margins to 25 mm, use the font Times New Roman, typeface 12 points and line spacing one and half.

The submitted manuscript should include the following parts:

- name and SURNAME of the author(s) – up to 5 authors
- affiliation of the author(s), ORCID Id (optional)
- title of the work
- key words
- abstract (about 500 characters)
- text of the paper divided into: Introduction, Material and Methods, Results and Discussion, Conclusions, References and Summary
- references in APA style are listed fully in alphabetical order according to the last name of the first author and not numbered; please find the details below
- post and mailing address of the corresponding author:

  Author's address:
  Name, SURNAME
  Affiliation
  Street, number, postal code, City
  Country
  e-mail: adress@domain

- Plagiarism statement (https://srees.sggw.edu.pl/copyright)

Reference formatting

In the Scientific Review Engineering and Environmental Sciences the APA 7th edition style is used.

Detailed information

More information can be found: https://srees.sggw.edu.pl